DOCTORAL THESIS

Geological, Geochemical and Mineralogical Characterization of Non-Metallic Mineral Deposits in the La Paz Region, Bolivia

Ariana Zeballos

Ore Geology

LULEÅ UNIVERSITY OF TECHNOLOGY

LULEÅ
UNIVERSITY
OF TECHNOLOGY

Geological, Geochemical and Mineralogical Characterization of Non-Metallic Mineral Deposits in the La Paz Region, Bolivia

Ariana Zeballos

Luleå University of Technology
Department of Civil, Environmental and Natural Resources Engineering
Division of Geosciences and Environmental Engineering

Cover picture: An inhabitant lady from the Micaya Village, painting a vessel.

Printed by Luleå University of Technology, Graphic Production 2018

ISSN 1402-1544
ISBN 978-91-7790-098-6 (print)
ISBN 978-91-7790-099-3 (pdf)

Luleå 2018

www.ltu.se

"Not everything that counts can be counted,
and not everything that can be counted, counts"

(Albert Einstein)

ABSTRACT

Industrial mineral resources are a promising source of economic development in Bolivia where the mining industry's main focus is on metalliferous deposits. The industrial mineral resources in Bolivia are of large quantity, even though they remain only locally known, as well as understudied to a large degree.

This thesis aims to show the industrial mineral mining potential of La Paz and Bolivia as a whole. Bolivia's resources of industrial minerals can potentially be used for numerous industrial applications. Three deposits have been geologically and mineralogically characterized. In addition, the potential applications of the mined products are addressed.

Firstly, the Micaya deposit, located at the Micaya village south-west of La Paz city, comprising two whitish kaolinite-bearing occurrences, was investigated. The material is currently used in tableware production. The Micaya deposit is situated in a Palaeozoic sequence in the Altiplano basin. The general mineral composition of the occurrences is 56 vol.% quartz, 21 vol.% muscovite, 18 vol.% kaolinite and <5 vol.% feldspar. The kaolinite-bearing sediments were formed through enhanced weathering of the muscovite-rich siltstones aided by groundwater remobilization along permeable fault zones. Micaya kaolinite is suggested to be suitable for industrial applications.

Secondly, the Choquetanga deposit, located south-east of La Paz city and currently mined for Sn and W, is associated with a coarse-grained granitic batholith that was studied for its feldspar characteristics in this work. Geologically, the Choquetanga area is dominated by a Palaeozoic sedimentary sequence intruded by the porphyritic granite from the Quimsa Cruz batholith in the south-east of the Eastern Cordillera. The Quimsa Cruz batholith is composed of megacrystalline granite with 5–10 cm long orthoclase, albite and oligoclase crystals that contain a considerable alkali content of $\Sigma K_2O,Na_2O$=7.84–10.25 wt.%.

Thirdly, the La Fabulosa deposit, located north-west of the Eastern Cordillera, was studied for its feldspar occurrences hosted in granites and pegmatites. The deposit is composed of a metasedimentary sequence of Palaeozoic age intruded by the Sorata batholith, which comprises two-mica granites, granodiorites and pegmatites with an alkali content of $\Sigma K_2O,Na_2O$=7.41–14.25 wt.%, hosted in the minerals microcline, orthoclase and oligoclase.

The potential raw materials from the three studied industrial mineral deposits were evaluated for use in ceramic applications. In addition, nine non-metallic occurrences, most of them currently mined and located at Oruro (one zeolite

occurrence), Potosí (one diatomite and one montmorillonite occurrence), La Paz (three clay deposits and one diatomite occurrence) and Santa Cruz (two kaolin deposits) have been sampled. Mineralogical and lithogeochemical characterization of the materials have been performed to address higher-value applications for the deposits.

X-ray diffraction (XRD) and inductively coupled plasma mass spectrometry (ICP-MS) were used to identify the mineralogical and lithogeochemical composition of the host rocks to the deposits. Scanning electron microscopy (SEM) were performed on the kaolinite-bearing materials to characterize the microstructure in the rocks. This indicates mineral paragenesis and has therefore implications for mineral deposit formation. Physical tests on the ceramic specimens, such as drying shrinkage (Choquetanga 0.20 vol.%, La Fabulosa 0.31 vol.%), firing shrinkage (Choquetanga 1.66 vol.%, La Fabulosa 1.59 vol.%), bending strength (Choquetanga 69.55 N/mm^2, La Fabulosa 70.20 N/mm^2), water absorption (Choquetanga 2.13 vol.%, La Fabulosa 0.58 vol.%) and Mohs hardness value of 7, demonstrate the potential application of the studied industrial minerals in the production of floor tile ceramics.

The results of this work show the geological potential for industrial mineral exploitation in Bolivia. It is expected that these investigations will serve as a starting point and encouragement for future geological research and mineral exploration with important implications for the supply of industrial minerals for the growing industrial sector of Bolivia.

Acknowledgments

This study was supported by the Swedish International Development Cooperation Agency (SIDA), through the project "Non Metallic Minerals Resources for the Development of Poor Bolivian Regions", a competitive project between the San Andrés University of La Paz (UMSA) and Luleå University of Technology (LTU).

The Institute of Metallurgy and Material Science (IIMETMAT) and Institute of Geology and Environmental Research (IGEMA), both from the San Andrés University in La Paz, are acknowledged for their technical support during the development of the numerous mineralogical and technical tests, and technical support during the field trips.

Mario Blanco, my supervisor and friend, who has been my guidance during each field work in Bolivia and my mentor in the beautiful science of mineral and elemental analyses with X-Ray diffractometer and X-Ray fluorescence techniques. He has always been very helpful during this project and other ones in which we have worked together, my deepest gratitude to you.

Pär Weihed and Christina Wanhainen have been my guidance at LTU, to whom I express here my thanks and gratitude during the development of this study.

My colleagues and friends, in Sweden and Bolivia, who have provided the extra fun during this journey. I wish to thank the people who helped me with technical and administrative issues here at LTU. Thanks to Milan Vnuk, for the layout of the figures in the manuscripts, and for the compilation of the thesis. Thanks to Glenn Bark for the comments during the revision of the kappa of the thesis. Tobi Kampmann who provides his expertise, comments and has taken the time to review the kappa of the thesis and edit the figures on it.

Thanks to my family that have always supported me throughout my studies. A special thanks to my husband, who has always been there for me and his understanding and support during the long time periods that we have been away from each other.

List of Publications

I. Zeballos, A., Weihed, P., Blanco, M. and Machaca, V. 2016. *Geological, mineralogical and chemical characterization of Devonian kaolinite-bearing sediments for further applications in the ceramic (tiles) industry in La Paz, Bolivia*. Environmental Earth Sciences 75, 15 pp.

II. Zeballos, A., Machaca, V., Blanco, M. and Weihed, P.. *Pegmatite and megacrystic granite as a source of feldspar for ceramic applications in Bolivia (manuscript)*

III. Zeballos, A., Machaca, V, Blanco, M and Wanhainen C. *Application of a kaolinite-bearing sediment for industrial purposes in Bolivia (manuscript)*.

IV. Zeballos, A., Weihed, P., Blanco, M. and Machaca, V. 2017. *Characterization of some non-metallic resources in Bolivia: An overview of their potentiality and their application in specialized formulations*. Environmental Earth Sciences 76, 15 pp

The following conference proceedings and reports have been published in the course of the project, and are related to the doctoral studies:

- Machaca V., **Zeballos A**. y Blanco M. *Caracterización de Feldespatos de pegmatitas que ocurren en la Mina Fabulosa, con una perspectiva aplicativa*. Memorias XVIII Congreso Geológico Boliviano. Potosí - Bolivia, 2009, 7 pp.

- **Zeballos A**, Machaca V, Blanco M. *Caracterización Mineralógica y Físicoquímica de una lutita blanca de la localidad de Micaya*. Memorias XVIII Congreso Geológico Boliviano. Potosí - Bolivia, 2009, 5 pp.

- **Zeballos A**, Weihed P, Blanco M and Machaca V. *Geological, Mineralogical and chemical characterization of kaolinite from Micaya, La Paz- Bolivia*. IMA. Budapest - Hungria, 2010, 1 pp.

- **Zeballos A**, Weihed P, Blanco M and Machaca V. *Granitic rocks as a source of* $K_2O + Na_2O$ *for ceramic applications in Bolivia*. MECC. Miskolc - Hungary, 2012, 1 pp.

- **Zeballos A**, Weihed P, Blanco M and Machaca V. *Sintetización de Mullita a partir de arcillas caoliníferas de la región de Micaya, La Paz*. XX Congreso Geológico Boliviano. La Paz – Bolivia 2012, 5 pp.

- Blanco M, Acarapi W, **Zeballos A** and Balanza R. *Potencial industrial de los recursos diatomíticos de las localidad de Charaña y Bella Vista (Departamentos de La Paz y Potosí)* XX Congreso Geológico Boliviano. La Paz – Bolivia 2012, 6 pp.

- **Zeballos A**, Weihed P, Blanco M and Machaca V. *Mullite synthetization at low temperature*. SGA Meeting. Uppsala - Sweden, 2013, 3 pp.

- **Zeballos A**, Weihed P, Blanco M and Machaca V., 2014. *Aplicación de Materias Primas Bolivianas en Productos Cerámicos de Revestimiento*. Revista Boliviana de Geociencias 6: 47-59.

- **Zeballos A**, Weihed P, Blanco M and Machaca V., 2014. *Sintetización de Mullita a partir de arcillas caoliniferas de la Región de Micaya, La Paz*. Revista Boliviana de Geociencias 6: 61-67.

- **Zeballos A**, Blanco M, 2017. *Zeolitas Naturales en Bolivia*. Journal of the Geosciences Museum-Brazil 4: 34-39.

- **Zeballos A**, Blanco M, Weihed P, Nina L and Hidalgo C. *Caracterización mineralógica y química de zeolitas tipo clinoptilolita en el departamento de Chuquisaca, Bolivia*. XXII Congreso Geológico Boliviano. Santa Cruz – Bolivia 2016, 5 pp.

Author's contribution

Paper I: I performed the mapping, sampling and structural interpretation of the area and constructed the geological profile of the transversal section. Supervision and assistance during field work was given by Vladimir Machaca and Mario Blanco. XRD analyses, quantification by Rietveld method, and ICP-MS interpretations were carried out by me. The scanning electron microscopy was carried out by me and Johanne Mouzon. Geological and mineralogical interpretation of the formation of the kaolinite-bearing deposit was performed by me. Geophysical field work was carried out by Rodolfo Ayala (Geophysics consultant) and me, while interpretation of the geophysical data was carried out by Rodolfo Ayala. Physical tests on the ceramic specimens were carried out by me. I wrote the manuscript, which was reviewed by Pär Weihed. Additional reviews were given by Eduardo Palenque.

Paper II: Field work with mapping, sampling and structural interpretation of the area was carried out by Vladimir Machaca and me. Supervision during the field work was given by Mario Blanco. Petrographical interpretation and ICP-MS interpretations were carried out by me. Physical tests on the ceramic specimens were carried out by me and Vladimir Machaca. I wrote the manuscript, which was reviewed by Pär Weihed. Additional reviews were given by Nils Jansson.

Paper III: Physical tests on the ceramic specimens were carried out by me and Vladimir Machaca. The ramp/hold firing programme for the mullite synthesis was designed by me. Gravimetrical treatments, XRD analyses, ICP-MS interpretations and scanning electron microscopy were carried out by me. I wrote the manuscript, which was reviewed by Christina Wanhainen.

Paper IV: I sampled the different mineral deposits and performed textural studies. Supervision and assistance during the field work was given by Vladimir Machaca and Mario Blanco. The XRD analyses, ICP-MS interpretations and scanning electron microscopy were carried out by me. Quantification of the mineralogical phases was carried out by me. Geological and mineralogical interpretation of the non-metallic deposits was performed by me. I wrote the manuscript, which was reviewed by Pär Weihed.

CONTENTS

1. INTRODUCTION

1.1. Context of this thesis work – the Non-Metallic Minerals Project

This thesis work is an integral part of the national umbrella project "Non Metallic Minerals Resources for the Development of Poor Bolivian Regions (2006-2018)" (herein named "Non-Metallic Minerals Project"), which was initiated in early 2006 for the development of the Micaya village, with funding granted by the Swedish International Development Cooperation Agency (SIDA) - Universidad Mayor de San Andrés (UMSA). The Non-Metallic Minerals Project has focused on four fundamental aspects: 1) Evaluation of geological, mineralogical and elemental non-metallic resources in Bolivia, that can be used in the production and synthesis of ceramics, zeolites, among other applications, and allow the establishment of a database of exploitable and industrializable non-metallic mineral resources in Bolivia; 2) Production of materials of industrial and/or environmental interest through phase transformations of non-metallic minerals, at laboratory or bench scale, as well as the knowledge transfer about these processes to productive community units and/or productive partnerships; 3) Implementation of integrated production centres for processing of non-metallic resources to value-added products helping to improve the quality of life of Micaya's inhabitants, and 4) Development of skills and capacities for non-metallic mineral processing through specialized human resources training. This thesis comprises the results of the geological evaluation of three deposits in La Paz region and the proposal for the application of these non-metallic minerals and the study of new deposits in Bolivia.

The Micaya Village and the associated deposit have been the main target to all these studies, practices and applications of the achieved results. A comprehensive training centre was established in the village in 2012 with the Japanese International Cooperation Agency (JICA) funding, in which the project team can transfer the acquired knowledge to the population through workshops. Hence, the local people are enabled to develop businesses for the production of, for example, value-added kitchen ware and artistic pottery.

The Non-Metallic Minerals Project represents an important milestone to confront the development challenges of Bolivia, not only in the public sector, but also in the private sector and civil society organizations. Also, it is important to note that there is a fundamental objective in the Bolivian national policy to strengthen mining activities and exploitation of Bolivian natural resources (mainly regarding non-metallic minerals).

1.2. Background of the studies performed in this thesis work

There have been extensive geological studies on the metallic resources (including tin, lead, copper, gold and silver) of Bolivia. In recent years, the mining of equally widespread industrial mineral resources has increased in Bolivia, but there is a lack of geological studies, as well as geochemical and mineralogical characterization of these deposits. Knowledge about these characteristics and the potential application of the mining products would allow for a more profitable commercialization of the material.

Due to a general lack of information about the national Bolivian resources of industrial minerals, the overall raw material imports have grown by over 20% in 2016 (Cámara Nacional de Industrias, 2017). For the reason mentioned above, many Bolivian companies mostly work with imported raw materials from foreign countries (Quispe, 2014), which provide the material properly characterized (regarding mineralogy, geochemistry and physical properties). Examples are the raw materials used in the tile industry (e.g. kaolin, feldspar for flux action and mullite), which could instead be supplied from Bolivian deposits at lower prices.

This study provides detailed geological and geochemical information about three industrial mineral deposits from La Paz (Fig. 1; Micaya, Choquetanga and La Fabulosa), along with a general lithogeochemical and mineralogical characterization of nine other deposits at La Paz (four), Oruro (one), Potosí (two) and Santa Cruz (two) (Fig. 1). The results will be a basis for the establishment of geological knowledge about currently under-explored industrial mineral deposits, as well as for future investigations in the non-metallic resource sector, both in the La Paz region and in entire Bolivia.

2. GEOLOGICAL FRAMEWORK OF BOLIVIA

Based on the geography of Bolivia, Montes de Oca (1983) has divided the national territory in geological provinces. Based on varying tectonic interpretations, a modification of the units' names has been suggested by Sempere et al. (1988), even though the general geological framework is widely accepted. Later on, Suarez (2000) has redefined Bolivia into six geological provinces based on the geo-tectonic framework (Fig. 1). Each province (from west to east: Western Cordillera, Altiplano Basin, Eastern Cordillera, Subandean Belt, Chaco-Beni Plain and Precambrian Shield) has unique geological characteristics. The provinces Western Cordillera, Altiplano Basin, Eastern Cordillera and Subandean Belt make up the Mesozoic–Cenozoic Andean orogeny in Bolivia (Arce, 2002; Arce, 2007).

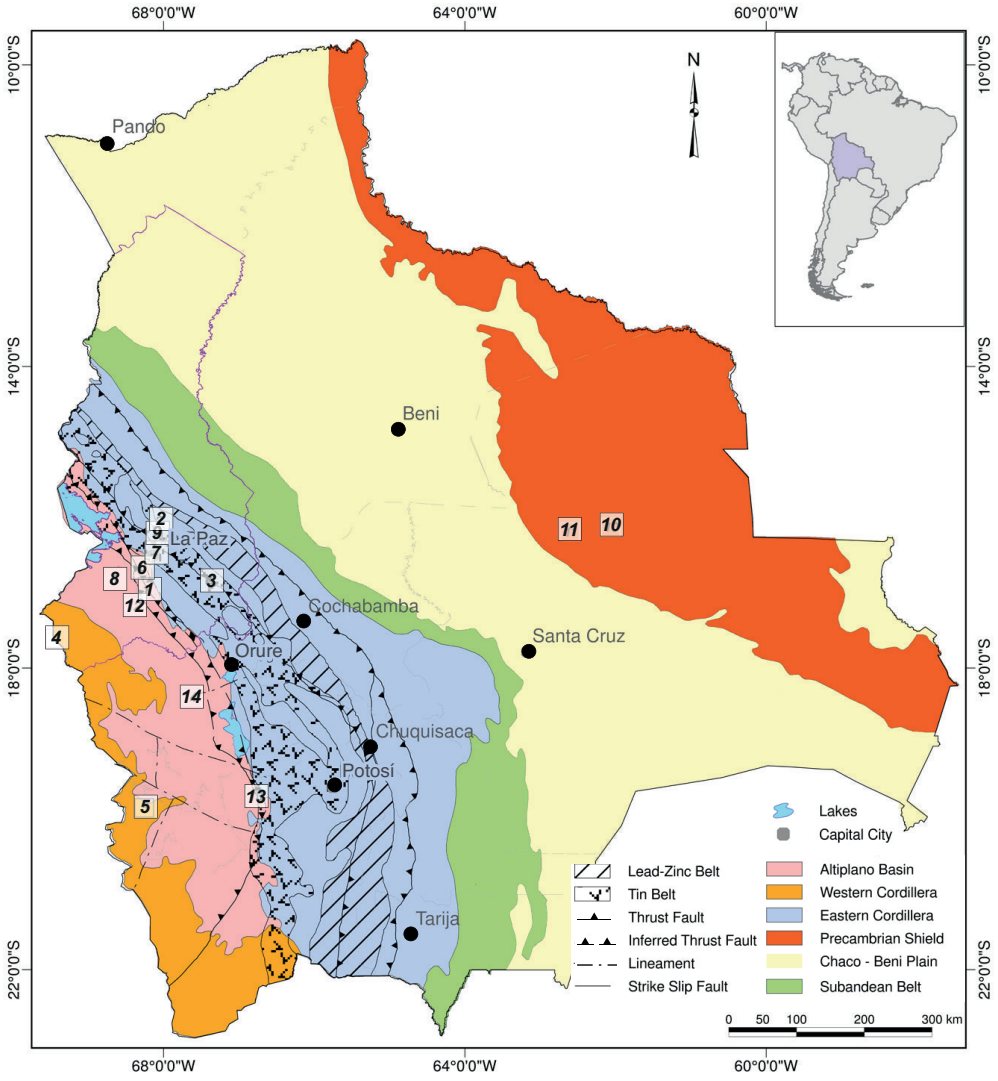

Figure 1: Geological provinces of Bolivia: Western Cordillera, Altiplano Basin, Eastern Cordillera, Subandean Belt, Chaco-Beni Plain and Precambrian Shield. Located in the figure are the studied non-metallic deposits: **1)** Micaya kaolinite deposit in La Paz region; **2)** Choquetanga feldspar deposit in La Paz region; **3)** La Fabulosa feldspar deposit in La Paz region; **4)** Charaña diatomaceous earth deposit in La Paz region; **5)** Murmutani diatomaceous earth deposit in Potosí; **6)** Viacha illite deposit in La Paz; **7)** Llojeta illite clay deposit in La Paz, **8)** The Quimsa Chata kaolin occurence in La Paz; **9)** The Zongo refractory minerals occurence in La Paz; **10)** The La Bella kaolin deposit in Santa Cruz; **11)** Benton kaolin deposit in Santa Cruz ; **12)**Villa Putuni montmorillonite deposit in La Paz; **13)** The Río Mulatos montmorillonite deposit in Potosí; and **14)** The Corque zeolite deposit in Oruro.

The Western Cordillera (Fig. 1) comprises mountain peaks with the highest altitudes in Bolivia and consists of volcanic deposits of Miocene to recent age (Kussmaul et al., 1975). The partly active volcanoes are aligned and younging from north to south from Miocene to recent in age (<0.011 Ma; Castaños and Rodrigo, 1978). The lava and pyroclastic deposits from these volcanoes extend over the Altiplano basin and fill large depressions in the terrain. The eruptive centres are near the border with Chile and Peru.

The Altiplano basin (Fig. 1) is a series of extensive interandean foreland basins, controlled tectonically by complex lateral horst and graben structures (Aranibar, 1984). These basins received sediments from convergent fold and thrust belts. The region represents an extensive flat plain that is interrupted by isolated mountain chains and was formed during the Cenozoic (Suarez, 2000).

Rock units in the Altiplano basin comprise a strongly folded Palaeozoic basement and a cover of sedimentary and volcanic rocks of Cretaceous to Cenozoic age (Kussmaul et al., 1975). Subsurface data suggest prolonged periods of crustal shortening and a model of thin-skinned tectonics including the development of fold and thrust belts, fault zones, and intermountain foreland basins (Sempere et al., 1990). Crustal shortening along the Altiplano basin commenced in the late Oligocene and terminated in the middle Miocene (Sempere et al., 1990). Basin fill was dominated by erosion of the Western Cordillera during late Eocene–Oligocene, but Neogene shortening in the Eastern Cordillera and Subandean Belt provinces led to a subsequent dominance of younger sediments derived from the east (Fig. 1; Horton et al., 2002) and deformed under a compressional regime during the Miocene (Sempere et al., 1990). At 9–10 Ma the uplift of the Eastern Cordillera accelerated (Benjamin et al., 1987; Marshall et al., 1993), causing a strong dissection of its western slope and the edge of the Altiplano basin (Hérail et al., 1993). At the same time, the faults in the central and western part of the basin were reactivated by compressional tectonics, which resulted in crustal shortening and thickening of the Altiplano basin, as well as tectonic uplift (Marshall et al., 1993).

The Eastern Cordillera (Fig. 1), extending from Peru in the north-west to Argentina in the south, is a well-studied and significant province regarding metallic mineralization. It is limited to the west by the Coniri and San Vicente faults, which separate it from the Altiplano basin, and to the east by a long front thrust fault, which forms the boundary to the Subandean Belt (Suarez , 2000; Fig. 1). The Eastern Cordillera includes polyphase deformed Ordovician to recently sedimented shale, siltstone, limestone, sandstone, slate and quartzite sequences (Suarez, 2000; Arce and Goldfarb, 2009). Following Permian to Jurassic rifting, these sedimentary rocks were uplifted during Andean compression, which may

have commenced in Late Cretaceous (McQuarrie et al., 2005). Thin Cretaceous fluvio-lacustrine and possibly marine deposits overlie folded and faulted Palaeozoic rocks with a pronounced angular unconformity, and are generally only exposed in isolated synclinal cores (Kennan et al., 1995). These mainly Palaeozoic clastic and metamorphic rocks represent folded flysch basin sediments that were deposited along the ancient Gondwana margin and later deformed during the middle to late Palaeozoic (Kennan et al., 1995; Jacobshagen et al., 2002; Arce and Goldfarb, 2009). According to geochronological studies (Jacobshagen et al., 2002), metamorphism and deformation of the basement occurred as a result of the Hercynian orogeny of late Carboniferous to early Permian age (Evernden et al., 1977; McBride et al., 1983; Avila, 1994; Lamb and Hoke, 1997; Gillis et al., 2006).

Compositions of the granitic rocks in the Eastern Cordillera range from granitic, syeno-granitic, monzogranitic, granodioritic, and tonalitic (Sugaki et al., 1988; Avila, 1990; Farrar et al., 1990). The magmatism in the Eastern Cordillera evolved in two stages. The first stage developed in the north and took place during the Triassic to early Jurassic (225 to 195.4 Ma; McBride et al., 1983). The second stage of magmatism commenced during the Palaeocene–Eocene and include volcanic and intrusive, rhyolitic flows (McBride et al., 1983; Argandoña and Vargas, 2004), as well as granodiorites (Schneider and Halls, 1985). K-Ar ages of southern plutons in the Eastern Cordillera range between 28.4 and 23.6 Ma and confirm a Cenozoic Age (McBride et al., 1983).

The Eastern Cordillera hosts many important metallic resources. The Bolivian tin belt extends for approximately 900 km in a NW–SE to N–S trending direction along this cordillera (Fig. 1; Arce and Goldfarb, 2009), where the continental crust is thickest (~150 km; Lamb et al., 1997).

The Subandean Belt (Fig. 1) constitutes a complex system of narrow longitudinal ranges, separated by wide syncline valleys. Tectonically, it represents a complex fold and thrust belt, separated from the Eastern Cordillera by a NW/N-S trending thrust fault (Fig. 1), which forms an important structure related to the formation of oil traps (Castaños and Rodrigo, 1978; Suarez, 2000). Not fully economically developed metallic and non-metallic mineral resources include alluvial gold beds formed by the erosion of Upper Miocene to Pliocene conglomerates (Herail et al., 1991). Local alluvial diamond occurrences have also been reported (Oppenheim, 1943).

The Chaco-Beni Plain is characterized by semi-consolidated sediments from alluvial plains, that overlie the Precambrian Shield basement and tertiary sediments (Harrington, 1968). The industrial mineral exploitation is limited to sediments used for aggregates in the construction industry (Suarez, 2000).

The Precambrian Shield (Fig. 1) comprises granitic and metamorphic rocks (Russo, 1966). The geological history of the Bolivian Precambrian Shield begins ~2000 Ma (Litherland et al., 1989) which is reflected by a complex interplay of igneous and tectonothermal events. The mineral resources in the area include schist-hosted orogenic gold (Arce and Goldfarb, 2009) and manganese veins to the north (Russo, 1966), as well as kaolin resources derived from hydrothermal alteration of granitic rocks with columbite-tantalite occurrences (Paper IV). East of the Precambrian Shield, beryllium-rich pegmatite dykes intrude the metasedimentary sequence (Arduz and Buitrago, 1992). North-east of Santa Cruz city (Fig. 1), cassiterite alluvial deposits occur in the same suite of pegmatites (Suarez, 2000). South-east of this city, magnetite-cupriferous gabbro bands containing bornite and chalcocite have been reported, as well as secondary concentrations of nickel formed through Tertiary erosion cycles (Suarez, 2000) overlying the ultramafic rocks in the area (Arduz and Buitrago, 1992).

3. LOCAL GEOLOGICAL FRAMEWORK OF THE LA PAZ REGION

The La Paz region is located at the boundary between the Altiplano basin and the Eastern Cordillera in the south and with the Subandean Belt in the north (Fig. 1). It is composed of a variety of Palaeozoic to Cenozoic rocks, which are prospective for metal deposits including silver, lead, zinc, gold and tin, but also for non-metallic minerals formed by hydrothermal alteration, lacustrine sedimentary accumulations and weathering.

The Palaeozoic rocks were deformed by intense tectonic activity from the beginning of the Andean orogeny, until the formation of the Andean mountain chain during the Mesozoic (Suarez, 2000). These rocks were folded and faulted, with tectonic blocks thrusted to the east (Sempere et al., 1990). The tectonically formed lineaments and escarpments have acted as major pathways for fluvial and glacial processes (Suarez, 2000).

Three deposits have been the main focus of this doctoral project: the Micaya kaolinite-bearing deposit is located 50 km south-west, the La Fabulosa feldspar deposit 48 km north and the Choquetanga feldspar deposit 94 km south-east of La Paz city (Fig. 1).

The Micaya deposit (Fig. 2), comprises two kaolinite-bearing occurrences hosted in sedimentary rocks. The deposit has been mined for some years by the local population for raw materials to produce tableware. However, detailed geological mapping and sampling have only been carried out in 2006, in the course of this doctoral project.

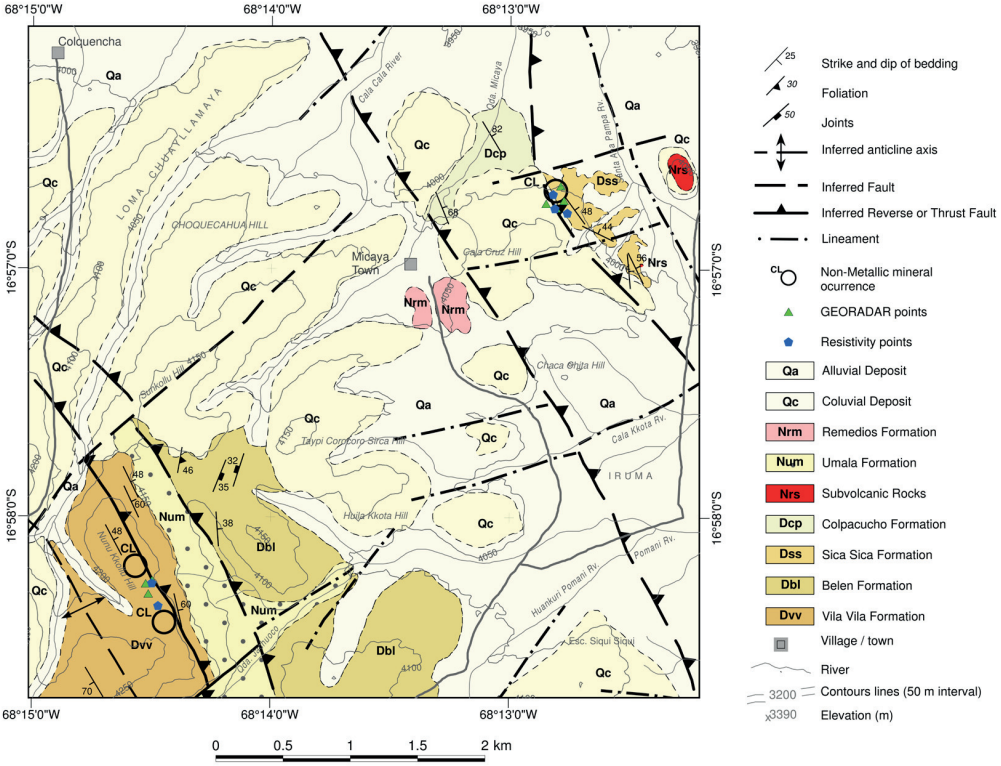

Figure 2: Geological map of Micaya (modified from the Calamarca Geological Sheet, N°5943, Esc 1:100000)

The Choquetanga feldspar deposit is hosted in feldspar-phyric granite of the Quimsa Cruz batholith (Fig. 3). The La Fabulosa feldspar deposit is located at 4400 m.a.s.l in the Sorata Triassic batholith (Fig. 4), which is surrounded by a metamorphosed sedimentary sequence of Palaeozoic age (GEOBOL, 1995). Close to the contact between the intrusive rocks and the sedimentary sequence, contact-metamorphic rocks such as meta-sandstones, schists and slates occur. In the Sorata batholith, Sn-W mineralization is hosted in irregular pegmatite dykes and sills (GEOBOL, 1982), both of which intruded the granites and the sedimentary sequence (Fig. 4).

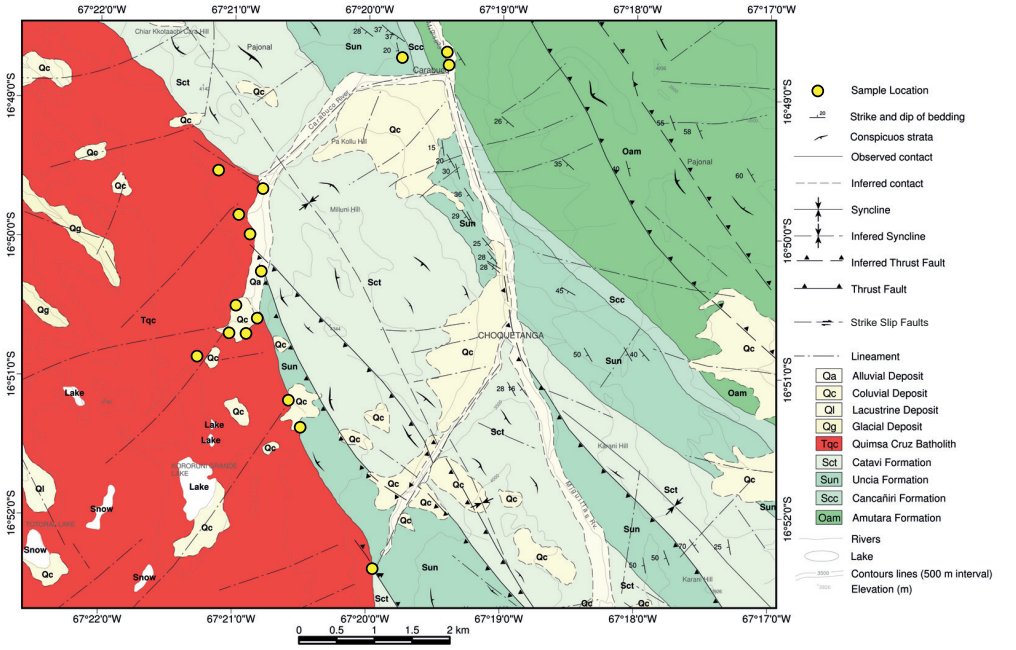

Figure 3: Geological map of Choquetanga (modified from the Inquisivi Geological Sheet, N°6143, Esc 1:100000)

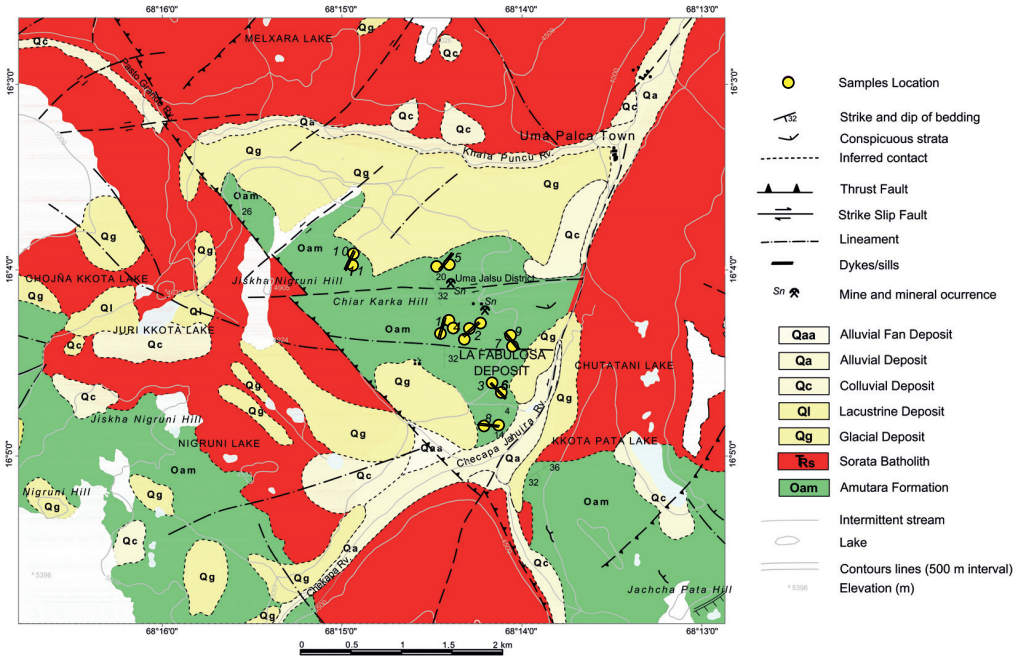

Figure 4: Geological map of La Fabulosa (modified from the Milluni Geological Sheet, N°5945, Esc 1:100000)

3.1. Industrial mineral deposits of the southern La Paz region

The La Paz region hosts several industrial mineral deposits (kaolinite, feldspar and refractory minerals) that have intermittently been mined by the small-scale mining industry. Although these deposits show promising potential, they have not been studied in detail and the materials remain uncharacterized. A proper characterization is essential for an economic evaluation of the deposits. The literature (Avila, 1989; Escobar et al., 1999; Rivas, 2002) indicates several industrial mineral deposits in the La Paz region, but only two have been studied previously and are related to this study: a kaolin deposit hosted by the Quimsa Chata dacite (Fig. 1) and a refractory mineral deposit, with andalusite and cordierite hosted by the Zongo batholith (Fig. 1).

3.1.1. Previously reported kaolin occurrences

The Quimsa Chata kaolin occurrence is located 56 km south-west of La Paz city (Fig. 1) and has been studied and open-pit mined for metallic ores. In the Quimsa Chata district, Pb-Au-Ag mineralization occurs in polymetallic veins as a product of the argillic alteration of the sandstones of the Miocene Tiwanaku formation, caused by the intrusion of the Quimsa Chata dacite (Orris et al., 1975). Escobar et al. (1999) studied the mineral alteration of the Quimsa Chata dacite for its kaolin content. Although promising geochemical assay data has been acquired, this kaolin deposit has never been actively mined.

3.1.2. Previously reported refractory mineral occurrences

North of La Paz city (Fig. 1), some andalusite mineral occurrences have been discovered. The andalusite formed during the Triassic through contact metamorphism caused by the cooling of regional batholiths (Farrar et al., 1990). The mineralization is hosted in sedimentary units in the form of andalusite crystals of up to 5 cm in length, and it constitutes 10 % of the total volume of the rock (Escobar et al., 1999). Cordierite has also been observed in this contact-metamorphic aureole (Arduz, 1976). Low grade metamorphism (greenschist facies) formed spherical cordierite globules, rich in inclusions of quartz, muscovite, biotite and graphite (Arduz, 1976; Escobar et al., 1999). Amphibolite metamorphism facies formed euhedral prismatic cordierite crystals (Arduz, 1976; Escobar et al., 1999). In other igneous units, staurolite has been observed (Escobar et al., 1999).

4. METHODS

4.1. Field work

In the three main study areas (Micaya, Choquetanga, La Fabulosa), selected outcrops were studied for geological characterization, and sampled (20 samples from the kaolinite occurrences (10 from each occurrence), 25 from the Choquetanga deposit and 25 from the La Fabulosa deposit) (Figs. 1, 5a and 5b) to determine rock type, mineralogy, lithogeochemistry and petrography.

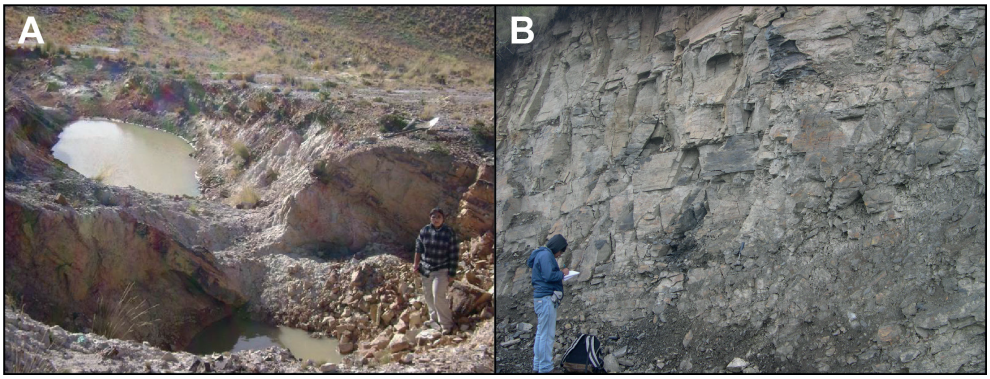

Figure 5: A) Photograph of the south-western occurrence in the Micaya deposit during field work; and B) Photograph of geological mapping work at the La Fabulosa deposit.

4.2. Mineralogical characterization

Optical microscopy

Petrographic analysis was performed on the kaolinite-bearing sediments, granite and pegmatite hand samples and 21 thin sections were made from the igneous rocks and from the kaolinite-bearing sediment. Thin sections were studied in an optical microscope with transmitted light, in order to define the mineralogy of the sampled rocks, as well as the composition and compositional variety of the feldspars (alkali source for ceramic tiles) and textural relationships in the kaolinite-bearing samples.

Scanning Electron Microscopy

Scanning electron microscopy (SEM) was performed on 50 samples. Microstructures in the samples were investigated, using an FEI Magellan 400 XHR (Extreme High Resolution) SEM fitted with an energy dispersive X-Ray spectrometer (EDX, X-MAX 80 mm2, Oxford instruments). An accelerating voltage of 1 kV and a current of 6.3 pA was used for high resolution imaging. The samples were power dispersed and dried in chloroform.

X-ray Diffraction

The mineralogical characterization (70 samples) of the raw material from the studied deposits (five deposits in La Paz, one deposit in Oruro, two deposits in Potosí and two deposits in Santa Cruz) and the ceramic slabs, was performed using a PANalytical Empyrean X-ray Diffractometer (XRD) equipped with a Cu LFF HR X-ray tube, a graphite monochromator and a PIXcel3D detector at Luleå University of Technology (LTU), Sweden. The diffractometer was operated at 30 mA and 40 kV. The scanning region of the diffraction angle 2 h was from 5° to 50° with a 0.026°/250s. At the IGEMA laboratory, La Paz, a X'Pert3 PANalytical instrument operating with Cu Kα radiation and time step increments of 0.010°/s, was used. Quantitative phase analyses of the kaolinite-bearing sediments were performed using XRD data and Rietveld refinements (Rietveld, 1967). The refinement was performed using the X'Pert High Score plus software.

Thermal analysis

Differential thermal analysis and thermo–gravimetric analyses were performed to understand the mineral transformation and the firing behaviour of the ceramic mixtures at high temperature. Six thermal analyses were carried out using a Netzsch STA 409C (simultaneous thermal analysis) equipment coupled with a mass spectrometer (MS) gas analysis system connected to the heated furnace outlet with a rotary pump. The sample carrier is located at the top of an analytical balance, in a vacuum tight casing. The high-temperature furnace is heated by tubular SiC heating elements and operates at temperatures from 25°C to 1550°C with possible heating rates between 0.1 and 50°C/min.

4.3. Lithogeochemistry

The samples for whole rock-analysis were prepared at the Institute of Geology and Environment at the Universidad Mayor de San Andrés, Bolivia. One hundred samples from the 12 studied deposits were analysed for major oxide and trace elements (igneous rocks). The analysis of the whole-rock samples was performed at ALS Scandinavia AB Laboratory, Luleå, Sweden using lithium borate fusion and inductively coupled plasma mass spectrometry (ICP-MS). Loss on ignition (LOI) was determined gravimetrically by heating powders up to 1000°C for one hour. Detection limits for major oxides are at 0.01 wt.%. The calculation of the normalized minerals from the igneous rocks was performed with the Niggli's Molecular Norm, using the algorithm given by Hutchison (1974) in the GCDkit software for geochemical data interpretations.

4.4. Technical quality test for floor tile application

To test the technical quality of the feldspar material for production of floor tile and to study the enhancement of the quality of the products, five physical parameters were determined in the ceramic specimens: Drying shrinkage, firing shrinkage, bending strength, water absorption and Mohs hardness value (Table 3). The ceramic slabs were tested according to national (Instituto Boliviano de Normalización y Calidad, 2014) and international standard methods (NB/ISO 10545-3:1995, NB/ISO 10545-4:2004) for ceramic tile products. The raw material was mixed and humidified (8.25 wt.% moisture content), immediately pressed into bars (18 MPa; size 8.025 mm x 29.5 mm x 6.20 mm). Measurements were taken at 24 h and 48 h and then subjected to firing at 1250°C in an electrical kiln.

4.5. Geoelectric and electromagnetic geophysical test in the Micaya deposit

Geophysical tests were performed using electrical resistivity tomography (ERT) and ground-penetrating georadar (GPR). Both methods were used for a basic estimation of the spatial relationship of the kaolinite-bearing layers within the host rocks. Five lines were established using a resistivity instrument, OYO Model geo-receptor JP-600. It has a sensitivity of 0.01 mV and digital recording capability. The unit operates at 2.5 A, and has a variable voltage of up to 1000 V. It operates using a 12 V battery and has four cable spools (100 m each) and 30 copper electrodes with a linear array of 10 m. The GPR studies were carried out in seven lines using a GEORADAR ZOND-12E instrument equipped with a 75 MHz monostatic antenna applying time windows of 120 ns, with 40 scans/s, and 512 samples per scan.

5. SUMMARY OF RESULTS

5.1. Geological and mineralogical character of the kaolinite-bearing sediments from the Micaya deposit

The kaolinite-bearing deposit in Micaya was first studied in detail during this thesis work. Even though geological mapping was performed in the area approximately 25 years ago, no references about the mineral occurrence have been found. The Micaya deposit is situated in a Devonian sedimentary sequence and contains two kaolinite-bearing occurrences (Fig. 2). The south-western occurrence is composed of sedimentary rocks of the Vila Vila Formation (Fig. 2), which comprises quartz sandstones and muscovite-rich limolites, whereas in the north-western occurrence the kaolinite-bearing sediments occur in the Sica Sica Formation, which is composed of muscovite-rich limolites interbedded with thin layers of sandstone (Fig. 2). Petrographical studies of the kaolinite-bearing sediment show

a homogeneous texture in the samples. Brown microcrystal agglomerations are recognized as clay mineral under plane-polarized light (Fig. 6a). Subhedral quartz and muscovite crystals are identified under cross-polarized light (Fig. 6b).

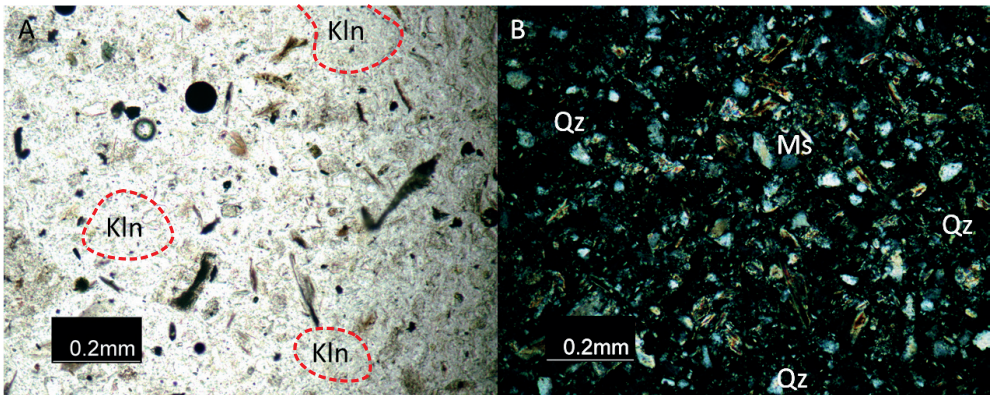

Figure 6: Images of the kaolinite-bearing sediment: **A)** Kaolinite crystal agglomerations are visible (plane-polarized light); **B)** Quartz and muscovite crystals are visible (cross-polarized light).

XRD analysis suggests the presence of three mineralogical phases from the north-east occurrence (Fig. 7a). It is composed of 50.8 vol.% quartz (3.36 Å), 35.4 vol.% muscovite (9.90 Å), and 13.8 vol.% kaolinite (7.12 Å) (Paper I). The rock from the south-western occurrence comprises four mineralogical phases: 56.3 vol.% quartz (3.36 Å), 12.2 vol.% muscovite (9.90 Å), 24.9 vol.% kaolinite (7.12 Å) and 6.7 vol.% feldspar (3.23 Å) (Paper I). The XRD pattern of the north-eastern and south-western materials (Fig. 7b) indicates high crystallinity for the quartz phase and poor crystallinity of the muscovite and kaolinite phases, corroborated with the microstructural images in which muscovite stacks (Fig. 8a) and irregular kaolinite plates (Fig. 8b) were identified**.**

Electrical resistivity tomography and ground penetrating radar data suggest 20 m of thickness for the kaolinite-bearing layer at the south-western deposit and 10 m thickness for the kaolinite-bearing layer at the north-eastern deposit in the Micaya area (Fig. 2).

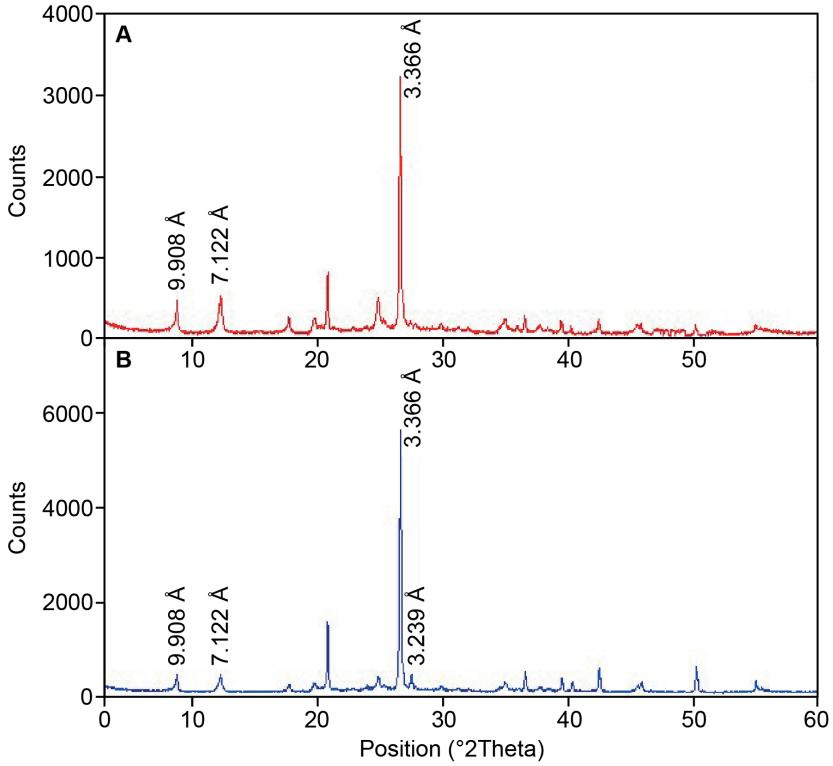

Figure 7: A) XRD pattern of the north-eastern kaolinite-bearing occurrence (Sica Sica unit). Quartz (3.36 Å), muscovite (9.90 Å) and kaolinite (7.12 Å) peaks were identified; **B)** XRD pattern of the south-western kaolinite-bearing occurrence (Vila Vila unit). Quartz (3.36 Å), muscovite (9.90 Å), kaolinite (7.12 Å) and feldspar (3.23 Å) peaks were identified.

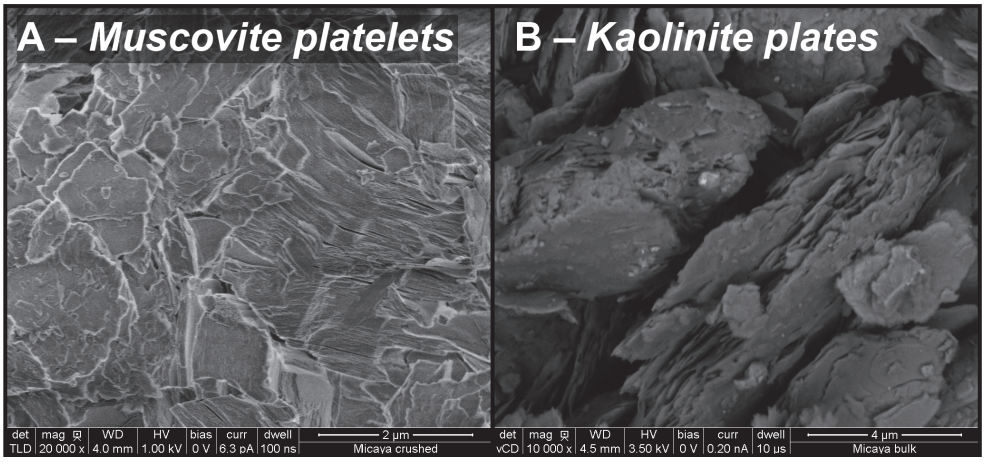

Figure 8: SEM images of the south-western kaolinite-bearing sediments from the Micaya deposit. **A)** Muscovite platelets **B)** Irregular edges in kaolinite plates.

5.2. Geological and lithogeochemical character of the Choquetanga and La Fabulosa deposits

The Quimsa Cruz batholith, in which the Choquetanga deposit is hosted (Fig. 3), intruded an Ordovician and Silurian sedimentary sequence west of the Eastern Cordillera (Fig. 1). The Ordovician Amutara Formation is composed of quartzite and dark shales, whereas the Silurian sequence trends from stratigraphically lowest diamictite (Cancañiri Formation) to shales (Uncia Formation) and stratigraphically highest quartzite and shales (Catavi Formation; Fig. 3). In the Quimsa Cruz batholith, potash feldspar is the most dominant mineral. It is represented by oriented orthoclase megacrysts (Fig. 9a) under microscope perthite texture is observed (Fig. 9b). The feldspar megacrysts occur in a granitic matrix, composed of euhedral biotite and plagioclase crystals (An; Fig 9c), as well as rounded quartz (Fig. 9d). The rock classification (modal mineralogy) as granite and quartz monzonite has been confirmed by the geochemical data (Fig. 10, Table 1; Middlemost, 1994). Modal analysis shows an average feldspar content of 62.53 % (orthoclase, albite and oligoclase), leading to a considerable alkali content in the rock (7.84–10.25 wt.%; Paper II) by arithmetic mean.

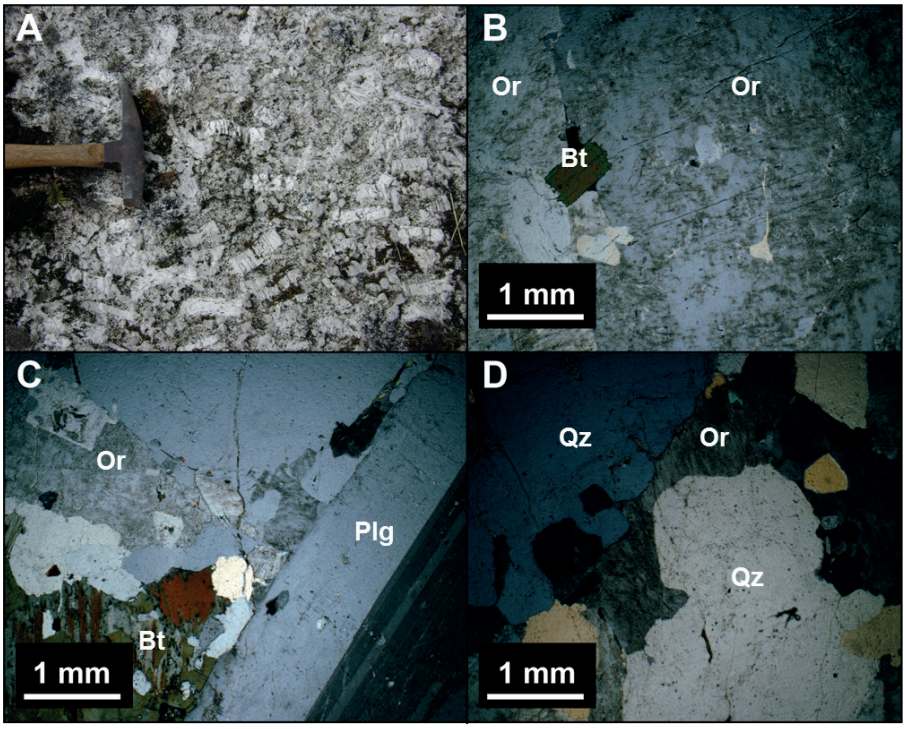

Figure 9: Images showing the Choquetanga deposit mineralogy. **A)** Oriented feldspar megacrysts of the Choquetanga deposit; **B)** Perthite texture in orthoclase, biotite is also observed; **C)** Twinned plagioclase, orthoclase and biotite crystals in the groundmass; and **D)** Rounded quartz crystals and orthoclase crystals in the groundmass.

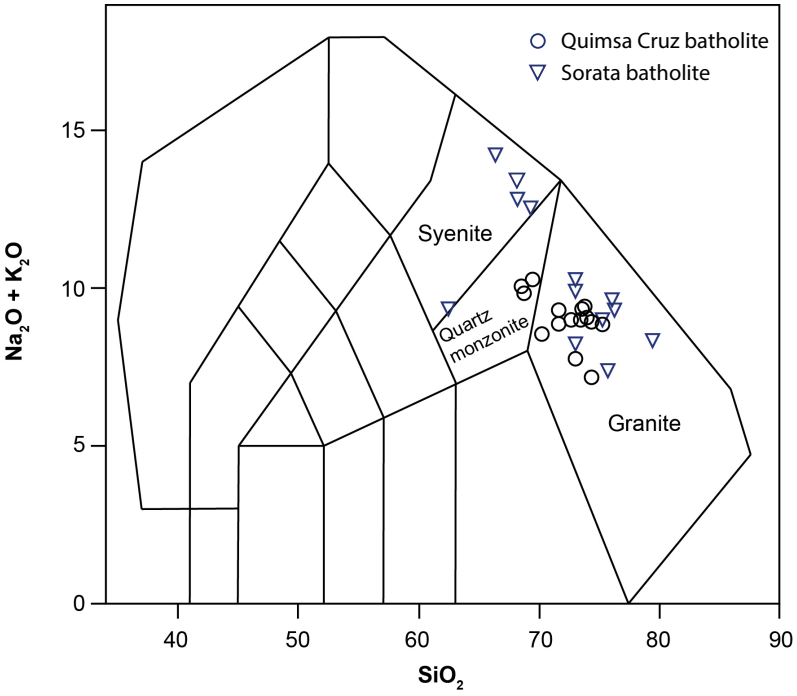

Figure 10: TAS (Total Alkali Silica) classification of igneous rocks from the Quimsa Cruz batholith and Sorata batholith samples (According to Middlemost, 1994).

The La Fabulosa deposit (Fig. 1) is hosted in granitic rocks of the Sorata batholith (Fig. 4). The Sorata batholith comprises granite and pegmatite dykes (Fig. 11a) that intruded Ordovician dark slates (Amutara formation). The rocks have a granite and syenite composition according to the Total Alkali Silica (TAS) diagram (Fig. 10, Table 2; Middlemost, 1994) and cross-cut the sedimentary rocks (Fig. 4). The pegmatites contain orthoclase-perthite crystals (Fig. 11b) with tourmaline inclusions (Fig. 11c), as well as well-developed quartz, muscovite and plagioclase (Fig. 11d). Modal analysis indicates feldspar (Fig. 11b) as the main mineral group in the pegmatite (65.73 %) with an alkali content of 7.41–14.25 wt.% (Paper II).

Table 1: Lithogeochemical and CIPW normative mineralogical composition of granite samples from the Quimsa Cruz batholith (Hutchison, 1974).

Chemistry (wt.%)															
	CHT-1	CHT-2	CHT-3	CHT-4	CHT-5	CHT-6	CHT-7	CHT-8	CHT-9	CHT-10	CHT-11	CHT-12	CHT-13	CHT-14	CHT-15
SiO_2	74.40	70.90	73.50	69.20	68.60	71.30	74.00	74.00	70.30	69.80	72.90	73.00	68.00	73.43	74.18
Al_2O_3	14.40	15.30	13.40	15.90	16.20	15.10	14.30	14.46	15.50	16.05	14.20	15.20	15.92	14.30	13.34
CaO	0.52	1.61	1.17	1.07	1.12	1.01	0.92	0.92	1.01	1.21	0.88	0.58	1.79	1.34	0.89
Fe_2O_3	1.70	3.51	3.50	2.28	3.33	1.29	0.95	0.95	1.32	1.19	1.24	1.25	1.75	1.63	1.06
K_2O	6.57	4.95	4.78	6.75	6.55	5.13	5.60	5.90	5.43	5.14	5.63	5.33	5.40	4.13	4.98
MgO	0.21	0.47	0.52	0.36	0.46	0.22	0.17	0.47	0.52	0.21	0.30	0.20	0.71	0.53	0.19
MnO	0.04	0.06	0.06	0.04	0.05	0.04	0.04	0.03	0.04	0.05	0.04	0.04	0.11	0.06	0.05
Na_2O	2.94	3.65	3.06	3.5	3.53	3.69	3.29	3.18	3.71	3.49	3.65	3.64	4.35	3.99	3.77
P_2O_5	0.15	0.21	0.26	0.18	0.22	0.18	0.16	0.17	0.18	0.20	0.18	0.18	0.48	0.11	0.06
TiO_2	0.09	0.33	0.37	0.26	0.30	0.30	0.09	0.09	0.12	0.14	0.11	0.11	0.70	0.25	0.14
LOI	0.50	0.40	0.30	0.50	0.30	1.10	0.90	0.84	1.10	1.30	0.9	1.00	0.85	0.29	1.56
Total	101.00	101.00	100.60	99.60	100.40	98.10	99.50	101.01	99.22	98.78	100.03	100.53	100.06	100.26	100.2
K_2O+Na_2O	9.51	8.60	7.84	10.25	8.66	8.82	8.89	9.08	9.14	8.63	9.28	8.97	9.75	8.12	8.75
Normative mineral composition (%)															
Qz	30.83	26.93	34.66	20.80	20.48	28.79	31.79	30.69	26.00	28.21	28.55	30.55	18.65	35.33	31.60
Co	1.84	1.51	1.68	1.34	1.80	2.12	1.53	1.57	2.15	3.10	0.94	2.83	0.82	2.20	0.28
Or	38.43	28.96	28.07	40.07	38.56	30.91	33.25	34.81	32.70	31.16	33.56	31.65	32.17	18.73	29.83
Ab	24.62	30.58	25.73	29.75	29.76	31.83	27.97	26.86	31.99	30.30	31.16	30.95	37.10	34.18	32.33
An	1.59	6.50	4.07	4.11	4.06	3.88	3.58	3.45	3.91	4.82	3.22	1.71	5.79	6.00	4.08
Mt	0.00	0.00	0.00	0.00	0.00	0.00	0.00	0.00	0.00	0.00	0.00	0.00	0.00	0.00	0.00
Hy	0.52	1.15	1.29	0.91	1.15	0.56	0.43	1.17	1.32	0.54	0.75	0.50	1.78	1.34	0.48
Il	0.09	0.13	0.13	0.10	0.12	0.09	0.08	0.06	0.09	0.11	0.09	0.09	0.24	0.13	0.11
Hm	1.68	3.48	3.48	2.29	3.32	1.32	0.96	0.95	1.35	1.22	1.25	1.26	1.76	1.65	1.07
Ru	0.05	0.26	0.31	0.21	0.25	0.08	0.05	0.06	0.08	0.09	0.07	0.07	0.58	0.19	0.09
Ap	0.35	0.51	0.62	0.45	0.54	0.45	0.38	0.40	0.43	0.49	0.43	0.43	1.15	0.26	0.14
Total	100.02	100.02	100.02	100.02	100.02	100.02	100.02	100.02	100.02	100.02	100.02	100.02	100.04	100.02	100.01
Total feldspar	64.64	66.04	57.87	73.92	72.38	66.61	64.80	65.12	68.60	66.27	67.94	64.30	75.06	58.91	66.24

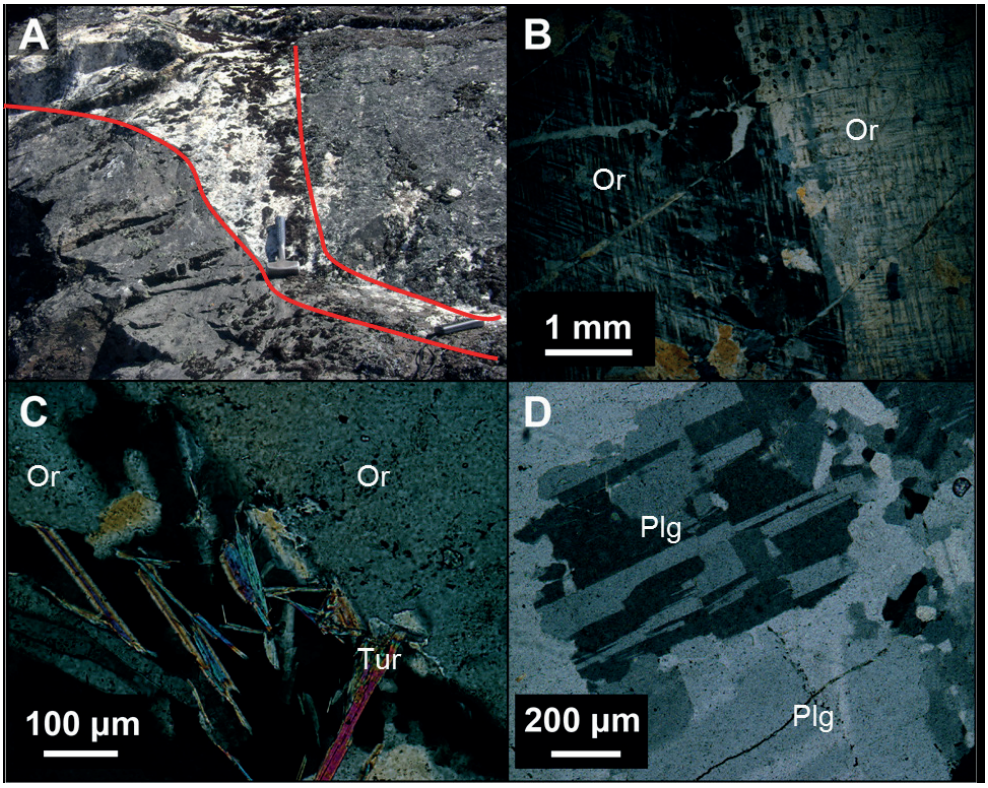

Figure 11: Images showing the La Fabulosa deposit mineralogy. **A)** Pegmatite dyke from the La Fabulosa deposit; **B)** Perthite texture in orthoclase crystals from the granite rock samples; **C)** Acicular tourmaline crystals and orthoclase crystals in the pegmatite rock samples; and **D)** Plagioclase crystals in the pegmatite rock samples.

In the AFM diagram (Fig. 12a) all the samples from the Sorata and Quimsa Cruz batholiths occupy the calc-alkaline affinity field. The SiO_2-K_2O diagram suggests a high-K, calc–alkaline character for the Quimsa Cruz and Sorata batholith samples (Fig. 12b). In the magmatic affinity diagram, the Quimsa Cruz and Sorata batholith samples are distributed between the alkaline and the highly-fractionated, calc-alkaline fields (Fig. 12c). In the aluminous character diagram (Fig. 12d), the Sorata batholith samples plot in the two-mica field, mostly as associated with muscovite. The Quimsa Cruz batholith samples plot in the II, III and IV fields, indicating association with biotite and pyroxenes (Figs. 12b and 12d).

Table 2: Lithogeochemical and CIPW normative mineralogical composition of granite samples from the Sorata batholith (Hutchison, 1974).

Chemistry (wt.%)															
	FAB-1	FAB-2	FAB-3	FAB-4	FAB-5	FAB-6	FAB-7	FAB-8	FAB-9	FAB-10	FAB-11	FAB-12	FAB-13	FAB-14	FAB-15
SiO_2	72.80	61.50	73.50	72.00	83.00	70.10	66.00	76.80	68.10	78.70	76.50	75.30	75.60	73.60	76.01
Al_2O_3	17.40	16.50	15.20	16.10	10.50	16.70	17.70	13.30	17.60	11.60	13.60	14.40	14.30	15.50	13.50
CaO	0.18	0.32	<0.10	0.28	0.29	0.18	<0.10	0.18	0.18	<0.90	<0.90	0.20	0.55	0.26	<0.90
Fe_2O_3	0.93	9.94	1.15	0.87	1.27	1.05	0.75	0.60	0.64	0.18	0.51	0.68	1.21	0.62	0.50
K_2O	2.85	7.54	5.13	7.89	1.15	10.80	12.30	7.58	10.30	6.47	6.90	6.23	4.90	7.01	6.90
MgO	<0.02	0.40	<0.02	0.04	0.07	0.02	<0.02	0.03	0.03	<0.20	<0.20	0.04	0.18	0.03	<0.20
MnO	0.04	0.10	0.24	0.03	0.04	0.02	0.01	0.02	0.02	<0.04	0.04	0.07	0.21	0.04	0.04
Na_2O	5.45	1.76	4.98	3.24	4.22	2.00	1.95	2.24	2.62	1.88	2.48	2.84	2.51	3.38	2.45
P_2O_5	0.21	0.25	0.62	0.34	0.16	0.38	0.83	0.26	0.38	0.26	0.34	0.27	0.25	0.34	0.33
TiO_2	0.01	0.08	0.00	0.00	0.02	0.00	0.00	0.01	0.01	<0.02	<0.02	0.02	0.14	0.01	<0.02
LOI	1.10	0.80	0.30	0.40	0.30	0.30	0.30	0.30	0.40	0.50	0.60	0.70	1.20	0.50	0.7
Total	99.90	98.40	100.8	100.8	100.7	101.3	98.90	101.1	99.90	99.10	100.4	100.1	99.20	100.80	99.80
K_2O+Na_2O	8.30	9.30	10.11	11.13	5.37	12.8	14.25	9.82	12.98	8.35	9.38	9.07	7.41	10.39	9.35
Normative mineral composition (%)															
Qz	30.76	31.93	26.00	22.50	48.15	9.19	14.07	31.10	24.66	36.36	26.85	35.83	36.83	30.39	34.47
Co	5.31	4.84	1.42	2.22	2.40	1.86	1.10	1.47	1.87	0.71	1.55	2.94	4.84	2.22	1.15
Or	16.73	39.61	29.54	46.40	7.51	68.89	67.91	46.56	53.03	42.25	45.37	36.26	31.36	39.12	40.69
Ab	45.81	13.24	41.06	27.28	39.45	18.27	15.42	19.70	19.32	17.58	23.35	23.66	23.00	27.01	20.69
An	0.00	0.00	0.00	0.00	0.44	0.00	0.00	0.00	0.00	2.59	1.99	0.00	1.19	0.00	2.31
Ms	0.10	0.08	0.76	0.10	0.08	0.07	0.03	0.04	0.03	0.29	0.09	0.17	0.30	0.10	0.07
Hy	0.05	0.89	0.05	0.10	0.19	0.05	0.05	0.08	0.07	1.05	0.50	0.10	0.49	0.07	0.50
Mt	0.02	0.14	0.00	0.00	0.04	0.00	0.00	0.02	0.02	0.04	0.04	0.04	0.29	0.02	0.04
Il	0.85	8.78	0.59	0.80	1.35	1.09	0.68	0.60	0.54	0.00	0.51	0.55	1.10	0.52	0.45
Hm	0.00	0.00	0.00	0.00	0.00	0.00	0.00	0.00	0.00	0.00	0.00	0.00	0.00	0.00	0.00
Ap	0.32	0.51	0.18	0.50	0.42	0.35	0.18	0.34	0.28	0.68	0.90	0.35	0.64	0.44	0.78
Total	99.96	100.02	99.61	99.89	100.02	99.75	99.43	99.89	99.80	101.55	101.15	99.90	100.03	99.88	101.15
feldspars	62.54	52.85	70.61	73.68	47.39	87.15	83.32	66.25	72.35	62.42	70.72	59.92	55.54	66.133	63.69

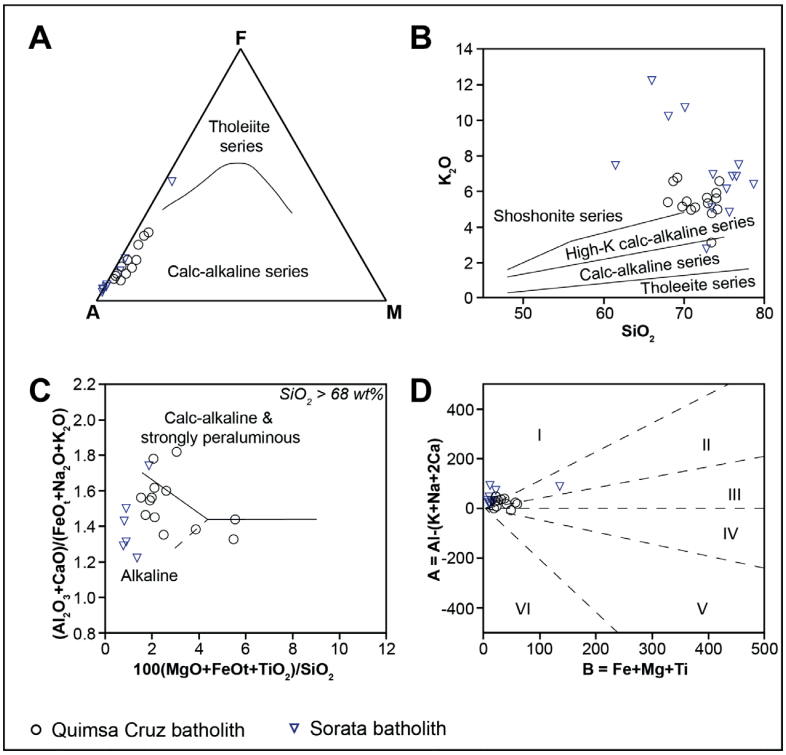

Figure 12: A) AFM diagram for tholeiite and calc-alkaline series classification for the Quimsa Cruz batholith and Sorata batholith (Irvine and Baragar, 1971); B) Rock classification diagram according to SiO_2-K_2O content in the rocks, for the Quimsa Cruz batholith and Sorata batholith (Peccerillo and Taylor, 1976); C) magmatic affinity rock classification diagram (Sylvester, 1989) from the Quimsa Cruz batholith and Sorata batholith; and D) B-A diagram from the Quimsa Cruz batholith and Sorata batholith (Debon and Lefort, 1983), reflecting alumina balance, as follows: Peraluminous domain I- muscovite>biotite, II-biotite<muscovite, III-biotite (+-minor amphibole) and Metaluminous domain IV- biotite, amphibole, +-biotite, V-clinopyroxene, +-amphibole, +-biotite, VI- usual mineral associations (carbonatites).

5.3. Physical properties of the potential kaolinite and feldspar deposits

The physical test results of the ceramic specimens from the Micaya kaolinite-bearing occurrences show: 1) Specimens from the north-eastern deposit exhibit 0.5 vol.% of drying shrinkage, 3.2 vol.% of firing shrinkage and 55.46 N/mm^2 of bending strength; 2) Specimens from the south-western deposit exhibit 0.7 vol.% of drying shrinkage, 5.1 vol.% of firing shrinkage and 55.70 N/mm^2 of bending strength (Paper I).

Table 3 shows the physical properties of the prototype ceramic specimens, i.e. floor tiles. Ceramic specimens conformed with the kaolinite-bearing sediment and feldspars at different concentrations.

Table 3: Physical test results on the ceramic specimens according to IBNORCA (2014). The kaolinite material belongs to the south-western kaolinite occurrence at Micaya.

specimen	Initial length (cm)	Drying length		Drying shrinkage (%)		Fired length (cm)	Firing shrinkage (%)	Bending strength (N/mm²)	Water absorption (%)	Mohs Hardness value
		24 hrs	48 hrs	24 hrs	48 hrs					
1	8.025	7.785	7.785	2.991	2.991	7.310	8.910	NE	<0.1	7
2	8.025	7.678	7.678	4.324	4.324	7.390	7.913	NE	<0.1	7
3	8.025	7.754	7.754	3.377	3.377	7.390	7.913	NE	<0.1	7
media	8.025	7.739	7.739	3.564	3.564	7.363	8.245	NE	<0.1	7
Kaolinite-bearing sediment from the Micaya deposit and feldspar from the Choquetanga deposit (50 vol.%–50 vol.%)										

specimen	Initial length (cm)	Drying length		Drying shrinkage (%)		Fired length (cm)	Firing shrinkage (%)	Bending strength (N/mm²)	Water absorption (%)	Mohs Hardness value
		24 hrs	48 hrs	24 hrs	48 hrs					
1	8.025	7.678	7.678	4.324	4.324	7.450	7.165	NE	<0.1	7
2	8.025	7.746	7.746	3.477	3.477	7.455	7.103	NE	<0.1	7
3	8.025	7.738	7.738	3.576	3.576	7.430	7.414	NE	<0.1	7
media	8.025	7.720	7.720	8.025	8.025	7.445	7.227	NE	<0.1	7
Kaolinite-bearing sediment from the Micaya deposit and feldspar from the La Fabulosa deposit (50 vol.%–50 vol.%)										

specimen	Initial length (cm)	Drying length		Drying shrinkage (%)		Fired length (cm)	Firing shrinkage (%)	Bending strength (N/mm²)	Water absorption (%)	Mohs Hardness value
		24 hrs	48 hrs	24 hrs	48 hrs					
1	8.025	7.875	7.875	1.869	1.869	7.705	3.988	66.405	1.683	7
2	8.025	7.826	7.826	2.48	2.48	7.855	2.118	68.543	1.723	7
3	8.025	7.861	7.861	2.044	2.044	7.770	3.178	69.563	1.794	7
media	8.025	7.854	7.854	2.131	2.131	7.770	3.094	68.179	1.733	7
Kaolinite-bearing sediment from the Micaya deposit and feldspar from the Choquetanga deposit (60 vol.%–40 vol.%)										

Table 3, cont.

specimen	Initial length (cm)	Drying length		Drying shrinkage (%)		Fired length (cm)	Firing shrinkage (%)	Bending strength (N/mm²)	Water absorption (%)	Mohs Hardness value
		24 hrs	48 hrs	24 hrs	48 hrs					
1	8.025	7.891	7.891	1.682	1.682	7.680	4.299	60.810	0.345	7
2	8.025	7.893	7.893	1.645	1.645	7.725	3.738	59.250	0.298	7
3	8.025	7.879	7.879	1.819	1.819	7.711	3.925	48.720	0.327	7
media	8.025	7.887	7.887	1.715	1.715	7.402	3.988	55.700	0.323	7
Kaolinite-bearing sediment from the Micaya deposit and feldspar from the La Fabulosa deposit (60 vol.%–40 vol.%)										

specimen	Initial length (cm)	Drying length		Drying shrinkage (%)		Fired length (cm)	Firing shrinkage (%)	Bending strength (N/mm²)	Water absorption (%)	Mohs Hardness value
		24 hrs	48 hrs	24 hrs	48 hrs					
1	8.025	7.995	7.995	0.374	0.182	7.89	1.682	69.050	2.213	7
2	8.025	8.011	8.011	0.174	0.243	7.892	1.657	55.560	2.077	7
3	8.025	8.003	8.003	0.274	0.198	7.893	1.645	60.090	2.120	7
media	8.025	8.003	8.003	0.274	0.207	7.760	1.661	69.550	2.136	7
Kaolinite-bearing sediment from the Micaya deposit and feldspar from the Choquetanga deposit (70 vol.%–30 vol.%)										

specimen	Initial length (cm)	Drying length		Drying shrinkage (%)		Fired length (cm)	Firing shrinkage (%)	Bending strength (N/mm²)	Water absorption (%)	Mohs Hardness value
		24 hrs	48 hrs	24 hrs	48 hrs					
1	8.025	7.985	7.985	0.498	0.299	7.888	1.707	70.350	0.630	7
2	8.025	7.997	7.997	0.349	0.320	7.900	1.558	69.750	0.459	7
3	8.025	7.999	7.999	0.324	0.312	7.903	1.520	70.510	0.660	7
media	8.025	7.993	7.993	0.390	0.310	7.897	1.595	70.200	0.583	7
Kaolinite-bearing sediment from the Micaya deposit and feldspar from the La Fabulosa deposit (70 vol.%–30 vol.%)										

Table 3, cont.

specimen	Initial length (cm)	Drying length		Drying shrinkage (%)		Fired length (cm)	Firing shrinkage (%)	Bending strength (N/mm²)	Water absorption (%)	Mohs Hardness value
		24 hrs	48 hrs	24 hrs	48 hrs					
1	8.025	8.002	8.001	0.287	0.287	7.73	3.676	59.15	1.768	6
2	8.025	7.998	7.996	0.336	0.336	7.789	2.941	51.792	1.657	6
3	8.025	8.004	8.004	0.262	0.262	7.756	3.352	58.729	2.01	6
media	8.025	8.001	8.000	0.295	0.295	7.758	3.323	56.557	1.811	6
Kaolinite-bearing sediment from the Micaya deposit and feldspar from the Choquetanga deposit (80 vol.%–20 vol.%)										
specimen	**Initial length (cm)**	**Drying length**		**Drying shrinkage (%)**		**Fired length (cm)**	**Firing shrinkage (%)**	**Bending strength (N/mm²)**	**Water absorption (%)**	**Mohs Hardness value**
		24 hrs	**48 hrs**	**24 hrs**	**48 hrs**					
1	8.025	7.989	7.992	0.449	0.436	7.750	3.427	66.405	0.730	6
2	8.025	7.991	7.991	0.436	0.424	7.761	3.29	66.405	0.759	6
3	8.025	7.991	7.997	0.424	0.349	7.776	3.103	66.405	0.860	6
media	8.025	7.990	7.993	0.436	0.403	7.762	3.273	66.405	0.783	6
Kaolinite-bearing sediment from the Micaya deposit and feldspar from the La Fabulosa deposit (80 vol.%–20 vol.%)										
specimen	**Initial length (cm)**	**Drying length**		**Drying shrinkage (%)**		**Fired length (cm)**	**Firing shrinkage (%)**	**Bending strength (N/mm²)**	**Water absorption (%)**	**Mohs Hardness value**
		24 hrs	**48 hrs**	**24 hrs**	**48 hrs**					
1	8.025	7.961	7.966	0.798	0.735	7.630	4.922	56.560	7.380	6
2	8.025	7.966	7.966	0.735	0.735	7.590	5.420	58.250	7.520	6
3	8.025	7.956	7.956	0.860	0.860	7.610	5.171	51.280	7.890	6
media	8.025	7.961	7.960	0.798	0.809	7.610	5.171	55.360	7.596	6
Kaolinite-bearing sediment 100 vol.%										

5.4. Industrial mineral resource potentiality of Bolivia

The Charaña and Murmutani diatomaceous earth deposits (Fig. 1) show similar crystallinity (Figs. 13a and 13b) with contaminant minerals such as muscovite, montmorillonite and halite. The Murmutani deposit shows considerable halite content, which is corroborated with the Na_2O_3 content (Table 4). The Villa Putuni clay deposit (Fig. 1) is composed of coloured layers of montmorillonite. The mineralogical analyses show montmorillonite and an amorphous phase (Fig. 13c), contrary to its analogue in Potosí. The Río Mulatos deposit (Fig. 1) is composed of crystalline montmorillonite, no amorphous material is visible in the XRD pattern (Fig. 13d). Two kaolin deposits have also been studied in Santa Cruz (Fig. 1). The La Bella kaolin deposit is characterized by high crystallinity (Fig. 13e), represented by long needle-shaped crystals of kaolinite (Paper IV). The mineralogical analysis of the Benton deposit shows kaolinite, sanidine and minor amounts of micaceous material (Fig. 13f). Both kaolin deposits show high alumina content and low iron content (table 4).

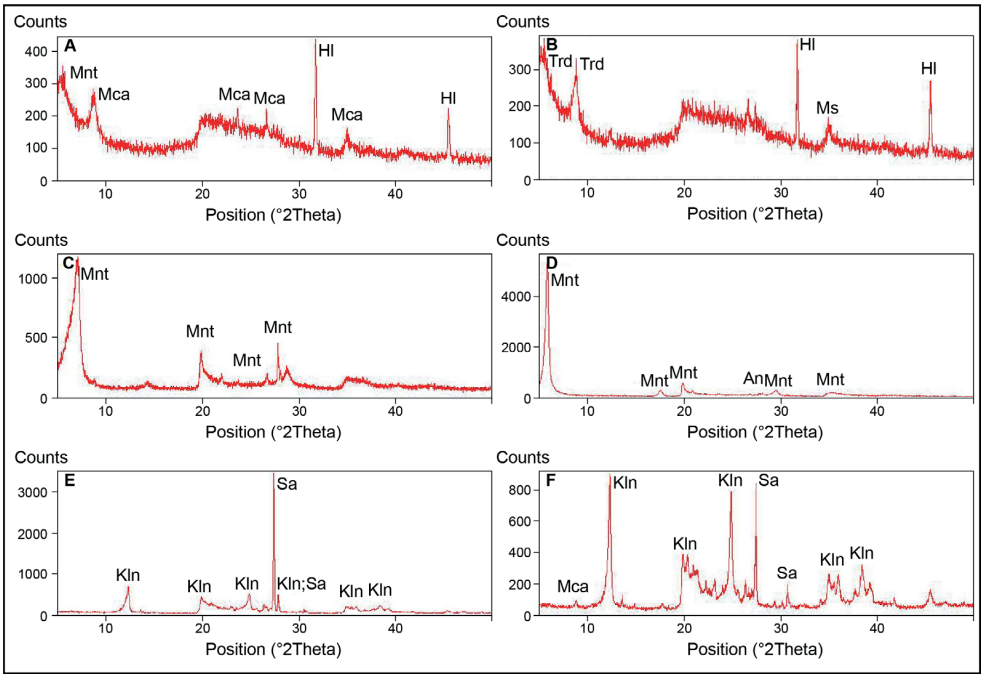

Figure 13: XRD pattern of the studied deposits: A) Charaña diatomaceous earth deposit in La Paz. Amorphous silica, halite and mica are identified; B) Murmutani diatomaceous earth deposit in Potosi. Amorphous silica, tridymite, halite and muscovite are visible; C) Villa Putuni montmorillonite deposit in La Paz. Montmorillonite and amorphous material are observed; D) Río Mulatos montmorillonite deposit in Potosí. Montmorillonite and anorthite are identified; E) La Bella kaolin deposit in Santa Cruz. Kaolinite and minor amounts of sanidine are identified; and F) Benton kaolin deposit in Santa Cruz. Kaolinite, muscovite and sanidine are visible.

Table 4: Mineralogical and lithogeochemical analyses of the Charaña diatomaceous earth deposit in La Paz, the Murmutani diatomaceous earth deposit in Potosí deposit, the Corque zeolite deposit in Oruro, the Villa Putuni montmorillonite deposit in La Paz, the Río Mulatos montmorillonite deposit in Potosí, the La Bella kaolin deposit in Santa Cruz, Benton kaolin deposit in Santa Cruz, Llojeta illitic clay in La Paz and the Viacha illitic clay in La Paz, using XRD and ICP-MS analysis.

Location of the deposit	Name	Origin	Mineralogy	Chemical composition (wt.%)						Microstructure configuration	Application
				SiO_2	Al_2O_3	Fe_2O_3	K_2O	CaO	Na_2O		
Charaña, La Paz	Diatomaceous earth	Lacustrine origin	Halite; phlogopite; montmorillonite	73.50	10.10	3.40	1.30	2.80	1.30	Microscopic algae skeletons	zeolite synthesis
Murmutani, Potosí	Diatomaceous earth	Lacustrine origin	Halite; tridymite; muscovite	72.10	8.49	1.30	1.60	1.47	5.00	Microscopic algae skeletons	zeolite synthesis
Corque, Oruro	Zeolite	Hydrothermal alteration of dacite sill	Mordenite; montmorillonite	59.20	15.20	1.22	0.56	2.83	0.83	Acicular crystals	agriculture
Villa Putuni, La Paz	Montmorillonite	Alteration of tuffaceous material	Montmorillonite; mordenite	57.30	10.00	2.40	0.47	0.60-7.81	2.63	clay plates	zeolite synthesis
Río Mulatos, Potosí	Montmorillonite	Alteration of tuffaceous material	Montmorillonite; anorthite	55.00	20.60	0.60	0.30	2.49	0.87	clay plates	drilling mud
La Bella, Santa Cruz	Kaolin	Hydrothermal alteration of granitic pegmatites	Kaolinite; sanidine	49.30	34.50	<0.10	1.86	<0.08	0.52	Acicular crystals	wall tile ceramic
Micaya, La Paz	Kaolinite-bearing sediment	Weathering of siltstones	Quartz; kaolinite; muscovite; feldspar	71.00	16.70	1.22	3.84	0.13	0.11	Plates	floor tile ceramic
Benton, Santa Cruz	Kaolin	Hydrothermal alteration of granitic pegmatites	Kaolinite; sanidine; phlogopite	49.80	29.30	0.10	3.89	<0.08	0.10	Acicular crystals	waste
Llojeta, La Paz	Illite	Lacustrine origin	Quartz; muscovite; montmorillonite	52.30	20.20	5.00	3.45	0.16	0.81	clay plates	red brick industry
Viacha, La Paz	Illite	Lacustrine origin	Quartz; clinochlore; muscovite	52.60	20.70	7.50	3.40	1.01	0.92	clay plates	red brick industry
Choquetanga, La Paz	Feldspar-rich granite	syn-collisional magmatic origin	Quartz; plagioclase; feldspar; biotite	71.70	14.90	0.95–3.51	4.13–6.75	0.52–1.79	2.94–4.35	n/d	floor tile ceramic
La Fabulosa, La Paz	Feldspar-rich granite and pegmatite dyke	syn-collisional magmatic origin	Quartz; feldspar; plagioclase; muscovite	72.60	15.10	0.50–1.27	1.15–12.30	0.10–0.90	1.76–4.98	n/d	floor tile ceramic

6. DISCUSSION

6.1. Geological and mineralogical characterization of the kaolinite-bearing deposit

Chemical and mineralogical characterization is the key to understanding and evaluating the better use of natural mineral mixtures as raw material for value-added products for different industry purposes. Therefore, kaolinite deposits formed from hydrothermal alteration of igneous rocks commonly become the favoured target of the paper and chemical industry, due to their crystallinity and purity (Keller, 1982; Murray and Keller, 1993) compared to kaolinite deposits derived from weathering of sedimentary rocks, which generally show poor crystallinity and contamination by minerals such as quartz and muscovite (Keller, 1982), as well as iron and magnesium. However, the mineralogical assemblage of the deposits from weathering are desirable for ceramic purposes, since quartz will give the ceramic the needed strength and kaolinite will give the necessary plasticity to form the green body (unfired ceramic body) of the ceramic (McCuistion and Wilson, 2006). In the La Paz area, one kaolinite-bearing deposit at Micaya has been evaluated (Fig. 1), which is formed by weathering of muscovite-rich siltstones from Devonian sedimentary units (Fig. 2). This suggests kaolinite formation from muscovite, and microstructural analysis suggests in-situ formation.

6.2. Exploitation of the non-metallic minerals beyond the exploration

In 2020 it is planned that 50 % of the Andean region and 25% of the Precambrian Shield in Bolivia will be geologically characterized (SERGEOMIN, 2016). Bolivia is considered an important player, related to the mineral and raw materials exportation in the world (World trade organization, 2017). The above mentioned facts, explain, the existence of currently exploited deposits in Bolivia without neither geological, nor mineralogical characterization of their mineral constituents (e.g. the Murmutani deposit, the Río Mulatos deposit and La Bella deposit).

Several studies have previously been performed on the filtering process, to remove colour and turbidity using montmorillonite and diatomite (Erdogan et al., 1996; Huttenloch, 2001; Martinovic et al., 2006). Filter industry for food and beverage are the main natural diatomite consumers (Martinovic et al., 2006). Diatomaceous earth resources must fulfil three fundamental conditions to be used in the industry: low contamination of sediments, low bulk density and high content of free amorphous silica (SiO_2) (Chang, 2002; Breese and Bodycomb, 2006). The Charaña diatomite deposit exhibits clay contamination (Fig. 13a) due to its lacustrine origin, but on the other hand, exhibits a high quantity of amorphous silica which is related to the algae skeletons content (Servant-Vildary, 1978). The

Murmutani deposit presents a high halite content (Table 4), among its mineral constituents, which exclude it from the food and beverage industries application (Breese and Bodycomb, 2006). Acarapi (2013) has leached, concentrated and treated both diatomaceous earth materials using the sintering process used by Akhtar et al. (2010). The Charaña diatomaceous earth could effectively increase the SiO_2 content by 25 wt. % and lower the bulk density, allowing for its use in the filter industry and synthesis of zeolites (García et al., 2015). The Murmutani diatomaceous earth is currently exploited and transported to Chile, for use in the cement industry (Juana Mita, 2014, personal communication), in which the diatomaceous earth has been used as a substitute to tuffaceous material to produce puzzolanic cement (Tagnit-Hamou et al., 2003).

Montmorillonite minerals are well known for their natural swelling properties in contact with water, which make them a natural absorbent (Eisenhour and Reisch, 2006). However, each industry has its own specifications of physical properties (e.g. swelling) (Eisenhour et al., 2006, Flanagan, 2015). The Villa Putuni deposit in La Paz (Fig. 1) exhibits amorphous silica (Fig. 13c), making the material highly reactive and therefore appropriate for zeolite synthesis process (Panoso, 2015) and is currently used in the cat litter industry due its swealling properties. The Río Mulatos montmorillonite has low iron contamination and crystalline structure (Fig. 13d). Therefore, it possesses important characteristics and can be used in the synthesis of other minerals, such as zeolite (Panoso, 2015).

The La Bella and Benton kaolin deposits were formed through hydrothermal alteration of pegmatites (Arduz et al., 1994). Therefore, they exhibit crystalline kaolinite (Fig. 13e and 13f) and high Al_2O_3 content (Table 4). Although they might be targets for the paper and chemical industry (Keller, 1982; Murray et al., 1993), due to its purity (Fig. 13e and 13f; Paper IV), the La Bella deposit is open-pit mined for the ceramic tile industry (Autoridad de Fiscalización de empresas, 2017). The price of kaolin is 160 $/ton and 50 $/ton (Statista, 2017) for the paper/paint-grade and for the ceramic-grade, respectively**.** The Benton deposit is mined for its tantalum/niobium content, while the kaolin goes to the waste (Paper IV), followed by an infiltration in the soil. The tantalite is composed of 60 % Ta and 3–5 % Nb and is a naturally occurring radioactive mineral (Paper IV) in pegmatites. Therefore, its exploitation has to be rigorously controlled.

Although each of these deposits could have formed under the same geological conditions as their analogues in other parts of the country, they have different mineralogical and geochemical characteristics that influence their industrial purposes. Therefore, their mineralogical and geochemical characteristics should be addressed before exploitation to reach better prices into the market.

6.3. Material suitability for the ceramic industry

For the tile industry, the content of sodium and potassium is an essential property. The alkali metals act as fluxing agents to lower the melting point of the mixture (Galan, 2003) and thus favour the glass development (Jensen and Bateman, 1979; Potter, 2006) and thereby reduce the porosity. Igneous rocks such as granites and pegmatites with an alkali content (ΣK_2O+Na_2O) between 5–14 wt. % are used as fluxing agents (Hughes, 2006). The alkali metals are hosted in minerals such as potassium feldspar and plagioclase. The presence of orthoclase increases the bending strength of the final ceramic product (Bennour et al., 2015), whereas sodium-feldspar-containing materials make the ceramic product brittle (Swapan and Kausik, 2003).

The ceramic specimens from the south-west deposit in Micaya show high porosity (Table 3). The muscovite content in the kaolinite-bearing raw material increases the porosity due to expansion of the muscovite stacks at high temperature (Cole and Crook, 1968). The ceramic specimens (kaolinite-bearing sediment+feldspar choquetanga/fabulosa) show enhancement in drying shrinkage and water absorption after the addition of the feldspathic material (Table 3), due to the glass development in the slabs during firing (Jensen and Bateman, 1979; Potter, 2006). The raw material, which is composed of quartz and aluminosilicate minerals such as muscovite and kaolinite (Figs. 7a and 7b), form a silicon-aluminium-oxygen network providing the mechanical strength during firing (Ismailova and Borisova, 1972).

The studied ceramic specimens show higher bending strength (Table 3) than those ceramic tiles currently marketed in Bolivia (35–55 N/mm^2: Fábrica Boliviana de Cerámica, 2018; Gladymar, 2015), as well as higher hardness (Table 3), compared to currently marketed ceramic tiles in Bolivia (Hardness 4; Uriarte, 2007). The mineral mullite has been thoroughly studied due to its thermal properties in the ceramic bodies (Lu et al., 2004) as well as the mechanical properties that this mineral imparts to the tile ceramics (Reyes et al., 2013) such as bending strength. The high bending strength observed in the ceramic tiles has been determined to be a result of the mullite transformation from the kaolinite (Brindley and Nakahira, 1959a, 1959b, 1959c), during firing. Although the mineral mullite requires higher temperature to form (Brindley and Nakahira, 1959a, 1959b, 1959c), it is believed that its formation might be promoted for the addition of alkali, lowering the melting point of the ceramic mixtures (Galan, 2003). Therefore mullite is observed in the ceramic slabs, at different feldspar concentrations (Figs. 14a, 14b, 14c and 14d).

In addition to the alkali content there are other technical specifications that a feldspathic material is required to meet to be used as a raw material in the ceramic industry, e.g. the iron and magnesium content, hosted in for instance biotite, ilmenite, pyroxene and tourmaline, as well as the calcium content in the mixture. Ions of iron and magnesium cause a colour change of the ceramic products during firing, therefore the documentation of their presence is important, especially if the material is envisaged to be used to produce white tiles. The iron content in the raw material (Table 4) has been determined to be too low to contaminate the colour of the final ceramic specimen (Paper III).

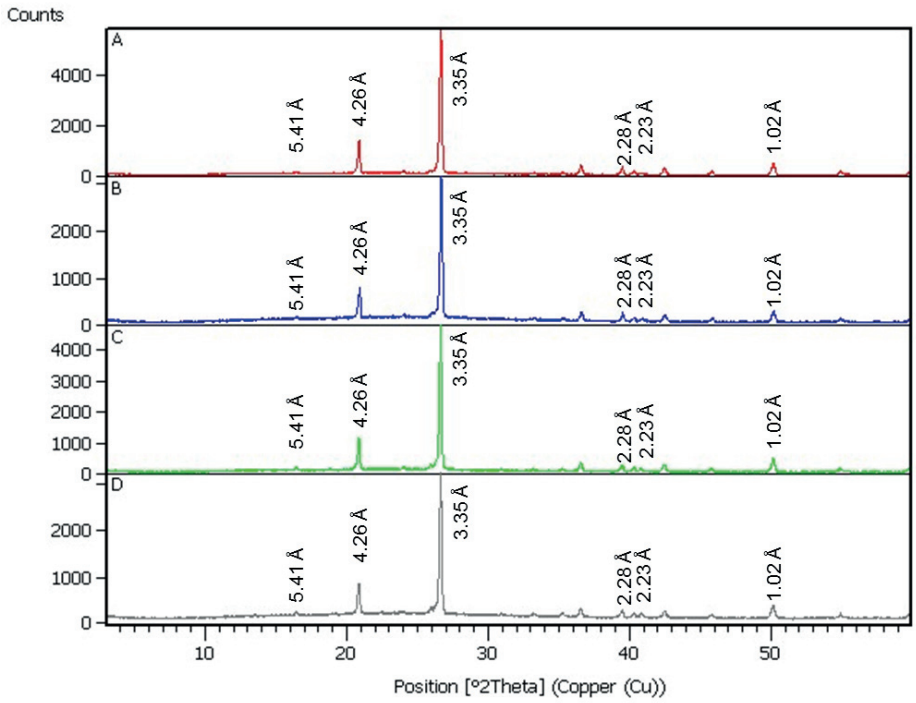

Figure 14: A) XRD pattern of the ceramic slabs, kaolinite-bearing sediments 70 vol.%–Choq 30 vol.%. Quartz (3.35 Å, 4.26 Å, 2.28 Å, 1.02 Å) and mullite (5.41 Å, 2.23 Å) peaks were identified; B) XRD pattern of the ceramic slabs, kaolinite-bearing sediments 70 vol.%–Fab 30 vol.%. Quartz (3.35 Å, 4.26 Å, 2.28 Å, 1.02 Å) and mullite (5.41 Å, 2.23 Å) peaks were identified; C) XRD pattern of the ceramic slabs, kaolinite-bearing sediments 80 vol.%–Choq 20 vol.%. Quartz (3.35 Å, 4.26 Å, 2.28 Å, 1.02 Å) and mullite (5.41 Å, 2.23 Å) peaks were identified ; D) XRD pattern of the ceramic slabs, kaolinite-bearing sediments 80 vol.%–Choq 20 vol.% Quartz (3.35 Å, 4.26 Å, 2.28 Å, 1.02 Å) and mullite (5.41 Å, 2.23 Å) peaks were identified.

7. CONCLUSIONS

Altogether to the mineralogical and chemical characterization of the studied materials, the kaolinite-bearing sediment from the Micaya deposit and the feldspars from the Choquetanga and La Fabulosa areas in the La Paz region, together with the technical characterization of the end product make as drawn the following:

- The Micaya deposit is hosted in sedimentary units of Devonian age. It comprises two whitish kaolinite-bearing occurrences, formed by weathering of micaceous siltstones. The Micaya deposit is composed of fine-grained quartz, muscovite, kaolinite and feldspar. The kaolinite-bearing sediments have been proven to be suitable for ceramic purposes in the floor tile industry.

- The Choquetanga deposit is hosted in the Quimsa Cruz batholith and comprises oriented orthoclase megacrysts with an alkali content of ΣK_2O+Na_2O=7.84–10.25 wt.%. The La Fabulosa deposit is hosted in the Sorata batholith. The Sorata batholith comprises granite and pegmatite dykes, with an alkali content of ΣK_2O+Na_2O=7.41–14.25 wt.%.

- A potential application of the kaolinite-bearing sediments from the Micaya deposit and the two studied feldspars from the Choquetanga and La Fabulosa deposits has been proven in floor tile production, with competitive physical properties.

- The importance of the mineralogical and lithogeochemical characterization prior to exploitation has been shown through the comparisson of the mineralogy and lithogeochemistry of six deposits currently exploited in Bolivia.

8. References

Acarapi W (2013) Estudio y aplicación de los recursos diatomaceous de las Localidades de Charaña y Bella Vista, departamento de La Paz y Potosí, Universidad Mayor de San Andrés, La Paz, Bolivia.

Akhtar F, Rehman Y and Bergström L (2010) A study of the sintering of diatomaceous earth to produce porous ceramic monoliths with bimodal porosity and high strength Powder Technology 201(3): 253–257.

Aranibar RO (1984) Megatrazas en el Altiplano de Bolivia y su influencia en la evolución de cuencas. Archivo YPFB (GXG-3082).

Arce BO (2002) Potencial geológico-minero de Bolivia: Memorias del XV Congreso Geológico Boliviano, Santa Cruz, Bolivia, October. Revista Técnica de YPFB 20: 18–24.

----- (2007) Guía de los Yacimientos metalíferos de Bolivia. La Paz, Bolivia, SPC Impresores, Minera San Cristóbal y Empresa Minera Unificada S. A. (EMUSA), 298 p.

Arce O and Goldfarb RJ (2009) Metallogeny of Bolivia. Newsletter of the Society of Economic Geologist. Number 79: 8–15.

Arduz M (1976) Estudio petrológico de las rocas metamorficas de un sector del Valle de Zongo. Revista Técnica de YPFB, 5(1): 33–58.

Arduz M and Buitrago O (1992) Minerales y rocas industriales en Bolivia: Una alternativa de diversificacio´n. Bol Soc Geol Bolivia – La Paz 27: 12–13.

Arduz M, Almeida L and Claure H (1994) Caolin y arcillas caoliníticas en Bolivia, consideraciones genéticas Final Proc. 7° Chilean Conf of Geology 2: 720–724.

Argandoña J and Vargas LH R (2004) Mineralización de la región de Yani-Charazani norte del Departamento de La Paz. Memorias del XVI Congreso Geológico Boliviano, Oruro, pp. 191–196.

Autoridad de Fiscalización de Empresas (2017) Estudio de Mercado de cerámicas para pisos y revestimientos en Bolivia Informe Final 47 p.

Avila SW (1989) Perspectivas sobre la explotacion y aplicación industrial de la andalucita de Yani – Zongo. CEDOMIN 11.

-----(1990) Tin-bearing granites from the Cordillera Real, Bolivia; a petrological and geochemical review. Geological Society of America, Special Paper 241: 145–159.

-----(1994) Ambiente Téctonico y Parámetros Geoquímicos de los granitos estanniferos Bolivianos. Revista Técnica de Y.P.F.B 15(1-2): 99–109.

Bennour A, Mahmoudi S, Srasra E, Boussen S and Htira N (2015) Composition, firing behaviour and ceramic properties of the Sjnène clays (Nortwest Tunisia) Journal of Applied Clay Science 115: 30–38.

Benjamin MT, Johnson NM and Naeser CW (1987) Recent rapid uplift in the Bolivian Andes; Evidence from fission-track dating Geology 15: 680–683.

Breese R and Bodycomb F (2006) Industrial Minerals & Rocks. In: Kogel J., Trivedi N., Barker J. and Krukowski S, editors. Diatomite: Society for Mining, and Exploration Inc p 433–450.

Brindley GW and Nakahira M (1959a) The kaolinite-mullite reaction series: I. A survey of outstanding problems. J. Am. Ceram. Soc., 42:311–-314.

Brindley GW and Nakahira M (1959b) The kaolinite-mullite reaction series: II. Metakaolin. J. Am. Ceram. Soc., 42:315–318.

Brindley GW and Nakahira M (1959c) The kaolinite-mullite reaction series: III. The high temperature phases. J. Am. Ceram. Soc., 42:319–324.

Cámara Nacional de Industrias (CNI) (2017) Ranking 2016: exportaciones e importaciones industriales. Revista de la Cámara Nacional de Industrias, La Paz, Bolivia 4(24): 14–16.

Castaños A and Rodrigo LA (1978) Sinopsis Estratigráfica de Bolivia. Edic. Academia Nacional de Ciencias de Bolivia, pp 8–19.

Chang LY (2002) Industrial mineralogy: materials, processes and uses 1st edition Prentice Hall 450 p.

Cole WF and Crook DN (1968) High-temperature reaction of clay mineral mixtures and their ceramic properties: IV, dimensional and weight changes on refiring and the pore-size distribution of fired kaolinite-muscovite-quartz mixtures with 25 wt.% quartz Journal of the American Ceramic Society 51(2): 79–84.

Debon F and Le Fort P (1983) A chemical mineralogical classification of common plutonic rocks and association. Earth Sci 73: 135–149.

Eisenhour D and Reisch F (2006) Industrial Minerals & Rocks. In: Kogel J., Trivedi N., Barker J. and Krukowski S, editors. Bentonite: Society for Mining, and Exploration Inc p 357–368.

Erdogan B, Demirci and Akay Y (1996) Treatment of sugar beet juice with bentonite, sepiolite, diatomite and quartamin to remove color and turbidity Applied Clay Science 11: 55–67.

Escobar DA, Bellot LJ and Jurado AE (1999) Minerales y Rocas Industriales. In: Riera, K. C., Troëng, B., Diaz, M. E., Jurado, A. E. (eds) Geología y Recursos Minerales del area La Paz – Copacabana – Estudios Integrados de los Recursos Minerales de Bolivia. Boletin del Servicio Nacional de Geología, pp 47–74.

Evernden JF, Kritz SJ and Cherroni C (1977) Potassium-argon ages of some Bolivian Rocks Economic Geology 72: 1042–1061.

Fábrica Boliviana de Cerámica (2018) Normas y especificaciones. Recuperado de http://www.faboce.com.bo.

Farrar E, Clark AH and Heinrich SM (1990) The age of the Zongo pluton and the tectonothermal evolution of the Zongo-San Gabán zone in the Cordillera Real, Bolivia. I International Symposium on Andean Geodynamics, Grenoble, pp. 171–174.

Flanagan D (2015) Minerals Yearbook. Clays and shales U.S.G.S 28 p.

Galán HE (2003) Mineralogía Aplicada. 1st ed. Madrid: Síntesis, 399 p.

García G, Aguilar-Mamani W, Cabrera S, Hedlund J and Mouzon J (2015) Preparation of zeolite A with excellent optical properties from clay J Alloys compd 619: 771–777.

GEOBOL (1982) Proyecto mina Fabulosa, etapas "B y C". Bull. Geol. Survey of Bolivia, N° 5.

GEOBOL (1995) Carta Geológica Milluni No. 5945. Escala 1:100000, Servicio Geológico de Bolivia (GEOBOL) and Geological Swedish AB (eds).

GEOBOL (1995) Carta Geológica Calamarca No. 5943. Escala 1:100000, Servicio Geológico de Bolivia (GEOBOL) and Geological Swedish AB (eds).

GEOBOL (1995) Carta Geológica Inquisivi No. 6143. Escala 1:100000, Servicio Geológico de Bolivia (GEOBOL) and Geological Swedish AB (eds).

Gillis R, Horton B and Grove M (2006) Thermocronology, geochronology, and upper crustal structure of the Cordillera Real: Implications for Cenozoic exhumation of the central Andean plateau Tectonic 25: TC6007

Gladymar (2015) Aspectos técnicos del porcelanato. Recuperado de http://www.gladymar.com.bo.

Harrington H (1968) Desarrollo Paleogeográfico de Sudamérica. Univ Nacional de Tucuman. Fund. Inst. M. Lillo. Misc N° 26. Tucuman – Argentina.

Hérail G, Fornari M, Viscarra G, Ruiz JA, Pozzo L and Dumont JF (1991) Les placers d'or de Bolivie: milieu de formation et structure geologique.- Symp. Intern. Sur les gisements d'or (La Paz): 115–143. Publ. ORSTOM.

Herail G, Rochat P, Baby P, Aranibar O, Lavenu A and Mascle G (1993) El Altiplano Norte de Bolivia: Evolución Geológica Terciaria. Actas del II Simposio de Estudios Altiplánicos, Santiago de Chile, pp.33–44.

Lu HY, Wang WL, Tuan WH and Lin MH (2004) Acicular Mullite Crystals in Vitrified Kaolin. Journal of the American Ceramic Society, 87: 1843–1847.

Horton BK, Hampton B, LaReau BN and Baldellon E (2002) Tertiary provenance history of the northern and central Altiplano (Central Andes, Bolivia) – A detrital record of plateau-margin tectonics. Journal of Sedimentary Research 72: 711–726.

Hughes W (2006) Minerals and metals availability in New South Wales Australia. New Department of Primary industries. 1st ed. Australia 58 p.

Hutchison CS (1974) Laboratory Handbook of Petrographic Techniques. John Wiley & Sons, New York, p. 1-527.

Huttenloch P, Roehl KE and Czurda H (2001) Sorption of nonpolar aromatic contaminants by chlorosine surface modified natural minerals. Environ. Sci. Technol. 35: 4260–4264.

Instituto Boliviano de Normalización y Calidad (IBNORCA) (2014) Catálogo de Normas Bolivianas. NB/ISO 10545-4:2005 Baldosas cerámicas— Determinación de la resistencia a la flexión y de la carga de rotura (correspondiente a la norma ISO 10545-4:1995-NB-259-78) Dirección General de Normas y Tecnología – Bolivia, Ministerio de Industria y Comercio, 14 p.

Irvine TN and Baragar WRA (1971). A guide to the chemical classification of the commmon volcanic rocks Can J Earth Sci.8: 523–548.

Ismailova MA and Borisova Kh B (1972) Low temperature bodies for ceramic tile Journal of Glass and Ceramics 29(8): 535–536.

ISO 10545-4 (2004) Determination of modulus of rupture and breaking strength. ISO, Geneva 20. www.iso.org

ISO 10545-3 (1995) Determination of water absorption, apparent porosity, apparent relative density and bulk density. ISO, Geneva 20. www.iso.org

Jacobshagen V, Müller J, Wemmer K, Ahrendt H. and Manutsoglu E (2002) Hercynian deformation and metamorphism in the Cordillera Oriental of Southern Bolivia, Central Andes. Tectonophysics 345: 119–130.

Jensen LM and Bateman MA (1979) Economic mineral deposits. In: John Wiley & Sons editors. United States of America, pp 496–505.

Keller WD (1982) Kaolin–a most diverse rock in genesis, texture, physical properties, and uses. Geol Soc Am Bull 93: 27–36.

Kennan L, Lamb S and Rundle C (1995) K-Ar dates from the Altiplano and Cordillera Oriental of Bolivia: implications for Cenozoic stratigraphy and tectonics. Journal of South American Sciences 8(2): 163–186.

Kussmaul S, Jordan H. and Ploskonka E (1975) Isotopic Ages of Tertiary Volcanic Rocks of SW – Bolivia. Geol. Sb. B 14: 111–120.

Lamb S and Hoke L (1997) Origin of the high plateau in the Central Andes, Bolivia, South America Tectonics 16(4): 623–649.

Litherland M, Annells RN, Darbyshire DPF, Fletcher CJN, Hawkins MP, Klinck BA, Mitchell WI, O'Connor EA, Pitfield PEJ, Power G and Webb BC (1989) The Proterozoic of the Eastern Bolivia and its relationship to the Andean mobile belt Precambrian Research 43(3): 157–174.

Martinovic S, Vlahovic M, Boljanac T and Pavlovic L (2006) Preparation of filter aids based on diatomites. Int. J. Miner. Process 80: 255-260.

Marshall LG, Sempere T and Gayet M (1993) The Petaca (Late Oligocene-Middle Miocene) and Yecua (Late Miocene) formations of the Subandean Chaco basin, Bolivian and their tectonic significance. Documents du Laboratoire de Geology de Lyon 125: 291–301.

McBride SL, Robertson RCR, Clark AH and Farrar E (1983) Magmatic and metallogenetic episodes in the northern tin belt, Cordillera Real, Bolivia. Geologische Rundschau 72(2): 685–713.

McCuistion J and Wilson I (2006) Industrial minerals & rocks. In: Kogel J, Trivedi N, Barker J, Krukowski S (eds) Ball clays. Society for Mining, and Exploration Inc, pp 343–356.

McQuarrie N, Horton BK, Zandt G, Beck S and DeCelles PG (2005) Lithospheric evolution of the Andean fold – thrust belt, Bolivia and the origin of the central Andean plateau. Tectonophysics 399: 15–37.

Middlemost E A K (1994) Naming materials in magma/igneous rock system. Earth Sci. Rev 37: 215–224.

Montes de Oca I (1983) Geografía y Recursos Naturales de Bolivia 1st ed Superel La Paz, 628 p.

Murray HH and Keller DW (1993) Kaolins, kaolins and kaolins: In kaolin genesis and utilization. Special publication no. 1. The Clay Minerals Society, pp 1–24.

Oppenheim V (1943) Diamond in the north-eastern Bolivian Andes. Economic Geology 38(8): 658–661.

Orris JG, Asher BS, Carrasco R and Claure ZM (1975) Other Industrial Deposits. In: Cox PD, Carrasco R, Andre RO, Hinojosa VA, Long RL (eds) Cooper deposits in sedimentary rocks. United States Government Press Office, pp 207–208.

Panoso Y (2015) Estudio geológico y caracterización del depósito bentonítico y sus aplicaciones potenciales en la localidad Putuni – Condoroca, Provincia Pacajes. Departamento de La Paz Graduated thesis, Universidad Mayor de San Andrés, La Paz, Bolivia.

Pecerillo A and Taylor SR (1976) Geochemistry of Eocene calc-alkaline volcanic rocks from the Kastamonu area, Northern Turkey. Contrib Mineral Petrol 58: 63–81.

Potter J M (2006) Industrial Minerals & Rocks. In: Kogel J., Trivedi N., Barker J. and Krukowski S, editors. Feldspars: Society for Mining, and Exploration Inc 451–460.

Quispe A (11 de Septiembre del 2014) Faboce abre moderna planta de tecnogranito. La Razón de Bolivia on-line edition.

Reyes LSY, Serrato RJ and Sugita SS (2013) Microstructural characterization of sanitaryware, the relationship spinel and mullite Journal of ceramic processing Research 14(4): 492–497.

Rietveld HM (1967) Line profiles of neutron powder-diffraction peaks for structure refinement Acta Cryst 22: 151-152.

Rivas S (2002) Minerales No-Metálicos, Rocas Industriales y Gemas de Bolivia Landivar Press, Bolivia p 355.

Russo A (1966) Algunas Consideraciones Fisiográficas del Territorio Boliviano. Ind. Bol. Petr. (I.B.P) 6(2): 7–25.

Schneider A and Halls C (1985) Cronología de los procesos eruptivos y de mineralización en el campo volcánico de Los Frailes Kari Kari, Cordillera Oriental, Bolivia. Comunicaciones (Santiago) 35: 217–224.

Sempere T, Hérail G and Oller J (1988) Los aspectos estructurales y sedimentarios del oroclino boliviano.V Congreso Geológico Chileno 1: A127–A 142.

Sempere T, Hérail G, Oller J and Bonhomme MG (1990) Late Oligocene–early Miocene major tectonics crisis and related basins in Bolivia. Geology 18: 946–949.

SERGEOMIN (2016) Rendición pública, resultados y prioridades. Ministerior de minería y metalurgía, 60 p.

Servant-Vildary S (1978) Les diatomeés des dépôts lacustres quaternaires de I'Altiplano bolivien. Cah ORSTOM Sér Géol X(I): 25–35.

Statista (2017) Average kaolin price, www.statista.com.

Suarez SR (2000) Compendio de Geología de Bolivia. Revista Tecnica de Yacimientos Petroliferos Fiscales Bolivianos 18(1-2): 13–38.

Sugaki A, Kusachi I and Shimada N (1988) Granite-series and –types of igneous rocks in the Bolivian Andes and their genetic relation to tin-tungsten mineralization. Mining Geology 38(2): 121–130.

Swapan KD and Kausik D (2003) Differences in densification behaviour of K- and Na-feldspar-containing porcelain bodies Thermochimica Acta 406: 199–206.

Sylvester PJ (1989) Post-Collisional alkaline granites J Geol 97(3): 261–280.

Tagnit-Hamou A, Petrov N and Luke K (2003) Properties of concrete containing diatomaceous earth Aci Materials Journal 100(1): 73–78.

Uriarte (2007) Estudio de las características físico – mecánicas de las baldosas cerámicas que se fabrican y ofertan en el mercado nacional. Revista del Instituto de Ensayo de Materiales. Carrera de Ingeniería Civil – UMSA. Año 2, N-2, pp 29–40.

World trade Organization (2017) World trade statistical review: Purinational State of Bolivia, p.182 www.wto.org/statistics.

PAPER I

Geological, mineralogical and chemical characterization of Devonian kaolinite-bearing sediments for further applications in the ceramic (tiles) industry in La Paz, Bolivia

Ariana Zeballos, Pär Weihed, Mario Blanco & Vladimir Machaca

Published in:

Environmental Earth Sciences

(2016) 75:546

Environ Earth Sci (2016) 75:546
DOI 10.1007/s12665-015-5212-y

ORIGINAL ARTICLE

Geological, mineralogical and chemical characterization of Devonian kaolinite-bearing sediments for further applications in the ceramic (tiles) industry in La Paz, Bolivia

Ariana Zeballos[1,2] · Pär Weihed[1] · Mario Blanco[2] · Vladimir Machaca[2]

Received: 10 December 2014 / Accepted: 29 December 2015 / Published online: 25 March 2016

Abstract Clay minerals are widely distributed in Bolivia; among them, illitic clays are most common in the Altiplano where they are mined for use in the ceramic industry that has been growing in the last few years. In addition to illitic sediments, kaolinitic sediments have been recently discovered in sedimentary units in the Bolivian Altiplano. Residual ball clay occurrences in Devonian sedimentary units were studied as part of this work. Geological mapping and geophysical studies (ERT and GPR) were done for better understanding the origin of the deposits and were part of a preliminary study of the mineral potential to define the relationship with the host rock. Chemical and mineralogical techniques such as X-Ray Diffraction, Scanning Electron Microscopy and Inductively Coupled Plasma analyses were performed in samples from the studied area to verify the presence of kaolinite. Atterberg limits and behaviour of the raw material in ceramic specimens supported by chemical analyses show that this material is suitable for manufacturing tile ceramics. This study provides fundamental knowledge for deposit exploitation and future generation of an alternative source of employment for the inhabitants of Micaya.

Keywords Kaolinite · Ball clays · Altiplano · Ceramics · Siltstones

✉ Ariana Zeballos
Ariana.Zeballos@ltu.se

[1] Division of Geosciences and Environmental Engineering, Luleå University of Technology, Luleå, Sweden

[2] IGEMA, Universidad Mayor de San Andres, La Paz, Bolivia

Introduction

Kaolinitic sedimentary clays are referred as "Ball clays"; and are amended to ceramic bodies. Kaolinitic clays are used in ceramic manufacture to add plasticity and strength to the ceramic body (McCuistion and Wilson 2006). They are generally composed of clay-size particles of kaolinite, illite, sericite and poorly crystallized fine-grained quartz (Mooney 1996; McCuistion and Wilson 2006). The term ceramic "body" is used to describe the starting material composed mainly of clay, to be used for a specific ceramic purpose.

The chemical composition of kaolinite is $Al_2O_3 2SiO_2 2H_2O$, having 39.8 wt% alumina, 46.3 wt% silica and 13.9 wt% water. It is an important industrial mineral for several applications including paper coating and filling, ceramics, paints and plastics (Murray and Keller 1993). A common assemblage of Ball clay deposits includes kaolinite, quartz and minor amounts of halloysite, muscovite and feldspars (Murray 1988). Kaolinite is mainly processed as a raw material for use in the ceramic industry; for manufacture of wall tiles, white wares, chemical, and scientific wares, sanitary wares and refractories. Depending on the kaolinite content in ball clays, some deposits are suitable as fillers in paper coating and paints (Murray and Keller 1993).

Geologic occurrences of kaolinite

Kaolinite-bearing deposits can occur in primary residual and secondary diagenetic environments (Murray and Keller 1993). Keller (1982) describes three geologic environments where kaolinite forms. The first occurs in low temperature weathering environments, the second takes place in

hydrothermal systems and the third forms from the crystallization process from colloid-size sediment whose chemical composition is congruent with that of kaolinite. Kaolinite can form at relatively low temperature and pressure from alteration of primary potassium-bearing minerals where the most common parent minerals are feldspar and muscovite (Murray 1988). An example of a low temperature kaolinite deposits is in Santa Cruz, Bolivia, where low temperature alteration of pegmatites have formed economic kaolinite deposits. Although the most common kaolinite deposits were formed by alteration of granitic rocks, some deposits have been formed from arkosic sediments that were altered primarily by groundwater after deposition (Murray 1988; Murray and Keller 1993).

Grahamstown, South Africa is one of the best studied kaolinite deposits hosted in sedimentary rocks (Murray and Smith 1973; Murray 1988; Jacob et al. 2004; Agnello 2005).

The ultimate industrial use of kaolinite is determined by the geological conditions in which a kaolinitic deposit was formed and the physical and chemical properties of the associated mineral assemblage (Keller 1982; Murray and Keller 1993). Knowledge of the origin, diagenesis and chemical composition of the clay is essential for the exploitation and use of the raw material for ceramic production (Sanfeliu and Jordan 2009).

Major kaolin producing countries are the United States (5480 Mt), Brazil (2050 Mt) and Czech Republic (3550 Mt) (Virta 2012). Three main ball clay deposits have been identified in Bolivia, which are located in Batallas, Karhuisa and Warmimarka (Fig. 1), where illite is the plastic mineralogical phase identified in these deposits (Escobar et al. 1999). Illite and kaolinite occurs in sediments and rocks in the Bolivian deposits and the material is currently mined for use in the construction industry (Escobar et al. 1999). Although these deposits are actively mined, they are poorly characterized.

The study area is located in Micaya, La Paz, where kaolinite bearing sediments were hand mined by the local inhabitants for handmade kitchen pots. The kaolinitic sediments in the Micaya area were first studied by Blanco et al. (2005); their physical properties including texture were described by Zeballos et al. (2009), who identified quartz, muscovite and feldspar as important constituents of the kaolinite occurrences. The physical properties including textural characteristics such as grain size are relevant to the material suitability for use in ceramics. Complementary geological, mineralogical, chemical and physical characterization tests were performed in selected rock samples to define the origin of the deposits in the Micaya area and its suitability for use in ceramics manufacture. Geophysical studies were used to also help to identify the spatial relationship of the kaolinite-bearing layers.

There are few studies concerning mineralogical characterization and formation of kaolinite bearing sediments in the Bolivian territory. Previous studies identify kaolin as a by-product of intense alteration of pegmatites such as in Santa Cruz and as a by-product of intense alteration of granitic rocks such as in La Paz and Oruro (Orris et al. 1992; Escobar et al. 1999). However, the kaolinitic materials described in sedimentary units in the Altiplano, are scarcely mentioned and barely studied, hence the importance of the current work.

Geological setting

Regional geologic framework

The sedimentary sequence in the Altiplano is represented by Silurian and Devonian units, composed of sandstones grading into pelitic rocks in normal graded sequences (GEOBOL 1995), overlain by limestones from the Cumana unit, and matrix supported conglomerates and tuffs intercalated with Neogene siltstones.

Porphyritic rocks from the Letanias and Comanche–Miriquiri complex intrude the Palaeozoic sequence (Redwood 1986). The Letanias complex is calcalkaline and dacitic to andesitic in composition (Redwood 1986). Accessory minerals such as sphene, zircon and apatite were reported. All volcanic rocks display a holocrystalline matrix and flow texture. These rocks have been dated by K–Ar method at 16.6 ± 0.40 Ma (Redwood 1986). The Comanche–Miriquiri porphyritic complex is composed of dacites, rhyolites and andesites and has been dated at 15.7–17.9 Ma by K–Ar (Redwood 1986).

Cenozoic intrusive and volcanic rocks in the study area resulted in the deposition of pyroclastic materials formed during Neogene volcanism. The deposition of fine grained pyroclastic material filled paleo valleys and modified the relief of the area (Soria 1980). Ages of preserved tuffs in the Remedios Formation range from 5.2 to 4.6 Ma (GEOBOL 1995).

Local geology

The local stratigraphy of Micaya (Fig. 2) consists of Palaeozoic and Cenozoic sedimentary rocks. The Palaeozoic sedimentary rocks are intruded by Cenozoic, dacitic and andesitic rocks. Tertiary pyroclastic rocks including ash-flow tuffs are exposed in the area. The litostratigraphic succession is given in Fig. 3. Vila Vila and Sica Sica formations are the host units for the studied clay materials (Fig. 3). The terrain is characterized by wide fluvial valleys with adjacent upland areas including the Asunkollu (4188 m) and Nunu Kkollu hills (4200 m) (Fig. 2).

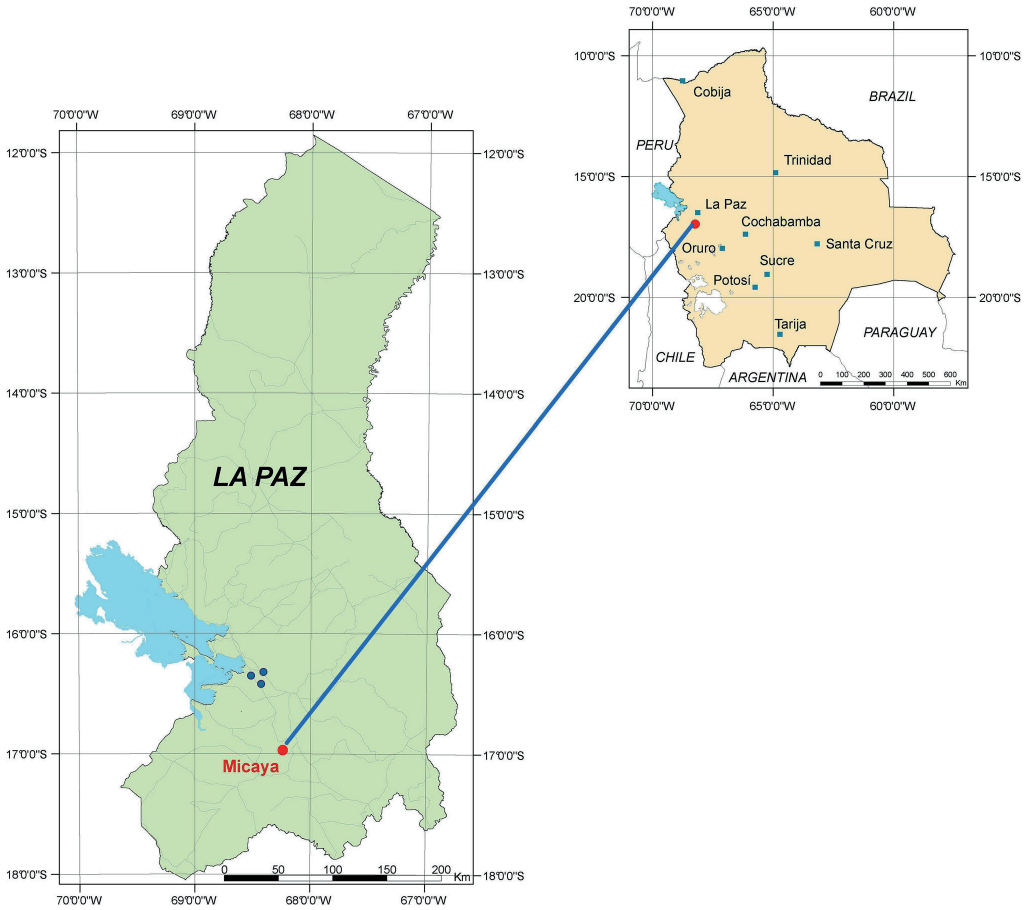

Fig. 1 Location map of the study area, Micaya and location of Batallas, Karhuisa and Warmimarka illitic deposits studied by Escobar et al. (1999)

Structural geology

The main structures in the Micaya area have a NW–SE (Fig. 2) orientation and they formed in response to the Andean orogeny, which is characterized by (SW–NE) directed compressional events. The deformation caused by the Andean uplift overprints earlier compressive deformation ascribed to the Hercynian orogeny (Martinez and Vargas 1990).

Faults in the Vila Vila and Sica Sica units are particularly important, because they form permeable hydrologic flow-paths, resulting in highly weathered siltstones, which are the parental sediments of the kaolinitic material. Enhanced weathering of siltstones along the fault zones due to water–rock interaction is thought to be an important process in forming secondary kaolinite (Zeballos et al. 2009).

Cenozoic volcanism

Cenozoic magmatism resulted in the deposition of fine pyroclastic materials (Remedios Formation) and intrusion of dacitic and andesitic subvolcanic rocks of the Letanias Complex (Soria 1980). Sedimentary units in the area were locally deformed causing visible folds and faults. The calc-alkaline porphyritic rocks of the Letanias Complex (16.6 ± 0.40 Ma by K–Ar; Redwood 1986) contain an abundance of sanidine phenocrysts, minor plagioclase and

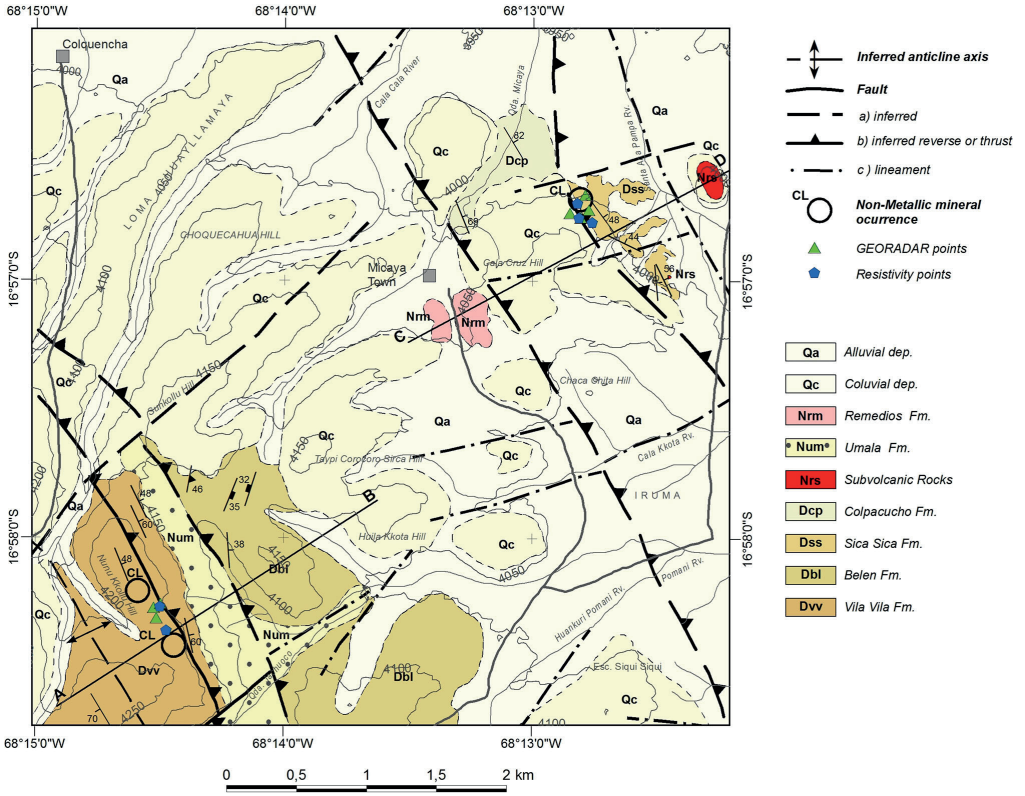

Fig. 2 Geologic map of Micaya modified from the Calamarca geologic map printed by GEOBOL (1995)

biotite. Some igneous bodies also contain rounded quartz phenocrysts and green or brown hornblende, with accessory sphene, zircon and apatite.

Materials and methods

Geological mapping (Figs. 2, 3) and structural profiles (Fig. 4a, b) were prepared to interpret the kaolinite-bearing deposit of Micaya in a geological context. Twenty semiconsolidated representative samples, 2–3 kg each were collected. Ten semiconsolidated clay samples from the Vila Vila formation and ten samples from the Sica Sica formation were also collected for analyses.

Chemical analyses were performed using Inductively Coupled Plasma–Atomic Emission Spectroscopy (ICP–AES) on the most representative samples and were carried out by ALS Scandinavia. Prior to the analysis the samples were dried at 105 °C, using a 0.1 g sample digested with 0.375 g $LiBO_2$ and dissolved in HNO_3. Loss on ignition (LOI) was determined gravimetrically by heating powders to 1000 °C for 1 h. ICP–AES analyses were completed on representative samples and the results are reported in "Appendix Table 1". Detection limits for major elements are 0.01 wt% and detection limits for most trace elements are 1–10 ppb. Mineralogy was determined by X-ray powder diffraction (Fig. 5) by a X'Pert3 PANalytical instrument using Cu Kα radiation and time step increments of 0.010°/s. Mineral identification and quantification were determined with the help of the X'-pert High Score Plus software. The quantification results were performed according to the Rietveld method (Rietveld 1969). The mineral kaolinite has a characteristic X-ray spectral peak at 12.32° (7.1 Å) (Brown and Brindley 1980; Moore and Reynolds 1997).

The microstructure of selected samples was investigated by scanning electron microscopy (Fig. 6a, b) (SEM, Magellan UHR) and Energy Dispersive X-ray Spectroscopy

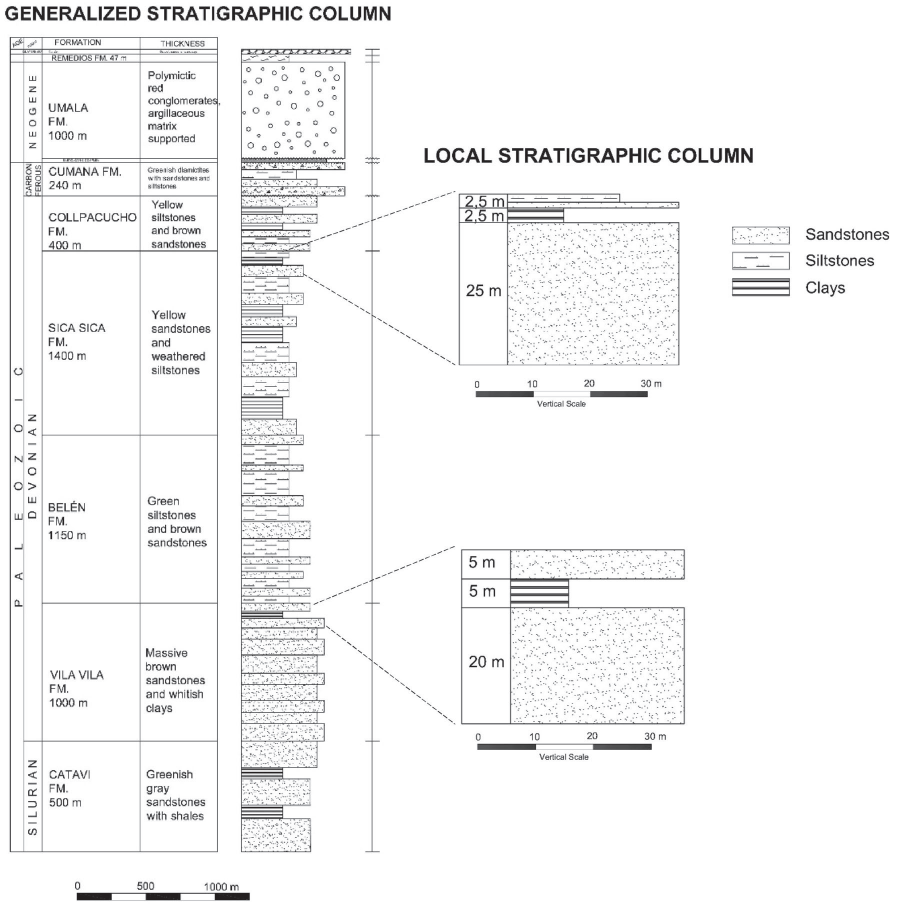

Fig. 3 Regional stratigraphic column of Micaya area and local stratigraphic columns based in geophysical tests

(EDX, X-MAX 80 mm^2, Oxford Instruments), in freshly broken surfaces of clays. An accelerating voltage of 1 kV and a current of 6.3 pA was used for high resolution imaging. Microanalyses were performed on samples mounted on an aluminium stub after powder samples were dispersed and dried in chloroform.

Preliminary physical tests commonly used on ceramic body were performed on ten ceramic specimens. Five samples from each deposit were selected and tested for: plasticity (ASTM D4318 2010), shrinkage (ASTM C326-09 2009), water absorption (ASTM C373-14 2014), Mohs scale hardness, bending strength (IBNORCA 2014; NB/ISO 10545-4:2005 2014) ("Appendix Table 2") and fired color (Munsell Chart 2009). The samples were dried and wet-ground (jaw crusher and porcelain grinder for 4 h; 350 mesh). Resulting powders were mixed, humidified (moisture content 8.25 wt%) and then pressed into bars (18 MPa; size 8.025 × 29.5 × 6.20 ± 1.0 mm; clay content 100 wt%). After drying (48 h at room temperature) the bars were fired (8 h; maximum temperature 1250 °C). The ceramic specimens were characterized by measuring the size variations after 24 and 48 h of pressing.

Geoelectric and electromagnetic geophysical tests

Geophysical tests (Figs. 7, 8) were performed using Electrical resistivity tomography (ERT) and Georadar (GPR). Both methods were used for a basic estimation of the spatial relationship of the kaolinitic layers within the host rocks. Five lines were established using georesistivity

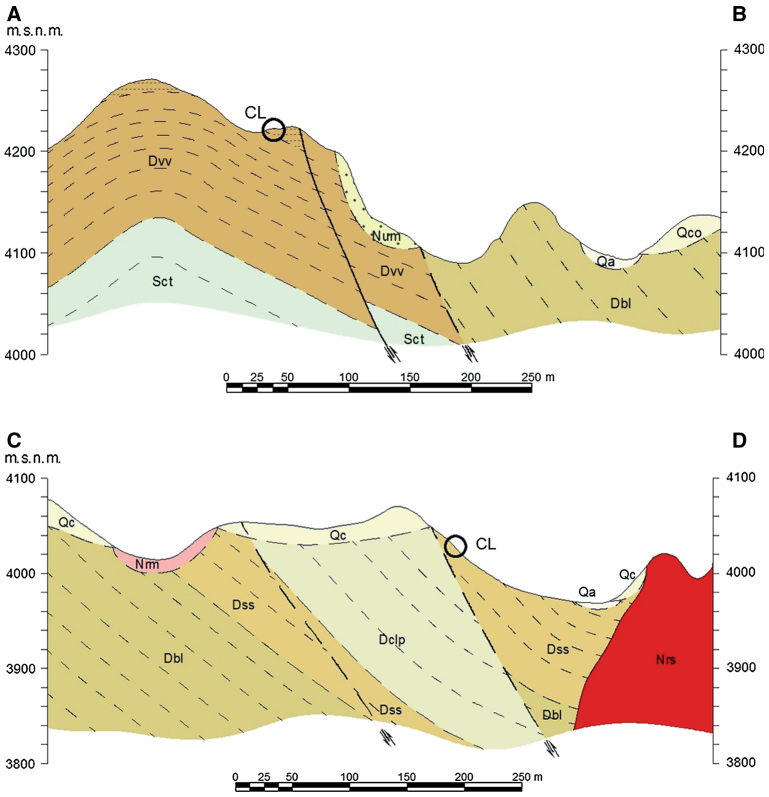

Fig. 4 **a** Geological profile (*A*–*B*) of the SW deposit and **b** geological profile (*C*–*D*) of the NE studied deposit. From the geologic sheet of Micaya

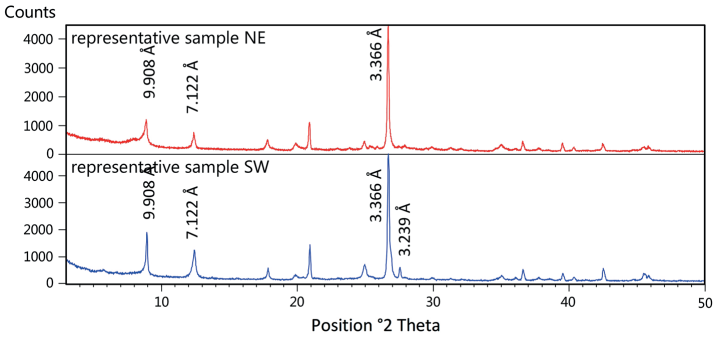

Fig. 5 Comparative XRD pattern of the kaolinitic layers. Four minerals were identified: Quartz (3.366 Å), muscovite (9.908 Å), kaolinite (7.122 Å) and feldspar (3.239 Å)

equipment. The resistivity instrument used was a OYO Model geo-receptor JP-600 brand. It has a sensitivity of 0.01 mV and digital recording capability. The unit operates at 2.5 amps and has a variable voltage of up to 1000 V. It operates using a 12 V battery and has four cable spools (100 m each) and 30 copper electrodes with a linear array of 10 m. The GPR studies were carried out in seven lines using a GEORADAR ZOND-12E instrument equipped with a 75 MHz monostatic antenna applying time windows of 120 ns, with 40 scans/s, and 512 samples per scan.

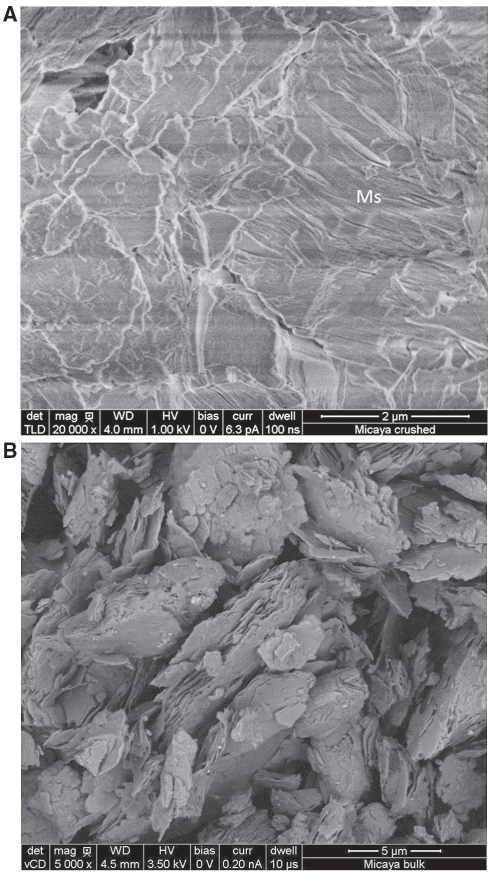

Fig. 6 SEM backscattered images of **a** Muscovite stacks in the NE deposit (Sica Sica sedimentary unit) and **b** microphotograph of the kaolinitic plates for the SW deposit (Vila Vila sedimentary unit) exhibit irregular edges, a characteristic texture in kaolinites form sedimentary rocks. Mineral abbreviations according to Kretz (1983)

Electrical and electromagnetic methods can be used to map subsurface variability according to electrical properties, caused by changes in lithology, structure and alteration. The geoelectric method (ERT) is used to measure the apparent resistivity (conductivity) of the rocks (János 2009). This method is based on the application of electric current into analysed bedrock and measurement of the intensity to its conductance. In electromagnetic methods (GPR), the electric current in the rocks induces a magnetic field (János 2009). The depth of investigation can range from less than a meter in the case of ground penetrating radar depending on the antenna used in the test (900 MHz—1.5 m depth; 200 MHz—9 m depth; 80–16 MHz—10–30 m depth), to tens and hundreds of meters depth for most other methods. Resolution of targets and detectability tend to decrease with increasing depth of burial (Watson et al. 2001).

Analytical results

Chemistry, mineralogy and microstructure

The chemistry and qualitative mineral assemblage of selected samples from Vila Vila (SW in the study area) and Sica Sica layers (NE in the study area) are shown in Appendix Table 1 and Fig. 5. The mineral assemblage of each layer was determined by XRD analyses showing a dominance of quartz, muscovite, kaolinite with subordinate feldspar, in the SW deposit; and quartz, muscovite and kaolinite in the NE deposit.

Silica content is consistently higher in Vila Vila samples (70.5–74 wt%) compared to the Sica Sica material (63.2–67.1 wt%). The Al_2O_3 content is higher in Sica Sica sediments (20.9–23.8 wt%) compared to Vila Vila sediments (17.0–17.9 wt%). The potassium content is similar in both layers and resides in muscovite and feldspars. The chemical results are consistent with the mineralogy of the material containing quartz, muscovite, kaolinite and lesser amounts of feldspars as shown in the XRD pattern (3.239 Å) (Fig. 5). The iron content ranges from 1.27 to 1.87 wt%. According to the Munsell color chart classification (2009), the raw ball clays are white (N9) to medium light grey color (N6) after kiln firing, which is consistent with the low iron content.

Mineralogical (Figs. 5, 6) and geochemical studies ("Appendix Table 1") have been performed in both kaolinitic beds from Micaya. Four mineralogical phases have been identified in the SW deposit (Vila Vila unit) (Fig. 5): quartz 56.3 wt%, muscovite 12.2 wt%., kaolinite 24.9 wt%, and feldspar 6.7 wt%. The studied material from the Sica Sica unit (NE deposit) was composed of quartz 50.8 wt%, muscovite 35.4 wt%, and kaolinite 13.8 wt% (Fig. 5).

The major element chemical composition of the Vila Vila unit is: SiO_2 (70.5–74.2 wt%) and Al_2O_3 (17–17.9 wt%), followed by 3.8–4 wt% of K_2O and comprising >90 % wt% total (on a volatile free basis) ("Appendix Table 1"). The Sica Sica layer compared to the Vila Vila unit is lower in SiO_2 (63.2–67.1 wt%), has higher Al_2O_3 (20.9–23.8 wt%) content and has a similar of K_2O (3–4.9 wt%) composition, comprising >95 % wt% (on a volatile free basis) ("Appendix Table 2").

The microstructure of the samples is shown in Fig. 6a and b. The SW deposit is composed mainly of kaolinite plates; the NE deposit mainly contains muscovite stacks. Secondary kaolinite after muscovite is observed in

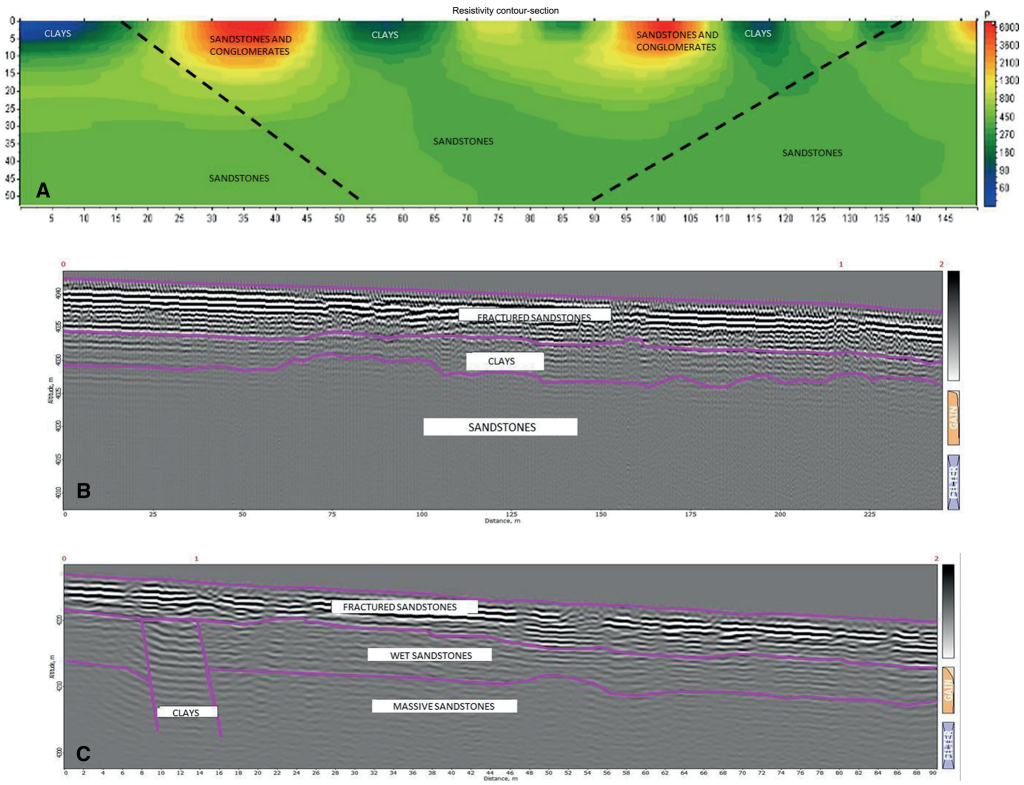

Fig. 7 Geoelectric tomography and ground penetrating radar results of the SW deposit

muscovite rich siltstones. The siltstones also contain quartz. Kaolinite is observed in both the SW and NE materials. The result of the Atterberg limits test shows a plasticity index of 4.03 for the SW samples and 4.01 for the NE samples, both reflecting zero plasticity according to the Casagrande chart (Casagrande 1932). These results reflect silt with low plasticity. The low plasticity is consistent with the predominant clay mineral being kaolinite (Bain 1971). "Appendix Table 2" shows the result of the physical tests performed on the ceramic specimens. The above results suggest that the kaolinite bearing materials are a suitable source for ceramic body.

Geophysical test

According to János (2009), the resistivity method has been proven to be useful in determining thickness and extent of horizontally stratified clay, sand and gravel deposits, being an important tool in geological, environmental and engineering surveys (Busby et al. 2004; de Oliveira Braga et al. 2006; Pànek et al. 2006; El Assel et al. 2011; Kumar 2012). Geoelectrical and electromagnetics methods are thought to be reliable and low cost methods to investigate underground lithology and subsurface structures and are easy to handle during field work (Burley et al. 1978; Sanner and Abbas 1998; Watson et al. 2001; EL-Qady et al. 2005).

Geophysical studies in the Micaya area (Fig. 2) were carried out through five resistivity lines (150 m) and seven GEORADAR lines. GEORADAR was performed in both occurrences to identify the spatial relationship of the kaolinite-bearing layers. The electrical resistivity tomography results are consistent with the ground penetrating radar results; both geophysical techniques show three lithological layers for the SW deposits: sandstones, conglomerates and clays (Fig. 7), and sandstones, siltstones and clays for the N–E occurrence (Fig. 8). Geographical position line length and approximate thickness of lithologic units are given in "Appendix Tables 4 and 5".

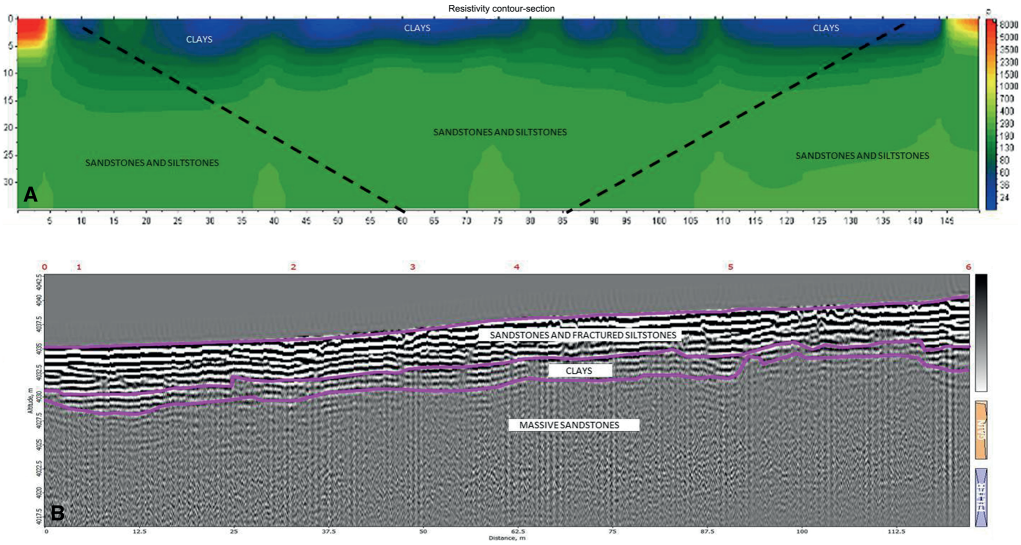

Fig. 8 Geoelectric tomography and ground penetrating radar results of the NE deposit

Fig. 9 Kaolinitic occurrence located in Micaya

Discussion and conclusions

Geological mapping (Fig. 2) in Micaya (La Paz) has identified two kaolinite-bearing occurrences in Devonian units consisting of sandstones in the Vila Vila formation and sandstones and siltstones in the Sica Sica Formation (Fig. 3). Kaolinitic material in the study area has been historically mined and minor mining is ongoing in the area (Fig. 9). The mined material has been used locally to manufacture white handmade kitchenware such as pots and dishes. Kaolinite is thought to be formed by enhanced weathering of siltstones containing potassium-rich minerals, such as muscovite and feldspars. Diagenetic kaolinite formation was aided by groundwater that interacted with rocks along permeable zones in folds and faults which increases the speed of breakdown of the primary minerals to clay minerals.

Mineralogical and geochemical studies performed in the kaolinitic beds show similarities in both materials. Although quartz, muscovite and kaolinite are the main mineralogical phases in both deposits, feldspar (6.7 wt%) is only observed in the Vila Vila unit (Fig. 5), the color and the fine-grained size and texture of the materials are similar.

The SiO_2 is consistently higher in the Vila Vila samples compared to the Sica Sica material ("Appendix Table 1"). A higher SiO_2 content is a desirable quality for floor tile ceramic materials. The Al_2O_3 content is higher in the Sica Sica sediments due the amount of muscovite. The K_2O content is similar in both layers and hosted in minerals such as feldspars and muscovite in the Vila Vila sediments and muscovite in the Sica Sica sediments. Both compositions indicate a favourable composition for ceramic materials production in which kaolinite will give plasticity to the mixture, whereas quartz and feldspar will increase the strength (McCuistion and Wilson 2006; Mooney 1996). The iron concentration is low (<2 wt%) for both layers ("Appendix Table 1"), and is desirable for tile manufacture.

Although "Ball clays" are well known for high plasticity and according to Bain (1971), kaolinitic materials derived from weathered sedimentary rocks tend to have a

high plasticity index (>10). This property can be reduced by the semiconsolidated character of the material or grain size of the material. In the Micaya samples, the reduction in the plasticity index of <5 is due to poor induration of the deposit. The plasticity index could affect, whether it can be used in ceramic body for various applications. Nonetheless ball clays will increase the green (unfired) strength after pressing (Mooney 1996; McCuistion and Wilson 2006). The green strength quality is visible in Appendix Table 2, where the ceramic specimens display high bending strength of >55 N/mm^2. The desirable average range in ceramic tiles must reach at least 50–55 N/mm^2 (ISO 10545-4).

Both deposits show similar chemical and mineralogical characteristics, suggesting in situ formation as a result of a contemporaneous alteration event affecting siltstones in both sedimentary units. Scanning electron microscopy analyses shows kaolinite pseudomorphs after muscovite in both areas (Fig. 6a), indicating diagenetic transformation of muscovite to kaolinite. These muscovite stacks contain voids within the plates due to the release of potassium during kaolinitization (Stoch and Sikora 1976; Manju et al. 2001). The rockforming mineral assemblage also suggests muscovite as the parent mineral for the kaolinite crystallization as no other phase has been identified as a likely precursor to kaolinite. Based on the shape of the kaolinite plates visible in the SEM images (Fig. 6b) and the kaolinite peaks from the XRD pattern (Fig. 5), we could conclude that the studied material exhibits poor crystallinity. The composition, heterogeneity and the irregular angular edges (Keller 1985; Fig. 6a, b) suggest primary formation, which is characteristic of actively growing crystals as a result of the on-going weathering process and is an indication of in situ formation. Differences in the kaolinite crystallization could be due to the physical characteristics of the host rock. Sandstones are competent and sometimes brittle during deformation resulting in a highly fractured rock with a high hydraulic conductivity compared with more plastic materials. Mineralogical and chemical similarities of both studied materials are apparent as the characterization reflects; therefore the samples also show similarities in the results of the physical tests for ceramic applications (Appendix Table 2).

Kaolinite bearing sediments were identified through geological mapping (Figs. 9, 10) and aided by mineralogical and physical tests. The geophysical results provide insight for a better understanding of the spatial relationship of the kaolinite-bearing units and the material potential for future exploitation.

The Micaya area is relatively arid; therefore the degree of water saturation in the soil is minor. Nevertheless the morphology of the area contributes to minor water accumulations during the rainy season. The reflections observed in geophysical profiles are mainly caused by the differences in lithology among the materials in contact, caused by the facies change within stratigraphic units. The ERT method does not provide a unique interpretation and is also insensitive to surface layers or features having similar electrical properties such as clays and siltstones and the GPR has limited depth of penetration in clay sediments. The frequency used must be high enough to resolve the target size and geometry, as the frequency increases small-scale features such as fine scale bedding, cracks and joints that become radar targets which reflect and scatter the signal. This results in clutter within the recorded data and reduces the amount of energy penetrating to depth. In addition, as the radar frequency increases the signal attenuation within the ground increases (Busby et al. 2004). Nevertheless, the combination of ERT and GPR methods has been able to distinguish two sedimentary units in the SW deposit (Fig. 7) having distinct geophysical signature, with a good correlation between them and one sedimentary unit in the NE deposit (Fig. 8). In each deposit three lithologic units were identified:

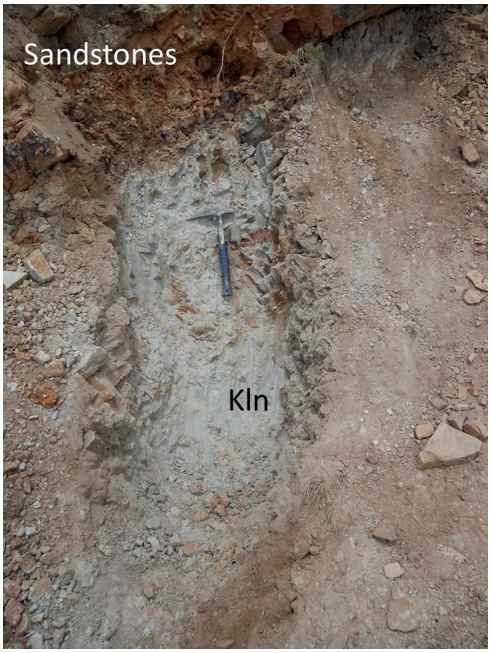

Fig. 10 Mine workings present in the area

In the SW deposit: *Lithologic unit 1,* is associated with Devonian sandstones and clays from the Vila Vila Formation (Fig. 3) and conglomerates from the Umala Formation (Fig. 3). It has a regular surface morphology according to the local erosion level. This layer has a high

GPR signature; mainly due to the fractured character of the strata. The material has been identified as fractured sandstones. In general, the ERT profiles show resistivities between 30 and 6000 Ω m for this level. *Lithologic unit 2*, is correlated to the first stratigraphic series that corresponds to irregular interbedded thin clay layers. The GPR-38 MHz profiles show some good reflectors that coincide with the interpretation of the geological mapping, although the lithologic contact between the upper and lower units is not well defined due the signature attenuation caused by the clays. The electric response for this layer is located below 80 Ω m. *Lithologic unit 3*, is thicker than the overlying units (about 50 m; "Appendix Table 3") and is related to the stratigraphic series consisting of a continuous sandstone beds. The electric response is over 1900 Ω m.

In the NE deposit: *Lithologic unit 1 is the uppermost unit* and is associated with Devonian sandstones and siltstones of the Sica Sica Formation (Fig. 3). This layer presents a high GPR signature mainly due the fractured character of the sandstone. In general, the ERT profiles show resistivities between 20 and 750 Ω m for this level. *Lithologic unit 2* is the second identified unit and corresponds to an irregular interbedded thin clay layer. The lithologic contacts between the upper and lower units are not well defined. The electric response for this layer is located below 300 Ω m. *Lithologic unit 3* is thicker than the previous units (about 30 m; "Appendix Table 3") and is related to a continuous sandstone horizon. In this case the electric response is over 9000 Ω m.

The geophysical methods used in the Micaya area for a preliminary investigation of the spatial relationship of the kaolinite-bearing layers have been proven effective in characterizing the mineralogical occurrences. Both, the GPR and ERT methods show similar results. The ERT method proved to be more effective in determining clay layer thickness in both occurrences, although the resolution has been reduced due to the electrode linear array configuration. According to Watson et al. (2001) and Busby et al. (2004) the GPR method is not recommended for clayey or very conductive terrains due to the attenuation of the radar signal by the conductive ground, so it is not possible to observe well defined lithologic contacts between clay and non-clay layers.

The results of the geological, analytical and geophysical investigations performed in the Micaya area provide important information concerning the economic potential of the sediments as an exploitable source of kaolinite. The important features of the resources are:

- Important potential for local use in ceramics manufacture. The deposit meets local standards for use in ceramic body.
- The mineral mixtures are fine grained which reduces energy use required for grinding. The mineral association is simple (quartz–kaolinite–muscovite–feldspar) and the presence of SiO_2, Al_2O_3 and Fe_2O_3 are within the allowable international determined parameters for white ceramic formulations, according to international and national parameters.
- The study area is accessible using existing infrastructure.

An assessment of pelitic sediments for use in ceramics includes the following characteristics: (1) reliable quantity of quartz, and clay; (2) low iron content and (3) good quality of the final products. Chemical composition of materials that can be unfavourable for use in ceramics are high SiO_2 and Fe_2O_3 concentrations, this composition raise the melting point of the mixture and adversely affects the quality of a raw material. On the other hand, lower quartz content reduces the strength of the ceramic specimen, also affecting the quality of the end product. High Fe_2O_3 concentrations are tolerable for building materials such as bricks. High Fe_2O_3 content however would prevent use for ceramic manufacture, because light colors are required. All these required characteristics are intimately related to the origin of the raw material.

The sedimentary source of the kaolinite-bearing sediments in Micaya is similar to those pelitic sediments studied in the Grahamstown deposits in South Africa. The pelitic sediments from Grahamstown are currently used in the ceramic industry and are acceptable for use in the ceramic production of wall tiles and white wares (Agnello 2005).

The XRD pattern (Fig. 5) of the studied mixtures supported by whole rock chemical analyses ("Appendix Table 1") defines the mineralogical composition of the kaolinitic materials as quartz and kaolinite along with muscovite and minor amounts of feldspar in each sedimentary unit. Based on the shape of the kaolinite plates and the kaolinite peaks from XRD pattern we infer that the studied material exhibits poor crystallization and the heterogeneity of the composition and the irregular edges suggest primary formation. Therefore we conclude that the kaolinite-bearing sediments located in Micaya are good raw materials for the ceramic tile industry; they are easy to access and easy to process due to the mineralogy of the material and feasibility for local mining and production.

Appendix 1

See Tables 1 and 2.

Table 1 Chemical analyses of the Vila Vila kaolinite bearing sediments

Location	Samples									
Vila Vila	M-1	M-2	M-3	M-4	M-5	M-6	M-7	M-8	M-9	M-10
SiO_2	71.30	72.70	74.20	72.30	72.10	71.40	71.50	72.00	70.50	72.40
$Al2O_3$	17.30	17.60	17.90	17.60	17.60	17.40	17.30	17.50	17.00	17.50
CaO	0.14	0.14	0.14	0.15	0.14	0.14	0.14	0.14	0.13	0.14
Fe_2O_3	1.28	1.29	1.32	1.30	1.29	1.30	1.29	1.32	1.27	1.31
K_2O	3.83	3.87	3.96	4.01	3.90	3.85	3.88	3.92	3.82	3.93
MgO	0.68	0.69	0.70	0.69	0.69	0.69	0.69	0.70	0.67	0.69
MnO	0.03	0.03	0.03	0.03	0.03	0.03	0.03	0.03	0.03	0.03
Na_2O	0.10	0.10	0.10	0.11	0.10	0.10	0.10	0.11	0.10	0.10
P_2O_5	0.07	0.07	0.08	0.07	0.08	0.07	0.07	0.08	0.07	0.08
TiO_2	0.96	0.97	0.99	0.98	0.97	0.96	0.95	0.97	0.94	0.97
LOI	4.40	4.40	4.30	4.30	4.40	4.40	4.40	4.40	4.30	4.40
Total	100.09	101.85	103.71	101.53	101.29	100.33	100.34	101.16	98.84	101.54

Table 2 Chemical analyses of the Sica Sica kaolinite bearing sediments

Location	Samples									
Sica Sica	M-1	M-2	M-3	M-4	M-5	M-6	M-7	M-8	M-9	M-10
SiO_2	65.20	67.10	65.30	63.20	65.90	66.20	66.90	65.40	66.30	65.70
Al_2O_3	21.80	20.90	22.90	23.80	22.30	21.90	22.80	21.90	22.80	21.90
CaO	0.47	0.48	0.47	0.47	0.48	0.47	0.47	0.46	0.47	0.47
Fe_2O_3	1.79	1.83	1.87	1.63	1.67	1.82	1.55	1.73	1.50	1.76
K_2O	3.93	3.54	3.68	3.71	3.96	3.86	3.01	4.04	4.93	3.93
MgO	0.60	0.80	0.74	0.61	0.60	0.60	0.60	0.60	0.59	0.60
MnO	0.02	0.02	0.02	0.02	0.02	0.02	0.02	0.02	0.02	0.02
Na_2O	0.67	0.60	0.70	0.67	0.67	0.66	0.67	0.67	0.66	0.67
P_2O_5	0.08	0.08	0.08	0.08	0.08	0.08	0.08	0.08	0.08	0.08
TiO_2	0.93	0.95	0.93	0.91	0.94	0.93	0.93	0.93	0.93	0.94
LOI	4.60	4.30	4.30	4.60	4.30	4.30	3.50	4.60	2.50	4.60
Total	100.09	100.59	100.98	99.70	100.90	100.85	100.52	100.43	100.78	96.74

Appendix 2

See Tables 3 and 4.

Table 3 Physical properties determined for kiln-fired Sica Sica samples

Sica Sica unit NE deposit	Initial length (cm)	Drying shrinkage (%)		Fired length (cm)	Firing shrinkage (%)	Bending strength (N/mm^2)	Water absorption (%)
		24 h	48 h				
1	8.025	0.675	0.582	7.880	1.806	49.050	6.900
2	8.025	0.593	0.543	7.700	4.049	55.560	6.850
3	8.025	0.604	0.598	7.670	4.423	60.090	6.780
4	8.025	0.654	0.603	7.760	3.302	57.800	5.990
5	8.025	0.635	0.599	7.810	2.679	54.820	6.800
Media	8.025	0.632	0.585	7.760	3.251	55.460	6.660

Table 4 Physical properties determined for kiln-fired Vila Vila samples

Vila Vila unit SW deposit	Initial length (cm)	Drying shrinkage (%)		Fired length (cm)	Firing shrinkage (%)	Bending strength (N/mm^2)	Water absorption (%)
		24 h	48 h				
1	8.025	0.809	0.747	7.630	4.922	56.560	7.380
2	8.025	0.747	0.747	7.590	5.420	58.250	7.520
3	8.025	0.872	0.934	7.610	5.171	51.280	7.890
4	8.025	0.802	0.765	7.590	5.420	54.300	7.620
5	8.025	0.809	0.781	7.620	4.764	58.150	7.670
Media	8.025	0.807	0.794	7.608	5.139	55.700	7.610

Appendix 3

See Tables 5 and 6.

Table 5 Initial and final UTM coordinates of the geophysical lines

Points	UTM coordinates (initial)		Z (m)	UTM coordinates (final)		Z (m)	Lithology and electromagnetic values	Depth	Lithological units
	E	W		E	N				
G1	580691	8123479	4042	580777	8123254	4037	Fractured sandstones ($k = 4.1$); clays ($k = 5.5$); massive sandstones ($k = 9.6$)	7; 3.5; 19 m	Vila Vila
G2	580710	8123403	4227	580781	8123445	4215	Fractured sandstones ($k = 6.5$); wet sandstones ($k = 10.8$); clays ($k = 4.5$); massive sandstones ($k = 9.6$)	5; 3; 20; 23 m	Vila Vila
G3	580739	8123505	4019	580819	8123353	4029	Fractured sandstones ($k = 6.6$); wet sandstones ($k = 6.3$); massive sandstones ($k = 10.8$)	5; 4; 20 m	Vila Vila
G4	583779	8126427	4008	583710	8126269	4040	Fractured sandstones ($k = 5.4$); wet sandstones and siltstones ($k = 6.3$); massive sandstones ($k = 5.1$)	2.5; 3; 20 m	Sica Sica
G5	583669	8126297	4037	583773	8126242	4042	Fractured sandstones and siltstones ($k = 6.3$); clays ($k = 3$); massive sandstones ($k = 6.6$)	3.5; 1.5; 20 m	Sica Sica
G6	583746	8126263	4042	583823	8126263	4015	Fractured sandstones and siltstones ($k = 6.6$); massive sandstones and siltstones ($k = 5.7$); massive sandstones ($k = 5$)	3.5; 5; 12 m	Sica Sica
G7	583802	8126319	4028	583694	8126354	4029	Fractured sandstones and siltstones ($k = 6.6$); massive clays and sandstones ($k = 5.7$); massive sandstones ($k = 5$)	3.5; 5; 20 m	Sica Sica

Lithology and thickness are shown according to Ground Penetrating Radar results, modified table from the GPR report of Micaya, Ayala (2015)

Table 6 Initial and final UTM coordinates of the geophysical lines

Points	UTM coordinates (initial)		Z (m)	UTM coordinates (final)		Z (m)	Lithology and resistivity values	Depth	Lithological units
	E	N		E	N				
T1	580782	8123314	4245	580695	8123441	4250	Sandstones, siltstones and clays (30–80 Ω m); medium to coarse sandstones (81–1000 Ω m); sandstones and conglomerates (1001–6000 Ω m)	5; 20; 50 m	Vila Vila
T5	580736	8123482	4190	580822	8123360	4190	Sandstones, siltstones and clays (10–50 Ω m); sandstones and siltstones (51–550 Ω m); sandstones and conglomerates (551–9000 Ω m)	5; 7; 30 m	Sica Sica
T4	583827	8126228	4050	583696	8126303	4050	Sandstones, siltstones and clays (2–19 Ω m); clays (19–20 Ω m); siltstones (21–99 Ω m); sandstones (100–750 Ω m)	5; 10; 15; 20 m	Sica Sica
T3	583734	8126261	4050	583799	8126404	4035	Clays (1–24 Ω m); sandstones and siltstones (25–300 Ω m); sandstones (301–400 Ω m); sandstones and conglomerates (401–5400 Ω m)	15; 25; 12; 30 m	Sica Sica
T2	583722	8126366	4020	583876	8126325	4020	Medium to coarse sandstones (140–1900 Ω m); sandstones and conglomerates (1901–9000 Ω m)	20; 70 m	Vila Vila

Lithology thickness are shown according to Electrical Resistivity Tomography results, modified table from the ERT report of Micaya, Ayala (2013)

References

Agnello VN (2005) The kaolin industry in the Republic of South Africa. Office of Minerals and Energy of the Republic of South Africa, South Africa

ASTM C326-09 (2009) Standard test method for drying and firing shrinkages of ceramic whiteware clays. ASTM International, West Conshohocken. http://www.astm.org. doi:10.1520/C0326-09

ASTM D4318-10e1 (2010) Standard test methods for liquid limit, plastic limit, and plasticity index of soils. ASTM International, West Conshohocken. http://www.astm.org. doi:10.1520/D4318

ASTM C373-14 (2014) Standard test method for water absorption, bulk density, apparent porosity, and apparent specific gravity of fired whiteware products, ceramic tiles, and glass tiles. ASTM International, West Conshohocken. http://www.astm.org. doi:10.1520/C0373

Ayala R (2013) Estudio geofísico del área de Micaya, municipio de Colquencha. Departamento de La Paz mediante Tomografías geoelectricas, Edu GEO Riesgos consultant

Ayala R (2015) Estudio geofísico del área de Micaya, municipio de Colquencha. Departamento de La Paz mediante Georadar, Edu GEO Riesgos consultant

Bain JA (1971) A plasticity chart as an aid to the identification and assessment of industrial clays. Clays Miner 9(1):1–17

Blanco M, Luna I, Conde J, Crespo P, Palenque E, Cabrera S (2005) Aplicacion de recursos naturales arcillosos de la localidad de Micaya en la obtencion de productos ceramicos. Final Proceedings of the Bolivian Conference on Geology, Sucre, pp 103–107

Brown G, Brindley GW (1980) X-ray diffraction procedures for clay mineral identification. In: Brindley GW, Brown G (eds) Crystal structures of clay minerals and their X-ray identification. Miner Soc Monogr 5:305–359

Burley AJ, Cornwell JD, Tombs JMC (1978) Geophysical field techniques mineral exploration. In: Crown (ed) Mineral reconnaissance reports. Report 2, pp 1–27

Busby JP, Cuss RJ, Raines MG, Beamish D (2004) Application of ground penetrating radar to geological investigations. In: British Geological Survey (ed) Internal reports. Report IR/04/21, pp 1–42

Casagrande A (1932) Research on the Atterberg limits of soils. Public Roads 12:3 **(pp 121–30, 136)**

Chart Munsell (2009) Geological rock—color chart. Munsell Colour Press, Miami

De Oliveira AC, Malagutti W, Dourado J (2006) Resistivity (DC) method applied to aquifer protection studies. Rev Bras Geofís 24(4):573–581

El Assel N, Kchikach A, Teixidó T, Peña JA, Jaffal M, Guerin R, Lutz P, Jourani E, Amaghzaz M (2011) A ground penetrating radar and electrical resistivity tomography prospection for detecting sterile bodies in the phosphatic bearing of Sidi Chennane (Morocco). Int J Gesci 2:406–413

El-Qady G, Hafez M, Abdalla AM, Ushijima K (2005) Imaging subsurface cavities using geoelectric tomography and ground-penetrating radar. J Cave Karst Stud 67(3):174–181

Escobar DA, Bellot J, Jurado AE (1999) Minerales y rocas industriales. In: Riera KC, Troëng B, Diaz ME, Jurado AE (eds) Integrated studies of the mineral resources of Bolivia. La Paz and Copacabana geological sheet. Geological Survey of Bolivia. Bulletin 22:47–74

GEOBOL (1995) Carta Geológica Calamarca No. 5943. Escala 1:100000, Servicio Geológico de Bolivia (GEOBOL) and Geological Swedish AB (eds)

IBNORCA (2014) Catálogo de Normas Bolivianas. NB/ISO 10545-4:2005 Baldosas cerámicas—Determinación de la resistencia a la flexión y de la carga de rotura (correspondiente a la norma ISO 10545-4:1995)

ISO 10545-4:2014 (2014) Ceramic tiles—part 4. Determination of modulus of rupture and breaking strength. ICS:91.100.23

Jacob RE, Mitha VR, Macpherson D (2004) The kaolinitic clay deposits on Beaconsfield, north of Grahamstown. S Afr J Sci 100:560–564

János F (2009) Mineral exploration. Development of basic earth science specialization—TÁMOP, report 4.1.2-08/1/A-2009-0033

Keller WD (1982) Kaolin—a most diverse rock in genesis, texture, physical properties, and uses. Geol Soc Am Bull 93:27–36

Keller WD (1985) The nascence of clay minerals. Clays Clay Miner 33:161–172

Kumar D (2012) Efficacy of electrical resistivity tomography technique in mapping shallow surface anomaly. J Geol Soc India 80:304–307

Manju CS, Narayanan Nair V, Lalithambika M (2001) Mineralogy, geochemistry and utilization: study of the Madayi kaolin deposit, North Kerala, India. Clays Clay Miner 49(4):355–369

Martinez C, Vargas E (1990) Sobre Las Deformaciones Sin-Sedimentarias Mesozoicas De La Región De Macha–Pocoata–Colquechaca, Norte De Potosí Cordillera Oriental De Bolivia. Rev Técnica YPFB 11:13–20

McCuistion J, Wilson I (2006) Industrial minerals & rocks. In: Kogel J, Trivedi N, Barker J, Krukowski S (eds) Ball clays. Society for Mining, and Exploration Inc, pp 343–356

Mooney JF (1996) Industrial minerals and their uses: a handbook & formulary. Noyes Publication, New Jersey, pp 467–481

Moore D, Reynolds R (1997) X-ray diffraction and the identification and analysis of clay minerals. Oxford University Press, Oxford **371 p**

Murray HH (1988) Kaolin minerals: their genesis and occurrences. In: Bailey SW (ed) Reviews in mineralogy, hydrous phyllosilicates. Mineralogical Society of America Publication no. 19

Murray HH, Keller DW (1993) Kaolins, kaolins and kaolins; In Kaolin genesis and utilization. Special publication no. 1. The Clay Minerals Society, pp 1–24

Murray HH, Smith JM (1973) The geology and mineralogy of the Grahamstown, South Africa kaolin deposit. In: Programs and abstracts, 22nd annual clays minerals conference, Clay Minerals Society

Orris JG, Asher-Bolider S, Soria EE, Enriquez RR, Bailey AE (1992) Laguna colorada. In: Cox PD, Carrasco R, Andre RO, Hinojosa VA, Long RL (eds) Cooper deposits in sedimentary rocks. United States Government Press office, pp 201–202

Panek T, Hradecky J, Silhan K (2006) Application of electrical resistivity tomography (ERT) in the study of various types of slope deformations in anisotropic bedrock: case studies from Flysch Carpathians. Stud Geomorphol Carpatho Balc, XLII, pp 57–73

Kretz R (1983) Symbols for rock-forming minerals. Am Miner 68:277–279

Redwood D (1986) Epithermal precious and base metal mineralization and related magmatism of the Northern Altiplano, Bolivia. Ph.D. thesis, University of Aberdeen

Rietveld HM (1969) A profile refinement method for nuclear and magnetic structures. J Appl Crystallogr 2(2):65–71

Sanfeliu T, Jordan MM (2009) Geological and environmental management of ceramic clay quarries: a review. Environ Geol 57:1613–1618

Sanner B, Abbas MA (1998) How can geophysical exploration help to determine GSHP ground properties?. The second Stockton international geothermal conference, New Jersey, p 10

Soria Flores A (1980) Estudio hidrogeológico del area Viacha, Surusaya y Villa Remedios. Tesis de Grado, Universidad Mayor de San Andrés, La Paz

Stoch L, Sikora W (1976) Transformation of mica in the process of kaolinization of granites and gneisses. Clays Clay Miner 24:156–162

Virta LR (2012) Clays. In: U.S. Geological Survey (ed) Mineral commodity summaries, USGS, Virginia, pp 44–45

Watson K, Fitterman D, Saltus RW, McCafferty A, Swayze G, Church S, Smith K, Goldhaber M, Robson S, McMahon P (2001) Application of geophysical techniques to minerals-related environmental problems. In: U.S. Geological Survey (ed) Open file report 01-458, USGS

Zeballos A, Blanco M, Machaca V (2009) Caracterización mineralógica y fisicoquímica de una lutita blanca de la Localidad de Micaya, La Paz. Final proceedings of the Bolivian conference of geology, Potosi, pp 102–106

PAPER II

Pegmatite and megacrystic granite as a source of feldspar for ceramic applications in Bolivia

Ariana Zeballos, Vladimir Machaca, Mario Blanco and Pär Weihed

Manuscript

(2018)

Pegmatite and megacrystic granite as a source of feldspar for ceramic applications in Bolivia

Ariana Zeballos[a,b], Vladimir Machaca[b], Mario Blanco[b] and Pär Weihed[a]

[a] *Department of Civil, Environmental and Natural Resources Engineering. Division of Geoscience , Luleå University of Technology, 971 87 Luleå, Sweden*

[b] *Instituto de Geología y del Medio Ambiente, Universidad Mayor de San Andrés, La Paz, Bolivia*

ABSTRACT

This paper characterizes and determines new sources of feldspars for ceramic applications in Bolivia. The Choquetanga and La Fabulosa areas are situated in the Eastern Cordillera, and are associated to the Bolivian tin belt. The Bolivian tin belt contain deposits that have been mined almost continuously since the 19th century for their W-Sn content. The present study shows the potential of these deposits as sources for feldspar used as raw materials for ceramic production.

Domestic production of feldspar for ceramic applications is currently lacking in Bolivia. Mineralogical and lithogeochemical analyses on thirty rock samples indicate an alkali content of 7.84–10.25 wt.% for the Choquetanga deposit and 7.41–14.25 wt.% for the La Fabulosa deposit. Normative mineral composition are similar to feldspar deposits exploited globally. The iron content of 0.95–3.51 wt.% for the Choquetanga deposit and 0.50–1.27 wt.% for the La Fabulosa deposit, together with a calcium content of 0.52–1.79 wt.% for the Choquetanga deposit and <0.10–0.90 wt.% for the La Fabulosa deposit shows suitability for ceramic aplications. These results along with preliminary results of ceramic tests on nine ceramic specimens (clay + feldspar), such as drying shrinkage (choq 4.30 vol.% and fab 3.84 vol.%), firing shrinkage (choq 2.16 vol.% and fab 3.49 vol.%), bending strength (choq 66.40 N/mm^2 and fab 72.13 N/mm^2) and Mohs hardness (around 7), indicate that both deposits would be suitable for feldspar exploitation. This along with easy access to the deposits indicate their potential for producing raw material for tile ceramic applications and generating economic growth in the studied areas.

Keywords: Granitic rocks, feldspars, K_2O + Na_2O, tile ceramics.

1. INTRODUCTION

The consumption of industrial minerals has increased globally in the last years and new mineral resources to be used as raw materials in future industrial applications are important to define. According to Parker (2008), the non-metallic mineral consumption is increasing and new materials are being developed in order to substitute for metals in various industrial applications. One of the largest industries to substitute metals is the ceramics industry where aplites, alaskites, granites, sands, and pegmatites are commonly regarded as the sources of feldspar (Potter, 2006). Several companies globally are currently extracting feldspathic materials from granitic rocks.

The ceramic industry in Bolivia has been growing in the last few years. Consequently, the non-metallic mineral consumption, i.e. feldspars and clays, used as raw materials in this industry, has also shown a significant growth. However, these raw materials are at present imported from adjacent countries such as Brazil and Argentina.

Intrusive rocks of the Bolivian Eastern Cordillera have been explored for metallic mineral resources such as gold, silver, lead, tungsten and tin since the last century. In 1929, the export of Bolivian tin reached 47000 t (Villalpando, 1988). The same minerals that can constitute non-metallic mineral deposits (e.g. clays, feldspars and quartz) occur as a gangue to the metallic ores. Recently, new legislation and mining policies in Bolivia opened up for more non-metallic mineral exploration and exploitations as a compliment to traditional metallic mineral deposit exploration and extraction.

Ceramic tiles, which are the end product of feldspars studied in this paper, are thin slabs made from clays, silica, fluxes (feldspars), colouring materials and other raw materials. They are mostly used as covering for floors, walls and façades (Moharem and Alla Eldin, 2007). The floor tile named "Loza" is prepared by dry pressing and is basically composed of white clays (50–70 vol.%), quartz (30–45 vol.%) and feldspar (5–25 vol.%) (Gonzales, 2003) and this particular floor tile will be the final ceramic product of the raw materials studied in this paper.

The discovery of promising alkali (K_2O+Na_2O) resources in two granitic rocks in the Eastern Cordillera area defines a new target for the non-metallic mineral exploration and more theoretical knowledge about deposits of non-metallic resources is called for. The aim of this study is to assess the potential of these two occurrences as sources of feldspars for ceramic applications. This is done by characterization of feldspar-bearing rocks using petrographic studies, lithogeochemical analysis using inductively coupled plasma–mass spectrometry (ICP-MS) and technical tests such as linear and firing shrinkage, bending strength and Mohs hardness value.

1.1. Review of global feldspar production

United States is the world's leading exporter of feldspars with many occurrences located south-east of North Carolina, such as Spruce Pine, Chalk Mountain and Green County. Spruce Pine is an alaskite and coarse-grained pegmatitic granite occurrence composed mainly of feldspars, making up 65% by volume of the total bulk rock comprising 8.5–9 wt.% in alkali content (Reed, 2004). In Chalk Mountain the igneous rock contains >50 wt.% feldspar (Reed, 2004). In Green county the Monticello granite has a feldspar content of 13.5 wt.%, and in the Jasper county the feldspar (13.6 wt.%) is mined from a granite (Potter, 2006). Another feldspar source in the United States is the Shadydale granite (Georgia) which displays a ΣK_2O+Na_2O=8.3 wt.%, and is processed in a plant to produce high-grade potassium feldspar (Potter, 2006). The Thatuna granodioritic batholith. In Idaho, north-west of United States is another source of feldspar with a significant Na_2O (4 wt.%) content and a total alkali content of 5 - 8 wt.% and around 1 wt.% of Fe_2O_3 (Browne, 2006).

In Italy, an aplite mined by Maffei contains a modal composition of 20 % sodium feldspar, 40 % potassium feldspar, 30% quartz and 10% other minerals. The end use includes floor and wall tile, glass, sanitary ware and table ware (Potter, 2006). In Uzbekistan, the Lyangar mine produces feldspars with 8.56 wt.% of alkali content, which are suitable for the manufacturing of high-voltage insulators, high-strength abrasive goods and fine ceramics (Kuzovlev et al., 1975).

South east of Australia two localities are the main target for feldsphatic materials: 1) The Oberon mining district which hosts resource of feldspar from the Rossdhu Granite, which is compositionally an alaskite and consists of quartz, feldspar and muscovite, with accessory garnet, magnetite, apatite, pyrite and zircon. The average total iron ($FeO+Fe_2O_3$) is low (0.5–0.9 wt.%) and the total alkali (K_2O+Na_2O) content is 8.0–8.5 wt.% (Hughes, 2006); 2) The mining district of Broken Hill Block, where pegmatite deposits are widespread (Lishmund, 1982), includes some large deposits of intermixed pegmatite and leucocratic quartz-feldspathic rock up to 10 km long, several kilometres wide and containing 60 % feldspar (microcline and albite) and about 40 % quartz, with a variety of accessory minerals including tourmaline, garnet and muscovite (Hughes, 2006).

2. GEOLOGICAL SETTINGS AND PETROGRAPHY

The Choquetanga and La Fabulosa areas are situated in the Eastern Cordillera of the Bolivian tin belt (Fig. 1) where physical and climatic conditions are cold and wet. The current topography in the area was formed predominantly by glacial processes giving rise to an alpine-type landscape with hanging valleys, cirques, arêtes and glacial lakes (Centellas, 1989). The annual precipitation is less than 700 mm/year (Andressen et al., 2007).

The Choquetanga and La Fabulosa deposits have been mined for their W-Sn content almost continuously since ancient times. The metallic ores are hosted by granites, granodiorites and pegmatites, which are described below.

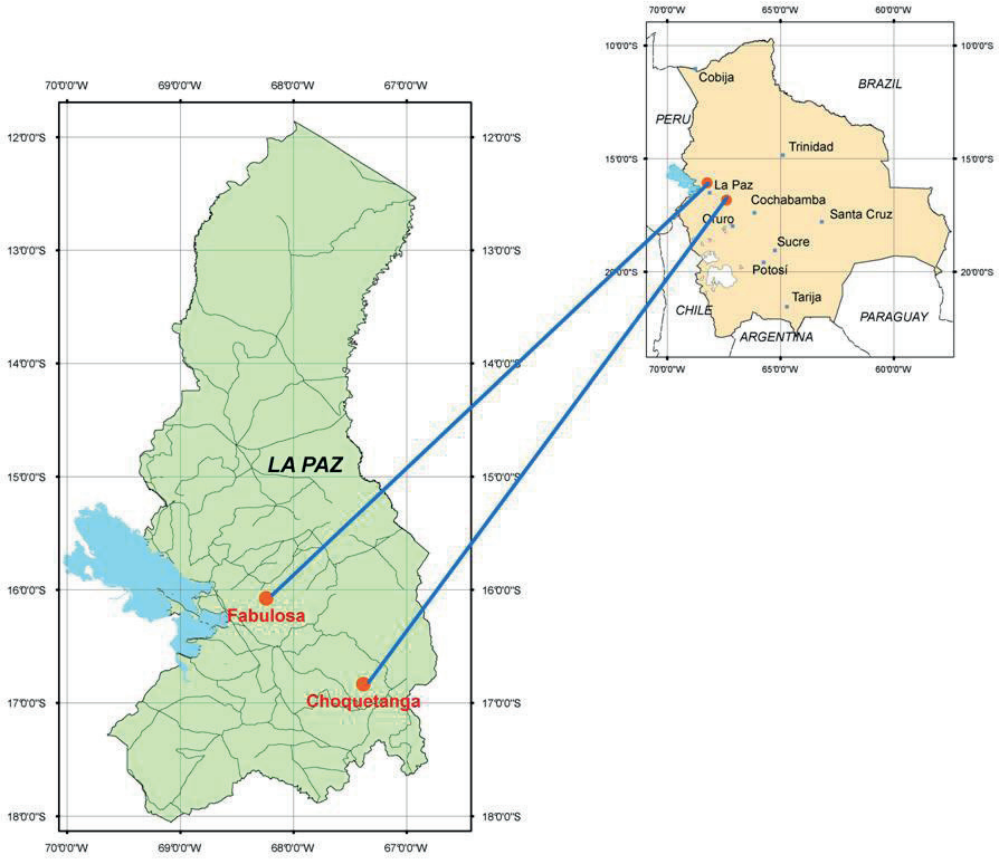

Figure 1: Location of the study areas. The Choquetanga area (67°23´00¨; 16°50´00¨) located in the Inquisivi province and La Fabulosa area (68°14´34¨; 16°04´29¨) located in the Larecaja province, both in the La Paz region, Bolivia.

2.1. Geology of the Choquetanga Area

The main sedimentary rock package in the Choquetanga area (Fig. 2) consists of Ordovician sandstone and quartzite from the Amutara formation interbedded with shales, a Silurian succession with dark diamictite of the Cancañiri formation, black shales of the Uncia formation, and quarzitic sandstones and black shales belonging to the uppermost Catavi formation. Intense physical weathering has formed colluvial deposits composed mainly of sedimentary clasts and blocks of granite which are derived from the Quimsa Cruz batholith with an aerial extension of 350 km^2, which intruded the supracrustal sequences (GEOBOL, 1995).

The Quimsa Cruz batholith is dominated by calc-alkaline porphyritic granite and granodiorite in the north (Evernden et al., 1977) and quartz-monzonite in the south (Cordero, 1967; McBride et al., 1983; Ávila, 1994). According to GEOBOL (1995) the emplacement of the Quimsa Cruz and other batholiths in the region are related to the subduction of the Nazca plate, and associated with felsic volcanic rocks. The Quimsa Cruz batholith was emplaced during post–cretaceous deformation under compressive conditions (Evernden et al., 1977; Ávila, 1994). The intrusive rocks in the north, have been dated at 25.9–23.6 Ma and those to the south at 23.3–20.7 Ma, using the K-Ar method on biotite (McBride et al., 1983).

2.2 Geology of the La Fabulosa Area

The La Fabulosa deposit is located north of La Paz City (Fig. 1); at 4400 m.a.s.l in the eastern part of the Bolivian Eastern Cordillera and in the south-eastern part of the Sorata Triassic batholith (Fig. 3). The Sorata Triassic batholith is surrounded by a metasedimentary sequence of Palaeozoic age which is characterized by rocks of the Ordovician Amutara formation, composed of grey to grey-green quartzite interbedded with sandstones and black shales. Close to the contact between the intrusive rocks and the sedimentary sequence, contact metamorphosed rocks such as meta-sandstone, schist and slate occur.

Quarternary deposits are widely distributed in the area, due to glacial processes. The glacial deposits consist mostly of till which are composed of poorly sorted and striated clasts from diverse lithologies supported by a clayey matrix. Intense physical weathering has formed colluvial deposits which are composed mainly of clasts of sandstones and igneous rocks, with blocks of granites (up to 8 m in diameter). Due to the existence of hanging valleys and cirques, several lakes exist, which are characterized by pelitic sedimentation. The colluvial deposits are associated with these lakes (Fig. 3).

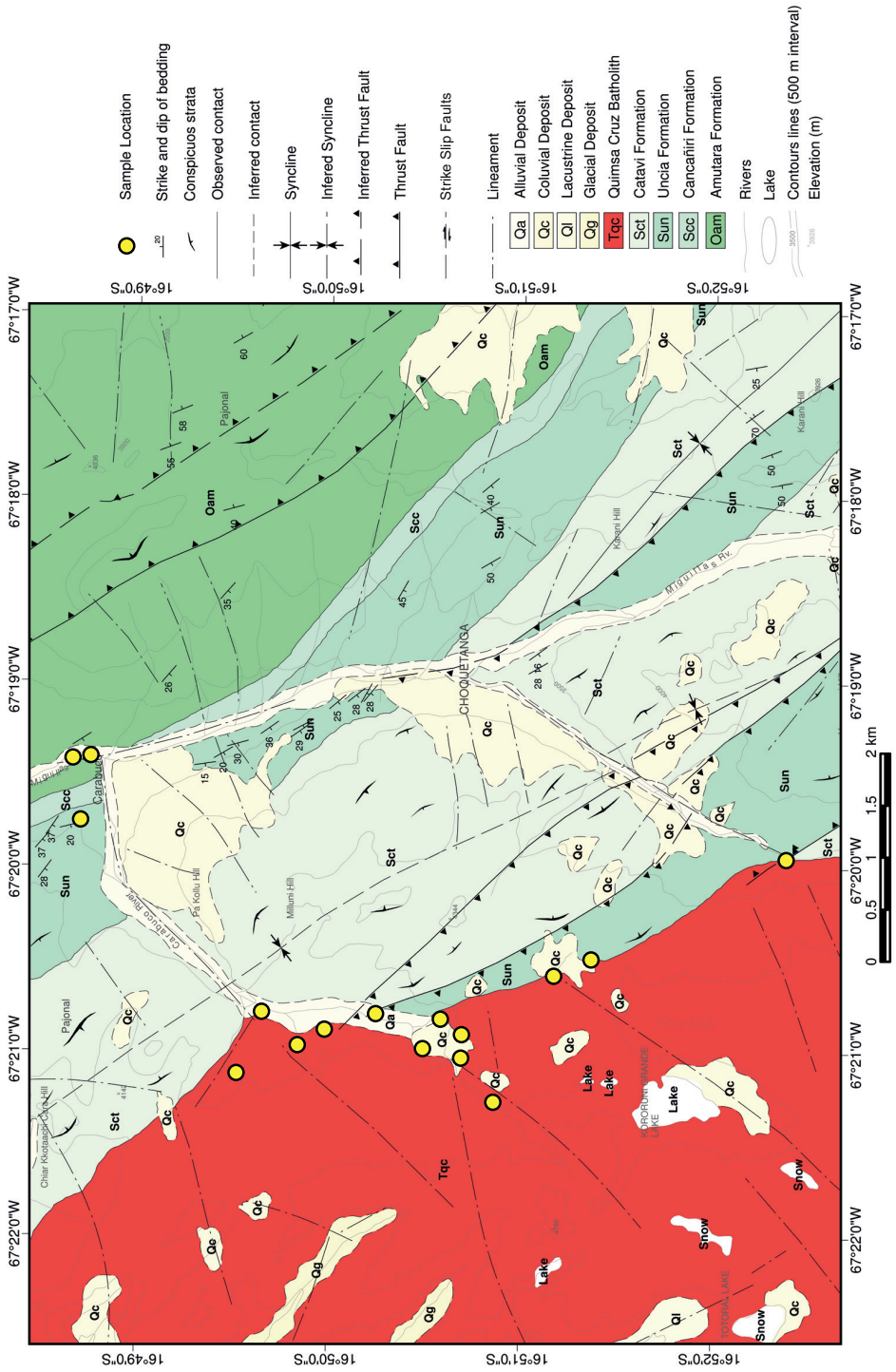

Figure 2: Geological Map of the Choquetanga area. (Modified from the Inquisivi Geological Sheet N°6143, Esc 1:100000, GEOBOL, 1995).

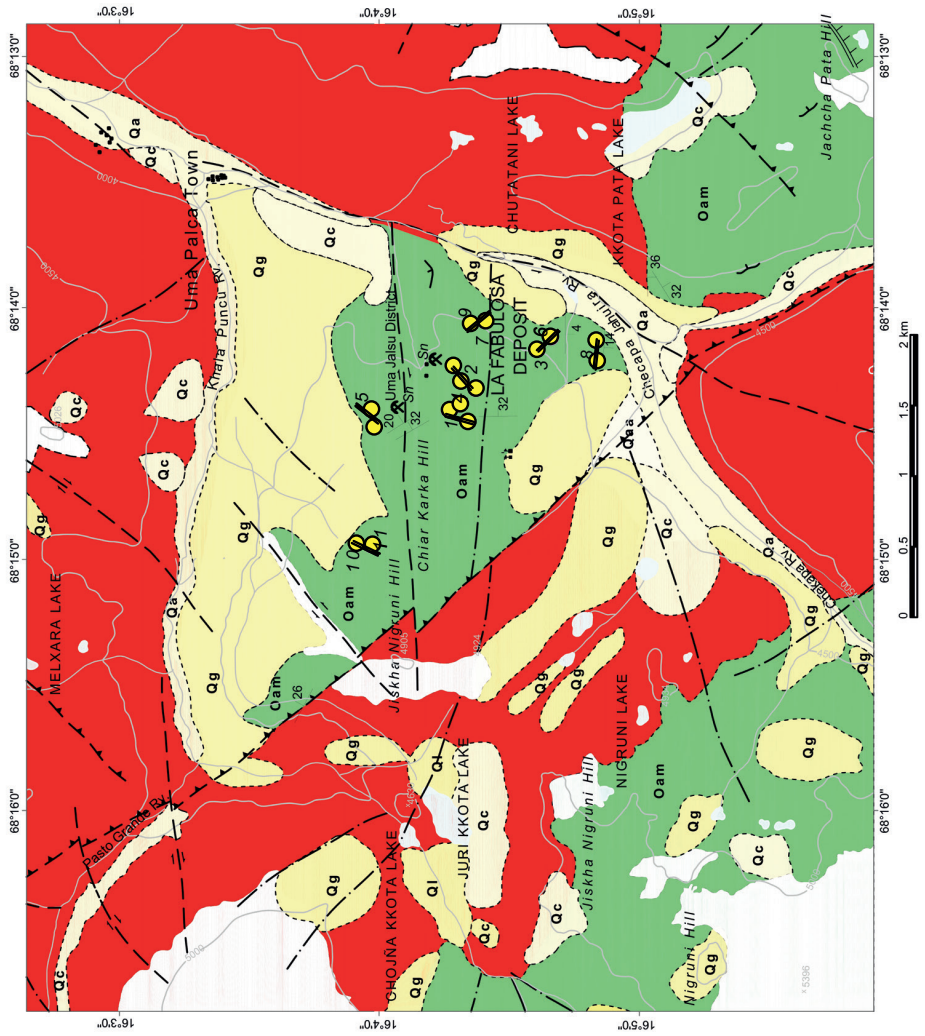

Figure 3: Geological Sheet of the La Fabulosa area. (Modified from the Milluni Geological Sheet N°5945, Esc 1:100000, GEOBOL, 1995).

The Sorata batholith comprises two-mica (muscovite and biotite) granite, muscovite granite, granodiorite and diorite and has been dated at 202–225 Ma using the K-Ar method on biotite (McBride et al., 1983). The granodiorite and diorite are hornblende-bearing and contain numerous xenoliths of sedimentary rock, aplite and leucocratic granite (Gorinova et al., 2009). The Sorata batholith is surrounded and intruded by numerous dykes and sills of pegmatite and aplite of late–magmatic origin consisting of coarse-grained feldspar, quartz, muscovite and tourmaline (GEOBOL, 1982) In the contact between the Sorata batholith and the sedimentary sequence, garnet and tourmaline are present in the metamorphic rocks (GEOBOL, 1982). According to Gorinova et al. (2009), lepidolite occurs in the pegmatite dykes in the southern part of the batholith, while in the central part, molybdenite is observed in the pegmatite dykes. A Sn-W mineralization is hosted by pegmatite in the adjacent sedimentary succession (GEOBOL, 1982).

3. METHODOLOGY

3.1. Petrography

Geological mapping was performed in both areas (Fig. 2 and Fig. 3) in order to characterize lithological units and geological features related to the feldspar deposits. Fifty unweathered igneous samples from granites and pegmatites were collected and prepared for petrographic studies. Thin sections were studied in an optical microscope with transmitted light in order to define the mineralogy and textural relationships of the feldspars as well as the modal abundance, composition and quality of the feldspar (Figs. 4 and 5)

3.2. Lithogeochemistry

Inductively coupled plasma mass spectrometry (ICP-MS) analysis of the samples was carried out at the ALS Scandinavia AB Laboratory in Luleå, Sweden. The samples were dried at 105 °C, using 0.1 g sample digested with 0.375 g $LiBO_2$ and dissolved in HNO_3. Loss on ignition (LOI) was determined gravimetrically by heating powders up to 1000 °C for 1h. Detection limits for main elements are 0.01 wt.% and detection limits for most trace elements are 1–10 ppb (table 1 and table 2). Major and trace element data were plotted in the rock classification diagram of Middlemost (1994) (Fig. 6). The total alkali content of the studied samples is herein defined as the arithmetic mean of the sum of K_2O, Na_2O and CaO, according to the lithogeochemical data (table 1 and table 2).

3.3. Physical tests

To test the quality of the feldspar material for production of floor tiles, ceramic slabs were prepared using the feldspar raw material from both deposits and were tested for ceramic tile applications. Four physical tests were performed: 1) drying shrinkage (vol.%), 2) firing shrinkage (vol.%), 3) bending strength (N/mm^2) and 4) Mohs hardness. Hardness is the resistance of a material to being scratched. The test is conducted by placing a sharp point of one specimen on an unmarked surface of another specimen and attempting to produce a scratch. This measurement was performed comparing the hardness of the ceramic specimens with the Mohs hardness table value (hardness of selected minerals). The ceramic specimens were tested according to national standard methods for ceramic tile products and were prepared according to Gonzales (2003), which states that a ceramic tile should be composed of 70 vol.% of clays + quartz and 30 vol.% of feldspars. Ceramic tile specimens were made using three raw materials: 1) a commercial ball clay, 2) a feldspathic material from the Quimsa Cruz batholith (choq), and 3) a feldspathic material from the Sorata batholith (fab). Three ceramic specimens with different mixtures of materials (table 3) were prepared and tested multiple times. The materials were mixed as follows: 1) ceramic specimen prepared by a ball clay (100 vol.%); 2) ceramic specimen prepared by a kaolinitic material (70 vol.%) + feldspathic material from the Choquetanga deposit (30 vol.%); and 3) ceramic specimen prepared by a ball clay (70 vol.%) + feldspathic material from the La Fabulosa deposit (30 vol.%).

4. RESULTS

4.1. Petrography

The samples from the Choquetanga area (Fig. 2) displays a porphyritic texture. The batholith is composed of subhedral crystals of orthoclase and microcline (5–10 cm) (Fig. 4A and 4B), rounded quartz crystals (1–2 cm) (Fig. 4A and 4C) and albite (An_8) and oligoclase (An_{11}) which are partly sericitized and show no visible intergrowths with quartz (Fig. 4C and 4D). Brown biotite crystals (iron-rich) with zircon inclusions are partly chloritized at the edges (Fig. 4D).

The La Fabulosa deposit (Fig. 3) is located in the Sorata batholith, and the studied rock samples are mainly collected from the pegmatitic dykes (Fig. 5A) which are common across the batholith (up to 0.80 m in widths and 200 m long). The batholith itself is composed of rounded grains of quartz with muscovite (Fig. 5B) and zircon inclusions in the feldspar and quartz. Petrographic studies of the pegmatites show partly sericitized oligoclase crystals (An_{15}) and slightly sericitized potassic feldspars (microcline and orthoclase) with inclusions of muscovite (Fig. 5C) and needle-shaped tourmaline crystals (Fig. 5D).

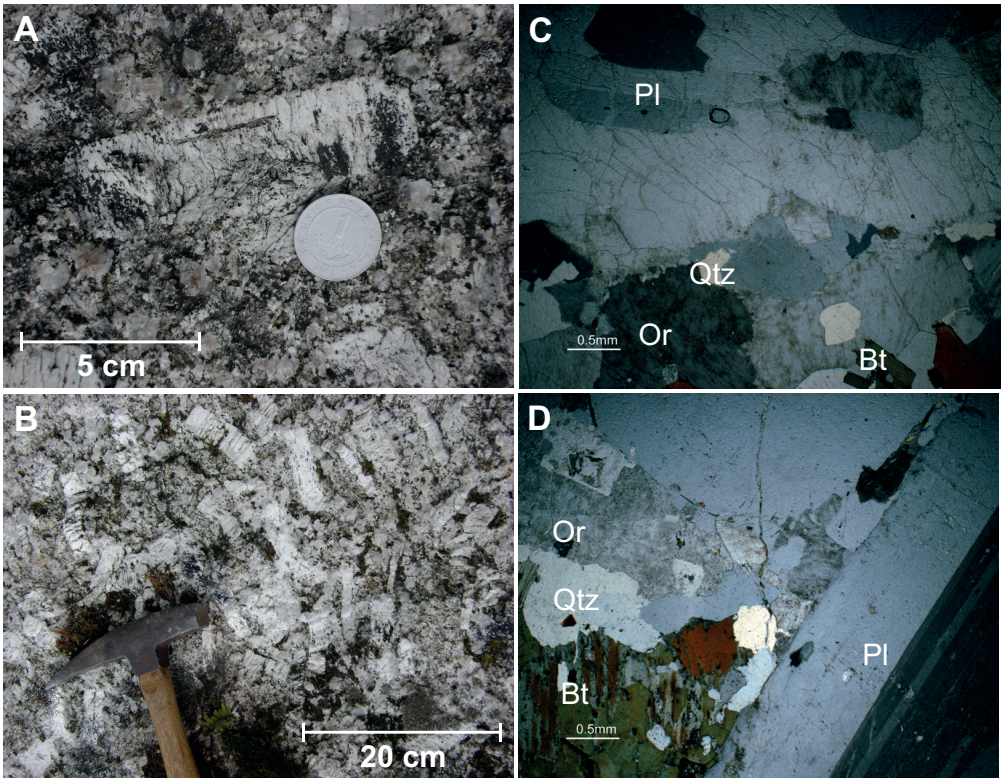

Figure 4: Photographs and micro-photographs from the Choquetanga deposit. **A)** and **B)** Photographs of feldspar-bearing granites with oriented feldspars megacrysts (5-10 cm); **C)** Plagioclase crystals, rounded grains of quartz and sericitized orthoclase crystals; **D)** Twinned plagioclase crystal and cloritized biotite (Mineral abbreviations according to Kretz, 1983)

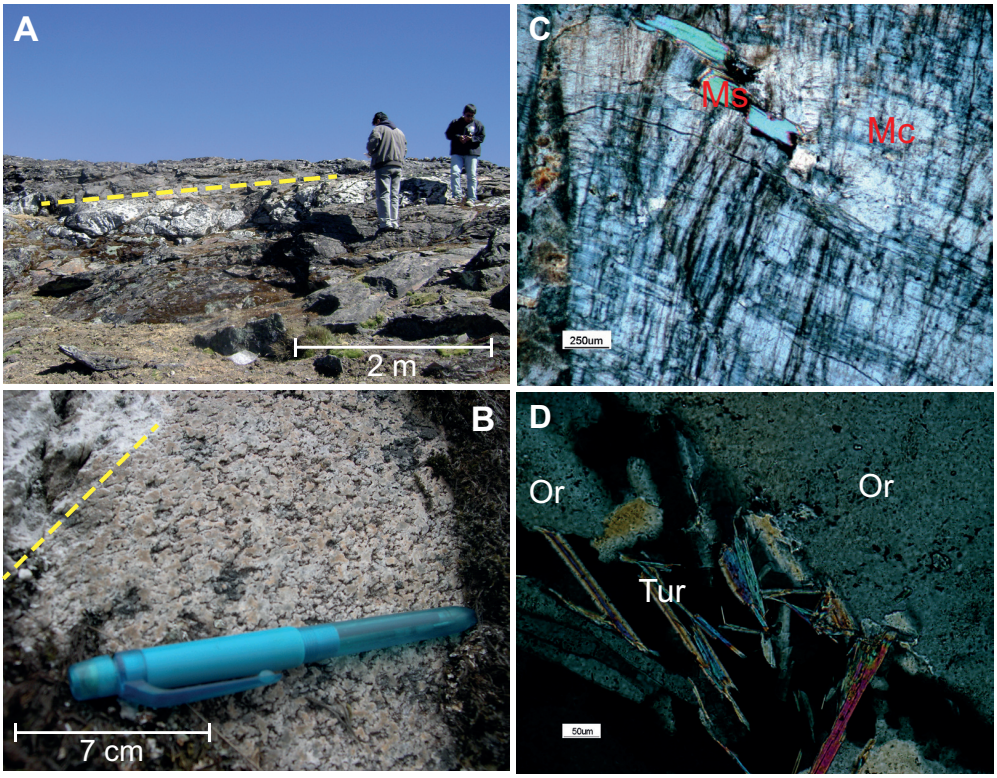

Figure 5: Photographs and micro-photographs from the La Fabulosa deposit. **A)** Pegmatite dyke **B)** Pegmatitic dykes in contact with the granitic Sorata batholith; **C)** Microcline crystal with muscovite inclusions; **D)** Needle-shaped tourmaline and sericitized orthoclase (Mineral abbreviations according to Kretz, 1983).

4.2. Lithogeochemistry

The chemical analyses show that the studied rocks are characterized by a considerable content of alkali, 7.84–10.25 wt.% (choq) and 7.41–14.25 wt.% (fab). The alkali content can be attributed to the high content of orthoclase and albite observed in the thin sections (Figs. 4 and 5) and modal analyses based on the lithogeochemical data (table 1 and table 2). The major element compositions of the rocks are shown in table 1 and table 2. According to the rock classification for igneous rocks from Middlemost (1994) the Quimsa Cruz batholit samples are classified as granites and quartz monzonite (Fig. 6). The samples from the Sorata batholith are classified as granite and syenite (Fig. 6)

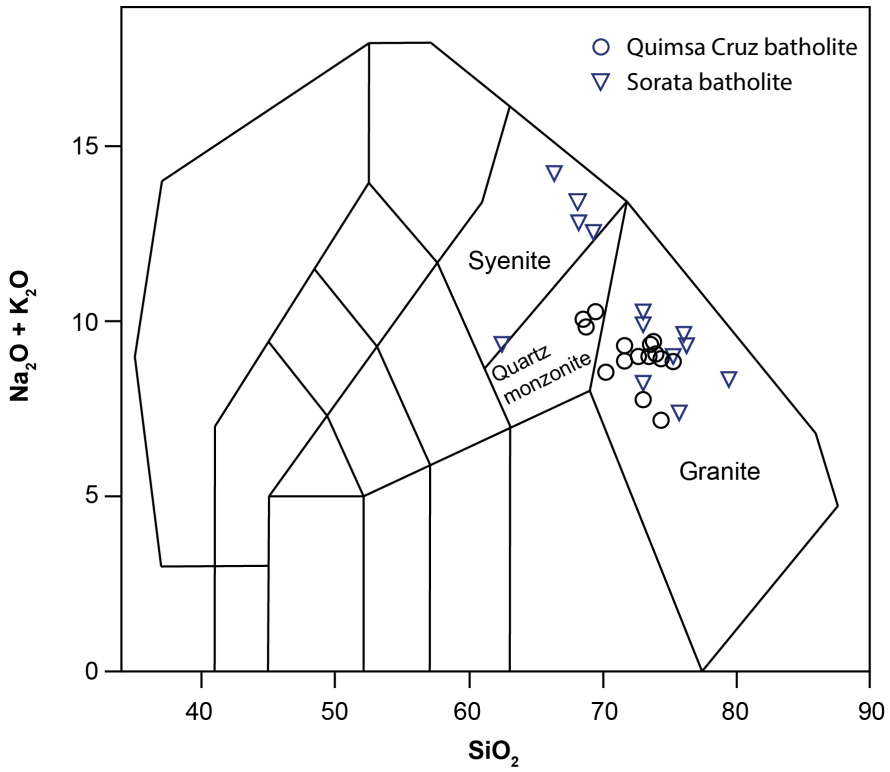

Figure 6: TAS (Total Alkali Silica) classification of igneous rocks from the Quimsa Cruz batholith and Sorata batholith samples (According to Middlemost, 1994)

Table 1: Mineralogical and chemical composition of the granite rock samples from the Quimsa Cruz batholith (Choquetanga deposit).

Chemical composition (wt.%)															
Al_2O_3	14.40	15.30	13.40	15.90	16.20	15.10	14.30	14.46	15.50	16.05	14.20	15.20	15.92	14.30	13.34
CaO	0.52	1.61	1.17	1.07	1.12	1.01	0.92	0,92	1.01	1.21	0.88	0.58	1.79	1.34	0.89
Fe_2O_3	1.70	3.51	3.50	2.28	3.33	1.29	0.95	0.95	1.32	1.19	1.24	1.25	1.75	1.63	1.06
K_2O	6.57	4.95	4.78	6.75	6.55	5.13	5.60	5.90	5.43	5.14	5.63	5.33	5.40	4.13	4.98
MgO	0.21	0.47	0.52	0.36	0.46	0.22	0.17	0.47	0.52	0.21	0.30	0.20	0.71	0.53	0.19
MnO	0.04	0.06	0.06	0.04	0.05	0.04	0.04	0.03	0.04	0.05	0.04	0.04	0.11	0.06	0.05
Na_2O	2.94	3.65	3.06	3.5	3.53	3.69	3.29	3.18	3.71	3.49	3.65	3.64	4.35	3.99	3.77
P_2O_5	0.15	0.21	0.26	0.18	0.22	0.18	0.16	0.17	0.18	0.20	0.18	0.18	0.48	0.11	0.06
TiO_2	0.09	0.33	0.37	0.26	0.30	0.30	0.09	0.09	0.12	0.14	0.11	0.11	0.70	0.25	0.14
LOI	0.50	0.40	0.30	0.50	0.30	1.10	0.90	0.84	1.10	1.30	0,9	1.00	0.85	0.29	1.56
Total	101.00	101.00	100.60	99.60	100.40	98.10	99.50	101.01	99.22	98.78	100.03	100.53	100.06	100.26	100.2
K_2O+Na_2O	9.51	8.60	7.84	10.25	8.66	8.82	8.89	9.08	9.14	8.63	9.28	8.97	9.75	8.12	8.75
Normative mineral composition (%)															
Qz	30,83	26,93	34,66	20,80	20,48	28,79	31,79	30,69	26,00	28,21	28,55	30,55	18,65	35,33	31,60
Co	1,84	1,51	1,68	1,34	1,80	2,12	1,53	1,57	2,15	3,10	0,94	2,83	0,82	2,20	0,28
Or	38,43	28,96	28,07	40,07	38,56	30,91	33,25	34,81	32,70	31,16	33,56	31,65	32,17	18,73	29,83
Ab	24,62	30,58	25,73	29,75	29,76	31,83	27,97	26,86	31,99	30,30	31,16	30,95	37,10	34,18	32,33
An	1,59	6,50	4,07	4,11	4,06	3,88	3,58	3,45	3,91	4,82	3,22	1,71	5,79	6,00	4,08
Mt	0,00	0,00	0,00	0,00	0,00	0,00	0,00	0,00	0,00	0,00	0,00	0,00	0,00	0,00	0,00
Hy	0,52	1,15	1,29	0,91	1,15	0,56	0,43	1,17	1,32	0,54	0,75	0,50	1,78	1,34	0,48
Il	0,09	0,13	0,13	0,10	0,12	0,09	0,08	0,06	0,09	0,11	0,09	0,09	0,24	0,13	0,11
Hm	1,68	3,48	3,48	2,29	3,32	1,32	0,96	0,95	1,35	1,22	1,25	1,26	1,76	1,65	1,07
Ru	0,05	0,26	0,31	0,21	0,25	0,08	0,05	0,06	0,08	0,09	0,07	0,07	0,58	0,19	0,09
Ap	0,35	0,51	0,62	0,45	0,54	0,45	0,38	0,40	0,43	0,49	0,43	0,43	1,15	0,26	0,14
Total	100,02	100,02	100,02	100,02	100,02	100,02	100,02	100,02	100,02	100,02	100,02	100,02	100,04	100,02	100,01
Total feldspar	64,64	66,04	57,87	73,92	72,38	66,61	64,80	65,12	68,60	66,27	67,94	64,30	75,06	58,91	66,24

Table 2: Mineralogical and chemical composition of the pegmatite rock samples from the Sorata batholith (La Fabulosa deposit).

Chemical composition (wt.%)															
	FAB-1	**FAB-2**	**FAB-3**	**FAB-4**	**FAB-5**	**FAB-6**	**FAB-7**	**FAB-8**	**FAB-9**	**FAB-10**	**FAB-11**	**FAB-12**	**FAB-13**	**FAB-14**	**FAB-15**
SiO_2	72.80	61.50	73.50	72.00	83.00	70.10	66.00	76.80	68.10	78.70	76.50	75.30	75.60	73.60	76.01
Al_2O_3	17.40	16.50	15.20	16.10	10.50	16.70	17.70	13.30	17.60	11.60	13.60	14.40	14.30	15.50	13.50
CaO	0.18	0.32	<0.10	0.28	0.29	0.18	<0.10	0.18	0.18	<0.90	<0.90	0.20	0.55	0.26	<0.90
Fe_2O_3	0.93	9.94	1.15	0.87	1.27	1.05	0.75	0.60	0.64	0.18	0.51	0.68	1.21	0.62	0.50
K_2O	2.85	7.54	5.13	7.89	1.15	10.80	12.30	7.58	10.30	6.47	6.90	6.23	4.90	7.01	6.90
MgO	<0.02	0.40	<0.02	0.04	0.07	0.02	<0.02	0.03	0.03	<0.20	<0.20	0.04	0.18	0.03	<0.20
MnO	0.04	0.10	0.24	0.03	0.04	0.02	0.01	0.02	0.02	<0.04	0.04	0.07	0.21	0.04	0.04
Na_2O	5.45	1.76	4.98	3.24	4.22	2.00	1.95	2.24	2.62	1.88	2.48	2.84	2.51	3.38	2.45
P_2O_5	0.21	0.25	0.62	0.34	0.16	0.38	0.83	0.26	0.38	0.26	0.34	0.27	0.25	0.34	0.33
TiO_2	0.01	0.08	0.00	0.00	0.02	0.00	0.00	0.01	0.01	<0.02	<0.02	0.02	0.14	0.01	<0.02
LOI	1.10	0.80	0.30	0.40	0.30	0.30	0.30	0.30	0.40	0.50	0.60	0.70	1.20	0.50	0.7
Total	99.90	98.40	100.8	100.8	100.7	101.3	98.90	101.1	99.90	99.10	100.4	100.1	99.20	100.80	99.80
K_2O+Na_2O	8.30	9.30	10.11	11.13	5.37	12.8	14.25	9.82	12.98	8.35	9.38	9.07	7.41	10.39	9.35
Normative mineral composition (%)															
Qz	30,76	31,93	26,00	22,50	48,15	9,19	14,07	31,10	24,66	36,36	26,85	35,83	36,83	30,39	34,47
Co	5,31	4,84	1,42	2,22	2,40	1,86	1,10	1,47	1,87	0,71	1,55	2,94	4,84	2,22	1,15
Or	16,73	39,61	29,54	46,40	7,51	68,89	67,91	46,56	53,03	42,25	45,37	36,26	31,36	39,12	40,69
Ab	45,81	13,24	41,06	27,28	39,45	18,27	15,42	19,70	19,32	17,58	23,35	23,66	23,00	27,01	20,69
An	0,00	0,00	0,00	0,00	0,44	0,00	0,00	0,00	0,00	2,59	1,99	0,00	1,19	0,00	2,31
Ms	0,10	0,08	0,76	0,10	0,08	0,07	0,03	0,04	0,03	0,29	0,09	0,17	0,30	0,10	0,07
Hy	0,05	0,89	0,05	0,10	0,19	0,05	0,05	0,08	0,07	1,05	0,50	0,10	0,49	0,07	0,50
Mt	0,02	0,14	0,00	0,00	0,04	0,00	0,00	0,02	0,02	0,04	0,04	0,04	0,29	0,02	0,04
Il	0,85	8,78	0,59	0,80	1,35	1,09	0,68	0,60	0,54	0,00	0,51	0,55	1,10	0,52	0,45
Hm	0,00	0,00	0,00	0,00	0,00	0,00	0,00	0,00	0,00	0,00	0,00	0,00	0,00	0,00	0,00
Ap	0,32	0,51	0,18	0,50	0,42	0,35	0,18	0,34	0,28	0,68	0,90	0,35	0,64	0,44	0,78
Total	99,96	100,02	99,61	99,89	100,02	99,75	99,43	99,89	99,80	101,55	101,15	99,90	100,03	99,88	101,15
feldspars	62,54	52,85	70,61	73,68	47,39	87,15	83,32	66,25	72,35	62,42	70,72	59,92	55,54	66,133	63,69

4.3. Physical tests

Physical test results are shown in table 3 and represents the average result of each mixture calculated by arithmetic mean of fifteen ceramic samples.

Table 3: Physical test results on the ceramic specimens according to IBNORCA (2014)

Ceramic Mixtures	Drying Shrinkage (vol.%)	Firing Shrinkage (vol.%)	Bending Strength (N/mm^2)	Mohs Hardness
Ball clays 100 vol.%	5.48	7.76	44.32	4
clay70 vol.%; Choquetanga 30 vol.%	4.30	2.16	66.40	7
clay70 vol.%;La Fabulosa 30 vol.%	3.84	3.49	72.13	7

5. DISCUSSION

According to Hughes (2006), the quality of feldspar used in the ceramic industry and the commercial potential of the source rocks depend on their alkali content (ΣK_2O+Na_2O+CaO must be 5–14 wt.%) and a low proportion of easily separated ferromagnesian minerals. A combined Na and K content of 10–15 wt.% makes it a good material to flux the body to below the required 0.50 wt.% water absorption (Galan, 2003). The studied deposits have a suitable alkali content of ΣK_2O+Na_2O+CaO=7.41–14.25 wt.% (table 1 and table 2). The chemical composition of a raw material is an important factor in the ceramic processing of tiles, and is related to the mineralogy and especially the amount of quartz, kaolinite and feldspars present in the mixture. The quartz and feldspar, which are similar in crystalline structure, are joined on firing by silicon-oxygen tetrahedra. This creates a generalized silicon-aluminum-oxygen network, which is responsible for the high mechanical strength and other technically important properties of the ware (Ismailova and Borisova, 1972). The amount of quartz in the raw material can be important as the volume of the ceramic increase during the transition of low quartz to high quartz. This physical change can occur because of the rapid transition during the firing process, and affects the final product since it may develop fractures (Schüller, 1979).

Feldspar is used as a fluxing agent to form a glassy phase for accelerating of the sintering process, and in the ceramic industry they are divided into potassium feldspars (orthoclase, microcline), sodium feldspars (albite) and calcium feldspars (anorthite) (Barth, 1969). Sintering temperature is defined as the firing temperature when water absorption of the fired body is 2 vol.%. Sokolár et al. (2017) demonstrated that among the feldspars, the most intensive fluxing agents are plagioclase, followed by potassium feldspars with a very similar fluxing effect.

The Coquetanga deposit is composed mainly of potassium feldspars such as orthoclase (32.19 %) and plagioclase such as albite and oligoclase (30.34 %), and the La Fabulosa deposit is mainly composed of potassium feldspars such as microcline and orthoclase (40.75%), whereas albite and oligoclase is observed in minor quantities (24.98%) (table 1 and table 2).

In addition to the importance of the alkali content in feldspar rocks, the content of the alkaline earth oxides CaO and MgO also play an important role in the final product quality, affecting the mechanical behaviour and colouring the final product. Increasing the lime (CaO) in the mixture leads to reaction with the metakaolin phase resulting from the phase transformation of the clay. This develops an anorthite-like composition phase formation thus promoting a glassy phase formation in the mixture (Sokolár et al., 2017). Furthermore, more lime-rich mixtures will need higher firing temperature in order to create an anorthite-like composition, which means more energy will be needed to obtain the final products (Sokolár et al., 2017). On the other hand, MgO promotes sintering in porcelain tiles, but also increase shrinkage (Ozturk and Ay, 2012). The presence of alkaline earth oxides also promotes the development of a less viscous liquid phase, which in turn reduces the open porosity, as long as it is operated within defined limits of compositions (Ozturk and Ay, 2012). Although the literature does not indicate exact limits of CaO and MgO content in the feldspathic rocks for application in floor tile ceramics, most of the companies work with a content <3 wt.% of alkali oxides (table 4; Kuzovlev et al., 1975; Reed, 2004; Potter, 2006).

The calcium content in the Choquetanga samples range from 0.52–1.79 wt.%, and <0.10 wt.% for the La Fabulosa samples. The CaO is hosted in plagioclase minerals such as anorthite and accessory minerals such as apatite. The magnesium content range from 0.17–0.71 wt.% in the Choquetanga samples to <0.02–0.20 wt.% in the La Fabulosa samples. The MgO is hosted in minerals such as pyroxene, which are present as inclusions in plagioclase crystals.

Table 4: Comparison of the chemical composition of feldspar-bearing samples from the Bolivian deposits and from international feldspar supplier companies (From Kuzovlev et al., 1975; Reed, 2004; Potter, 2006).

Chemical Composition wt. %	K_2O + Na_2O	CaO + MgO	Fe_2O_3	SiO_2	Al_2O_3
Quimsa Cruz intrusive, Bolivia	9,1	1,02	2,3	71,7	14,9
Pegmatitic occurrences, Bolivia	10,9	0,2	1.6	72,6	15,1
Spruce Pine, USA	7,6	0,9	1,6	70,2	14,5
Spruce Pine, 2nd locality, USA	8,5	0,9	0,4	74,4	15,4
Lyangar mine, Central Asia	8,56	0,88	0,19	25 - 30	----
Shadydale granite, Georgia	8,3	0,9	1,6	----	13,9
Feldspar Corp. Monticello, Green County	13,5	0,8	0,076	----	18
Feldspar Corp. Monticello, Jasper County	13,6	0,81	0,082	----	18,5
Rossdhu granite, Oberon-Autralia	8,0 - 8,5	----	0,5 - 0,9	----	----
Thatuna batholith, USA	9	----	1	----	----

The drawbacks of pegmatitic and granitic raw material are 1) the presence of impurities of iron minerals (biotite and magnetite) which contaminate the melt with dark spalls, and 2) a low K/Na ratio (Pavlunenko, 2010). The presence of iron is an important parameter in the choice of a raw material, since iron tends to colour the raw material during firing process, resulting in a red colour of the final product, thus limiting the end use of the product. Although the maximum Fe_2O_3 must be no more than 0.3 wt.%, the worldwide feldspar companies work with high iron content in the feldspatic rock (Browne, 2006; Hughes, 2006). The presence of higher amounts of Fe_2O_3 than the allowed limits may also contribute in unwanted variations of the colour towards grey rather than white (Dondi, 1994; Amaireh and Aljaradin, 2014). The chemical analysis of the studied samples indicates that the iron oxides (Fe_2O_3) content varies from 0.95–3.51 wt.% for the Choquetanga deposit and 0.50–1.27 wt.% for the La Fabulosa deposit.

In the Choquetanga deposit iron is mostly present in biotite as individual minerals and between mineral particles of quartz and feldspar. In addition hematite is present in the rock samples; and as component of mineral inclusions such as in tourmaline and along micro-fractures in quartz and feldspar such as in the La Fabulosa deposit. Biotite is the dominant host of iron in the mineral products of the studied materials. Hence, the iron minerals may need to be removed by flotation and magnetic separation (Hestnes et al., 2013; Amaireh and Aljaradin, 2014) if these materials are to be used in ceramic applications where colouration is undesired.

Swapan and Kausik (2003) have studied the densification behaviour of K- and Na-feldspars in porcelain bodies. Sodium feldspar-containing compositions exhibit high densification, which affects the bending strength of the tile product, making it brittle. At the same time, the soda feldspar reduce the firing shrinkage by the amalgamation of cavities and the production of the liquid phase in the product (Bennour et al., 2015), and therefore reduces the water absorption. On the other hand, the potash-feldspar-containing composition usually displays higher bending strength, which is related to the crystalline phase reactions during firing, as many as mineral reactions occur in the mixture, more crystalline phases will be created, increasing the bending strength (Jordan et al., 2008).

According to Uriarte (2007) and IBNORCA (NB-259-78; 2014) tiles should exceed level 4 on the Mohs scale. Shrinkage is the rate of change in length and width for inspection samples and is directly proportional to the total alkali content (Moharem and Alla Eldin, 2007).

Table 3 indicates an improvement of the physical properties, such as the firing shrinkage and bending strength, over the ball clay pure specimen when feldspar is added. The Choquetanga specimens shows better firing shrinkage (2.16 vol.%) due to the amalgamation of cavities, but lower bending strength (66.40 N/mm^2) because the brittleness of the sample. The La Fabulosa ceramic specimens shows lower firing shrinkage (3.49 vol.%) due to the viscosity of the melt which increase the porosity and yields higher bending strength (72.13 N/mm^2).

6. CONCLUSIONS

The alkali content of 7.84–10.25 wt.% for the Choquetanga deposit and 7.41–14.25 wt.% for the La Fabulosa deposit, together with an iron content of 0.95–3.51wt.% for the Choquetanga deposit and 0.50–1.27wt.% for the La Fabulosa deposit and a calcium content of 0.52–1.79 wt.% for the Choquetanga deposit and <0.10–0.90 wt.% for the La Fabulosa deposit, along with the preliminary results on the ceramic testing all indicate that the Choquetanga and La Fabulosa rocks have suitable properties to be used as raw materials in the production of floor tiles.

7. ACKNOWLEDGEMENTS

The authors thank Nils Jansson for his constructive and helpful comments. This study was supported by the Swedish International Development Cooperation Agency (SIDA). We are grateful to the Institute of Geological and Environmental Research (IGEMA), the Universidad Mayor de San Andrés in La Paz, Bolivia.

REFERENCES

Andressen LR, Monasterio M and Terceros LF (2007) Climatic regimes of the Bolivian Southern High Plateau: A region affected by desertification. Revista Geográfica Venezolana 48: 11-32.

Amaireh M and Aljaradin M (2014) Characterization of the Jordanian Feldspar Raw materials for application in the Ceramic and Glass Industries, Journ of Mining Engineering and Mineral Processing 3(2): 28-31.

Ávila SW (1994) Ambiente tectónico y parámetros geoquímicos de los granitos estanníferos bolivianos. Revista Técnica de Yacimiento Petrolíferos Fiscales Bolivianos 15: 9 – 109.

Barth TFW (1969) Feldspars (1st ed.), John Wiley & Sons Inc, 272 p.

Bennour A, Mahmoudi S, Srasra E, Boussen S and Htira N (2015) Composition, firing behaviour and ceramic properties of the Sjnène clays (Nortwest Tunisia) Journal of Applied Clay Science 115:30-38.

Browne LJ (2006) Helmer-Bovill feldspar, quartz, and kaolin mineral leases, latah county, Idaho. On behalf of i-minerals inc. Vancouver, B.C: 6, p 93.

Centellas CR (1989) Petrología metamórfica de Zongo (sector Chururaqui – Jacha Chahui). Tesis de grado, Universidad Mayor de San Andrés, La Paz – Bolivia, p 130.

Cordero G (1967) Estudio metalogenético del área Quime - Choquetanga Grande. Bull. Informe Técnico, SERGEOTECMIN.

Dondi M (1994) Compositional Parameters to evaluate feldspathic fluxes for ceramic tiles. Tile & Brick International 10: 77-84.

Evernden JF, Kriz S and Cherroni C (1977) Potassium – Argon Ages of Some Bolivian Rocks. Economic geology and the bulletin of the society of Economic Geologist, 72:1042 – 1061.

Galán HE (2003) Mineralogía Aplicada. 1st ed. Madrid: Síntesis, 399 p.

GEOBOL (1982) Proyecto mina Fabulosa, etapas "B y C". Bull. Geol. Survey of Bolivia, N° 5.

GEOBOL (1995) Carta geológica de Bolivia hoja Inquisivi Nº 6143. Escala 1:100.000, Servicio Geológico de Bolivia (GEOBOL) and Geological Swedish AB (eds).

GEOBOL (1995) Carta geológica de Bolivia hoja Mulluni Nº 5945. Escala 1:100.000, Servicio Geológico de Bolivia (GEOBOL) and Geological Swedish AB (eds).

Gonzales DI (2003) Arcillas cerámicas de construcción y cerámica fina: Impacto ambiental provocado por su extracción. In: Mineralogía Aplicada de Emilio Galán Huertos. Madrid: Editorial Sintesis S.A.
pp 83-104.

Gorinova E, Jimenez ChN, Tornos F, Chambi O, Aruquipa F (2009) Estudio petrológico preliminar de los granitoides de edad mesozoica del segmento norte de la Cordillera Oriental Boliviana. Congreso Geológico Boliviano, Potosí XVIII: 271 – 274.

Hestnes KH, Aasly K, Sandøy R and Sørensen (2013) Occurrence of iron in industrial granitic pegmatite Minerals Engineering 52: 21-30.

Hughes W (2006) Minerals and metals availability in New South Wales Australia. New Department of Primary industries. 1st ed. Australia 58 p.

Instituto Boliviano de Normalización y Calidad (IBNORCA) Norma boliviana NB-259-78, azulejos cerámicos Dirección General de Normas y Tecnología – Bolivia, Ministerio de Industria y Comercio, 14 p.

Instituto Boliviano de Normalización y Calidad (IBNORCA) (2014) Catálogo de Normas Bolivianas. NB/ISO 10545-4:2005 Baldosas cerámicas— Determinación de la resistencia a la flexión y de la carga de rotura (correspondiente a la norma ISO 10545-4:1995 - NB-259-78) Dirección General de Normas y Tecnología – Bolivia, Ministerio de Industria y Comercio, 14 p.

Ismailova MA and Borisova Kh B (1972) Low temperature bodies for ceramic tile Journal of Glass and Ceramics 29(8):535-536.

Jordan MM, Montero MA, Meseguer S and Sanfeliu T (2008) Influence of firing temperature and mineralogical composition on bending strength and porosity of ceramic tile bodies Journal of Applied Clay Science 42(1):266-271.

Kretz R (1983) Symbols for Rock-Forming Minerals. Am Miner 68: 277-279.

Kuzovlev KA, Ibadullaev IS, Kailinkin IV, Gabelko BA (1975) The economic effectiveness of a complex beneficiation of feldspar and quartz sands from the Kermin Seam. Russia, 835-837.

Lishmund SR (1982) Non-metallic and Tin Deposits of the Broken Hill District. New South Wales Bull: Geol. Survey New South Wales Bull 28.

McBride LS, Robertson RCR, Clark AH and Farrar E (1983) Magmatic and metallogenetic episodes in the northern tin belt, Cordillera Real, Bolivia. Geologische Rundschau 72:685 – 713.

Middlemost E A K (1994) Naming materials in magma/igneous rock system. Earth Sci. Rev 37: 215–224.

Moharem AF and Alla Eldin M S (2007) Properties and suitability of Wadi Zarieb Feldspars for ceramic industries in Egypt. Journal of Applied Science 7 (19): 2794 – 2799.

Ozturk ZB and Ay N (2012) An investigation of the effect ok alkaline oxides on porcelain tiles using factorial design Journal of Ceramic Processing Research 13(5): 635 – 640.

Parker P M (2008) The Worldwide market potential. In: The 2009-2014 World Outlook for Non-Metallic Mineral Mining and Quarrying. San Diego: ICON Group International, inc p 17-18.

Pavlunenko LE (2010) Feldspar materials in Ukraine-Raw Materials. Journal of Steklo I keramika 7:20-23.

Potter J M (2006) Industrial Minerals & Rocks. In: Kogel J., Trivedi N., Barker J. and Krukowski S, editors. Feldspars: Society for Mining, and Exploration Inc p 451-460.

Reed, R M (2004) Rob's granite page. http://uts.cc.utexas.edu/~rmr/.

Sokolár R, Keršnerová L and Šveda M (2017) The effect of different fluxing agents on the sintering of dry pressed porcelain bodies Journal of Asian ceramic Societies 5(3): 290 – 294.

Schüller KH (1979) Porcelain. Ceramic Monographs: A Handbook of Ceramic. Verlag Schmidt GMBH. Freiburg.

Swapan KD and Kausik D (2003) Differences in densification behaviour of K- and Na-feldspar-containing porcelain bodies Thermochimica Acta 406:199-206

Uriarte (2007) Estudio de las características físico – mecánicas de las baldosas cerámicas que se fabrican y ofertan en el mercado nacional. Revista del Instituto de Ensayo de Materiales. Carrera de Ingeniería Civil – UMSA. Año 2, N-2, pp 29 – 40.

Villalpando M J (1988) The tin ore deposits of Bolivia. In: Hutchison, C S. (eds) Geology of Tin Deposits in Asia and the Pacific. Springer, Berlin, Heidelberg, pp 201-215.

PAPER III

Application of a kaolinite-bearing sediment for industrial purposes in Bolivia

Ariana Zeballos, Vladimir Machaca, Mario Blanco and Christina Wanhainen

Manuscript

(2018)

Application of a kaolinite-bearing sediment for industrial purposes in Bolivia

[a,b]Ariana Zeballos, [b]Vladimir Machaca, [b]Mario Blanco and [a]Christina Wanhainen

[a] Department of Civil, Environmental and Natural Resources Engineering. Division of Geoscience, Luleå University of Technology, 971 87 Luleå, Sweden

[b]Instituto de Geología y del Medio Ambiente, Universidad Mayor de San Andrés, La Paz, Bolivia

ABSTRACT

An assessment of the possible application of Bolivian raw materials, such as kaolinite-bearing sediments, feldspars and low-grade synthetic mullite in the traditional ceramic industry was carried out based on the mineralogical and chemical properties of the raw material and the mineralogical and physical properties of the resultant ceramic slabs, which were porcelain stoneware enhanced by low-grade mullite.

Technical properties such as suitable composition (70 vol.% kaolinite-bearing sediment and 30 vol.% feldspar) and physical properties such as drying shrinkage (Choquetanga 0.20 vol.%, La Fabulosa 0.31 vol.%), firing shrinkage (Choquetanga 1.66 vol.%, La Fabulosa 1.59 vol.%), bending strength (Choquetanga 69.55 N/mm^2, La Fabulosa 70.20 N/mm^2), water absorption (Choquetanga 2.13 vol.%, La Fabulosa 0.58 vol.%) and Mohs hardness value of 7 of the traditional ceramic slabs show a potential for applications of the studied material. A comparison was made with the most popular floor tiles commercially marketed in Bolivia, and the physical properties of these commercial products were used as a reference for the suitability of the studied materials in ceramic products. In addition acicular crystals of low-grade mullite ($Al_2O_32SiO_2$) were obtained as a result of the dehydroxylation of the fired kaolinite-bearing sediment at 1250°C in a ramp/hold programme, through slow cooling. The phase transformation were investigated using X-ray diffraction, scanning electron microscopy and differential thermal and thermogravimetric analyses.

1. INTRODUCTION

The ceramic industry uses a wide variety of specifications, manufacturing methods, moulding and firing processes (Enrique and Amorós, 1985), which are listed in table 1. The physical and technical specifications used depend on the type of final product and are related to international standards, and defined by the International Organization for Standardization (NB/ISO 10545-3:1995, NB/ISO 10545-4:2004). The physical and technical specifications of the National Certification and Standardization Organization (IBNORCA, 2014), refer specifically to the testing of Bolivian ceramic tiles.

Table 1: Classification of Ceramic Materials (Gonzales, 2003, modified from Enrique and Amorós, 1985).

Type of Ceramic Material	Coating	Colour	Type of end product	Application	Firing Temperature	Raw Materials
Porous (Classic)	No coating	Coloured	Construction material	Bricks and roof tiles	900°C–1000°C	Calcareous marls, clay marls, calcareous clay-ferruginous
			Refractory	Refractory bricks	--------	Refractory clay, Al oxides, quartzite, magnetite, graphite, Zr, Cr, etc.
		White	Loza	Refractory bricks, Tableware and filters	1200°C – 1250°C	Whitish Clays
	With Coating	Coloured	Majolica	Tableware, faience mosaic	920°C–980°C	Calcareous clay and ferruginous clay
		White	Loza	Tableware, faience mosaic	900°C–1280°C	Whitish clays with feldspar, quartz and carbonate
Non Porous (Advanced)	No coating	Coloured	Gres	Red faience mosaic	950°C–1100°C	Whitish clays with feldspar and quartz
		White	Porcelain	Dental applications	1200°C	Kaolinitic and feldspathic clays
	With Coating	Coloured	Gres	Faience mosaic, resistant to chemical attack	1100°C–1300°C	Whitish clays with feldspar and quartz
		White	Porcelain	Insulating membranes of high and low voltage	1200°C–1600°C	Kaolinitic clays with quartz and feldspars, and refractory materials

Ceramic tiles are thin slabs made from clays, silica, fluxes (feldspars), colouring materials and other raw materials. They are used as covering for floors, walls and façades (Moharem and Alla Eldin, 2007). In general, the ceramic process passes through seven successive stages: (1) dressing of raw materials, (2) batching, (3) grinding, (4) pressing, (5) glaze processing, (6) standardizing relating to ceramic tiles and (7) firing (Moharem and Alla Eldin, 2007). During the firing process, a series of transformations that will govern the final properties of the ceramic products occurs (González et al., 1990).

Ceramic stoneware is an opaque vitreous mass, formed by high-plasticity and high-strength clays (Dondi et al., 1999). The ceramic properties of clay materials vary with the mineral composition of the clay and properties such as particle size distribution, presence of organic material, and non-clay mineral composition (e.g. iron content). Knowledge of the origin, diagenesis and physicochemical composition of the raw material is thus essential when designing suitable compositions for ceramic products (Sanfeliu and Jordan, 2009). Kaolinite is the most important clay mineral used in ceramic applications because of its colour and plasticity. These properties are imparted to the finished products through ceramic processing (Murray, 1988; Murray and Keller, 1993; Murray, 2007; King, 2009). Feldspars provide both alkali content and alumina and are used in the fine ceramic industry as a flux to form a glassy phase in the ceramic body, thus promoting vitrification and translucency (Potter, 2006). Potassium feldspar (orthoclase and microcline) increases the translucency, and provides good bending strength. Sodium feldspar (albite) lower the melting point of the mixture (Rodas, 2003; Potter, 2006), saving energy during firing.

The mineral mullite has the nominal chemical composition $3Al_2O_32SiO_2$, and its name is derived from the Isle of Mull outside of Scotland. It crystallizes in the orthorhombic system, has a very high melting point (1840°C) and is very scarce in nature. Mullite is widely used in the production of refractory materials; therefore it is necessary to optimize the synthesis process to produce marketable mullite at a low cost. The general transformation required for the production of mullite from pure kaolinite is as follows:

kaolinite – metakaolinite – spinel phase – primary mullite – mullite

Mullite displays excellent thermal properties in ceramic bodies by: 1) improving the thermal shock of ceramic bodies due to its low thermal expansion and 2) improving the resistance of the material after firing. The main uses of mullite include fabrication of porcelain refractory, refractory bricks, electrical insulators and pipe protectors. Triaxial porcelains acquire significant hardness and strength properties through mullite formation during calcination as a result of vitrification (Lu et al., 2004).

Since mullite formation mechanisms are strongly affected by the constitution and structure of its precursors, knowledge of their temperature-dependent development allows us to design the microstructure and properties of the final mullite to be used in ceramic applications. For example, mullite ceramics designated for structural applications at moderate temperatures should have a microstructure with small crystal sizes and a minimum number of pores, while small amounts of a glassy phase may be acceptable. In contrast, mullite for high-temperature structural applications must be glass-free, and a greater crystal size is favoured (Schneider and Komarneni, 2005). Various raw materials and preparation methods have been investigated in the production of sintered mullite, fused mullite and chemical mullite (Chen et al., 2004).

The aim of this study is to find new industrial applications of a kaolinite from a Bolivian clay deposit (Fig. 1). The raw material from this deposit is currently used in pottery and tableware. This research is intended to generate alternative jobs in Micaya, where the deposit is located (Zeballos et al., 2016), generating higher added-value products from the natural resources in the area. In this way, the results of this study will contribute to the development of the Bolivian ceramic industry, with porcelain stoneware, enhanced by mullite formation being produced by Bolivian natural raw materials such as clays and feldspars.

2. MATERIALS AND METHODS

2.1. Sample preparation for porcelain stoneware

For the definition of the technical specifications, three raw materials have been used for the preparation of ceramic slabs (Fig. 2). These raw materials have been mineralogically (Fig. 2) and chemically characterized (table 2) in previous studies and are as follows: 1) a kaolinite-bearing sediment from Micaya, composed of quartz, muscovite, and kaolinite, as well as small amounts of feldspar (Fig. 2; Zeballos et al., 2016), 2) a feldspar mixture (orthoclase-albite) from the Choquetanga deposit (Zeballos et al., 2012), and 3) a feldspar mixture (orthoclase-oligoclase) from the La Fabulosa deposit (Zeballos et al., 2012). The feldspar separation from the host rock was carried out at the Institute of Geological Research in La Paz, Bolivia (IGEMA). The raw materials were first dried and wet ground (with a jaw crusher and porcelain grinder for 4 h to -350 mesh). The resulting powders were mixed and humidified, with a moisture content of 8.25 wt.%, and then pressed at 18 MPa into 80.2 x 31.6 x 6.20 $\pm$ 1.0 mm bars. Five sets of ceramic specimens using the kaolinite-bearing material from the Micaya deposit and the feldspars from the Choquetanga (choq) and La Fabulosa (fab) deposit were prepared. Each mixture was prepared as follows: a) three ceramic

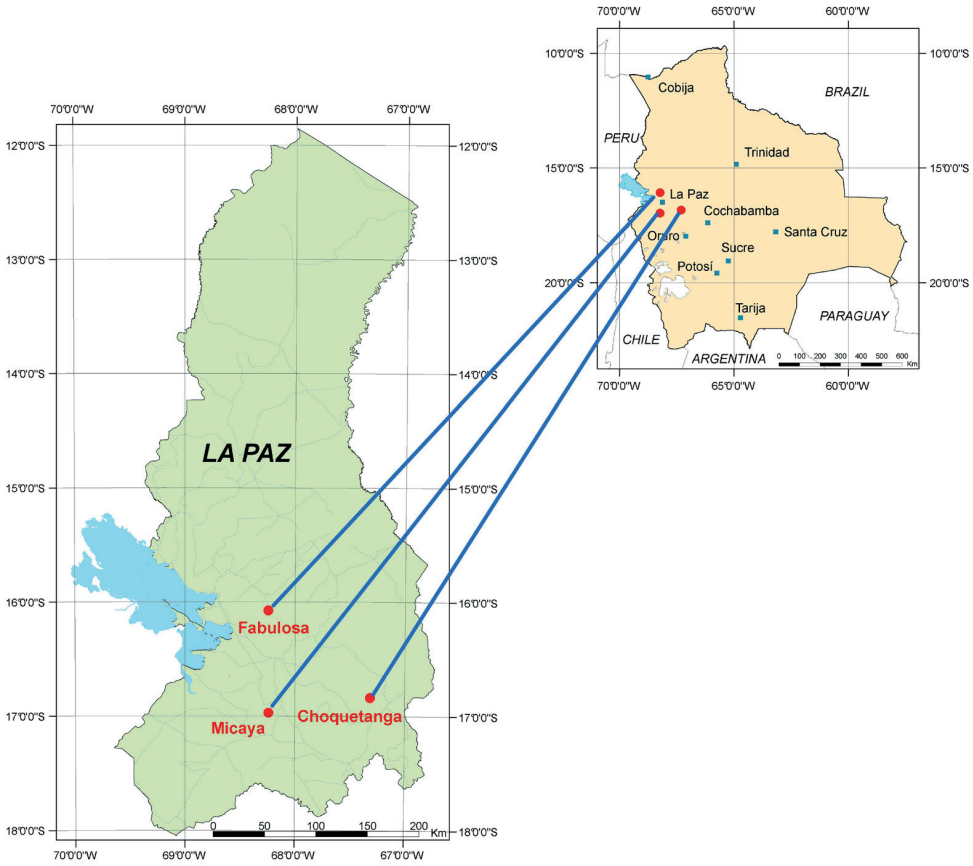

Figure 1: Map showing the location of the raw material deposits. Micaya, Choquetanga and La Fabulosa in La Paz, Bolivia.

slabs using 50 vol.%–50 vol.% kaolinite–feldspar choq/fab, respectively; b) three ceramic slabs using 60 vol.%–40 vol.% kaolinite–feldspar choq/fab, respectively; c) 70 vol.%–30 vol.% kaolinite–feldspar choq/fab, respectively; d) three ceramic slabs using 80 vol.%–20 vol.% kaolinite–feldspar choq/fab, respectively and e) three ceramic slabs using 100 vol.% from the kaolinite-bearing sediments. After drying for 48 h at room temperature, the bars were fired for 3 h with a maximum temperature of 1250°C.

Technical property tests were applied on each sample according to international standards (NB/ISO 10545-3:1995, NB/ISO 10545-4:2004). These include linear shrinkage, firing shrinkage, water absorption, Mohs hardness value, bending strength and fired colour. The physical characterization of the specimens (table 3) was carried out at the Institute of Metallurgy and Materials Research in La Paz, Bolivia (IIMETMAT).

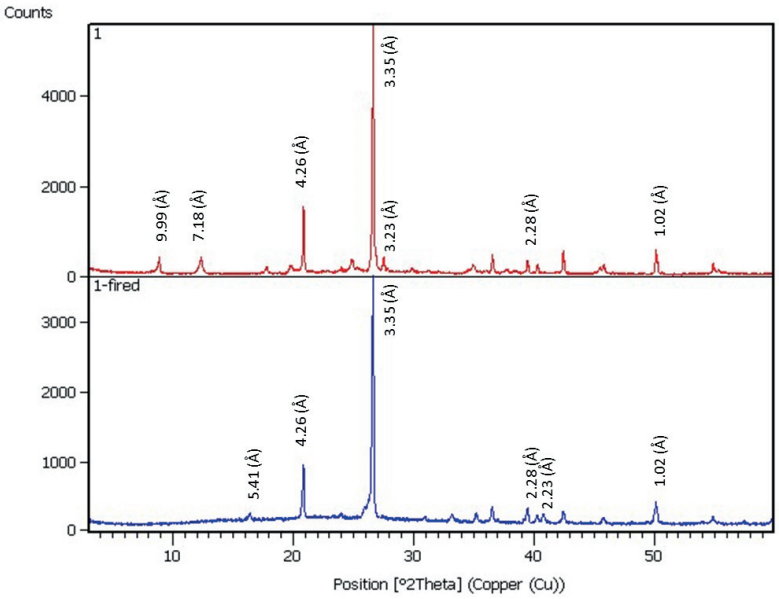

Figure 2: XRD patterns: 1) kaolinite-bearing sediment from the Micaya deposit, composed of quartz (4.26 Å, 3.35 Å, 2.28 Å and 1.02 Å), muscovite (9.99 Å), kaolinite (7.18 Å) and feldspar (3.23 Å); 1-fired) ceramic slab fired at 1250°C, two mineralogical phases are observed, quartz (4.26 Å, 3.35 Å, 2.28 Å and 1.02 Å), and mullite (5.41 Å and 2.23 Å).

Table 2: Chemical composition of the raw material, expressed as major oxides (wt.%).

	Micaya deposit	La Fabulosa deposit	Choquetanga deposit	Quartz-reduced material
SiO_2	71.30	70.10	68.60	57.30
Al_2O_3	17.30	16.70	16.20	32.80
CaO	0.13	0.18	1.12	0.29
Fe_2O_3	1.28	1.05	3.33	1.69
K_2O	3.83	10.80	6.55	5.27
MgO	0.68	0.02	0.46	1.07
MnO	0.02	0.02	0.05	0.04
Na_2O	0.09	2.00	3.53	0.11
P_2O_5	0.07	0.38	0.22	0.12
TiO_2	0.95	0.00	0.30	0.97
LOI	4.40	0.30	0.30	5.30
Total	95.70	101.3	100.40	99.45

Table 3: Physical test on the ceramic specimens: Drying shrinkage (vol.%), firing shrinkage (vol.%), bending strength (N/mm^2), water absorption (vol.%) and Mohs scale hardness.

specimen	Initial length (cm)	Drying length		Drying shrinkage (%)		Fired length (cm)	Firing shrinkage (%)	Bending strength (N/mm^2)	Water absorption (%)	Mohs Hardness value
		24 hrs	48 hrs	24 hrs	48 hrs					
1	8.025	7.785	7.785	2.991	2.991	7.310	8.910	NE	<0.1	7
2	8.025	7.678	7.678	4.324	4.324	7.390	7.913	NE	<0.1	7
3	8.025	7.754	7.754	3.377	3.377	7.390	7.913	NE	<0.1	7
average	8.025	7.739	7.739	3.564	3.564	7.363	8.245	NE	<0.1	7
Kaolinite-bearing sediment from the Micaya deposit and feldspar from the Choquetanga deposit (50 vol.%–50 vol.%)										

specimen	Initial length (cm)	Drying length		Drying shrinkage (%)		Fired length (cm)	Firing shrinkage (%)	Bending strength (N/mm^2)	Water absorption (%)	Mohs Hardness value
		24 hrs	48 hrs	24 hrs	48 hrs					
1	8.025	7.678	7.678	4.324	4.324	7.450	7.165	NE	<0.1	7
2	8.025	7.746	7.746	3.477	3.477	7.455	7.103	NE	<0.1	7
3	8.025	7.738	7.738	3.576	3.576	7.430	7.414	NE	<0.1	7
average	8.025	7.720	7.720	8.025	8.025	7.445	7.227	NE	<0.1	7
Kaolinite-bearing sediment from the Micaya deposit and feldspar from the La Fabulosa deposit (50 vol.%–50 vol.%)										

specimen	Initial length (cm)	Drying length		Drying shrinkage (%)		Fired length (cm)	Firing shrinkage (%)	Bending strength (N/mm^2)	Water absorption (%)	Mohs Hardness value
		24 hrs	48 hrs	24 hrs	48 hrs					
1	8.025	7.875	7.875	1.869	1.869	7.705	3.988	66.405	1.683	7
2	8.025	7.826	7.826	2.48	2.48	7.855	2.118	68.543	1.723	7
3	8.025	7.861	7.861	2.044	2.044	7.770	3.178	69.563	1.794	7
average	8.025	7.854	7.854	2.131	2.131	7.770	3.094	68.179	1.733	7
Kaolinite-bearing sediment from the Micaya deposit and feldspar from the Choquetanga deposit (60 vol.%–40 vol.%)										

Table 3: cont.

specimen	Initial length (cm)	Drying length		Drying shrinkage (%)		Fired length (cm)	Firing shrinkage (%)	Bending strength (N/mm²)	Water absorption (%)	Mohs Hardness value
		24 hrs	48 hrs	24 hrs	48 hrs					
1	8.025	7.891	7.891	1.682	1.682	7.680	4.299	60.810	0.345	7
2	8.025	7.893	7.893	1.645	1.645	7.725	3.738	59.250	0.298	7
3	8.025	7.879	7.879	1.819	1.819	7.711	3.925	48.720	0.327	7
average	8.025	7.887	7.887	1.715	1.715	7.402	3.988	55.700	0.323	7
Kaolinite-bearing sediment from the Micaya deposit and feldspar from the La Fabulosa deposit (60 vol.%–40 vol.%)										
specimen	**Initial length (cm)**	**Drying length**		**Drying shrinkage (%)**		**Fired length (cm)**	**Firing shrinkage (%)**	**Bending strength (N/mm²)**	**Water absorption (%)**	**Mohs Hardness value**
		24 hrs	**48 hrs**	**24 hrs**	**48 hrs**					
1	8.025	7.995	7.995	0.374	0.182	7.89	1.682	69.050	2.213	7
2	8.025	8.011	8.011	0.174	0.243	7.892	1.657	55.560	2.077	7
3	8.025	8.003	8.003	0.274	0.198	7.893	1.645	60.090	2.120	7
average	8.025	8.003	8.003	0.274	0.207	7.760	1.661	69.550	2.136	7
Kaolinite-bearing sediment from the Micaya deposit and feldspar from the Choquetanga deposit (70 vol.%–30 vol.%)										
specimen	**Initial length (cm)**	**Drying length**		**Drying shrinkage (%)**		**Fired length (cm)**	**Firing shrinkage (%)**	**Bending strength (N/mm²)**	**Water absorption (%)**	**Mohs Hardness value**
		24 hrs	**48 hrs**	**24 hrs**	**48 hrs**					
1	8.025	7.985	7.985	0.498	0.299	7.888	1.707	70.350	0.630	7
2	8.025	7.997	7.997	0.349	0.320	7.900	1.558	69.750	0.459	7
3	8.025	7.999	7.999	0.324	0.312	7.903	1.520	70.510	0.660	7
average	8.025	7.993	7.993	0.390	0.310	7.897	1.595	70.200	0.583	7
Kaolinite-bearing sediment from the Micaya deposit and feldspar from the La Fabulosa deposit (70 vol.%–30 vol.%)										

Table 3: cont.

specimen	Initial length (cm)	Drying length		Drying shrinkage (%)		Fired length (cm)	Firing shrinkage (%)	Bending strength (N/mm²)	Water absorption (%)	Mohs Hardness value
		24 hrs	48 hrs	24 hrs	48 hrs					
1	8.025	8.002	8.001	0.287	0.287	7.73	3.676	59.15	1.768	6
2	8.025	7.998	7.996	0.336	0.336	7.789	2.941	51.792	1.657	6
3	8.025	8.004	8.004	0.262	0.262	7.756	3.352	58.729	2.01	6
average	8.025	8.001	8.000	0.295	0.295	7.758	3.323	56.557	1.811	6
Kaolinite-bearing sediment from the Micaya deposit and feldspar from the Choquetanga deposit (80 vol.%–20 vol.%)										

specimen	Initial length (cm)	Drying length		Drying shrinkage (%)		Fired length (cm)	Firing shrinkage (%)	Bending strength (N/mm²)	Water absorption (%)	Mohs Hardness value
		24 hrs	48 hrs	24 hrs	48 hrs					
1	8.025	7.989	7.992	0.449	0.436	7.750	3.427	66.405	0.730	6
2	8.025	7.991	7.991	0.436	0.424	7.761	3.29	66.405	0.759	6
3	8.025	7.991	7.997	0.424	0.349	7.776	3.103	66.405	0.860	6
average	8.025	7.990	7.993	0.436	0.403	7.762	3.273	66.405	0.783	6
Kaolinite-bearing sediment from the Micaya deposit and feldspar from the La Fabulosa deposit (80 vol.%–20 vol.%)										

specimen	Initial length (cm)	Drying length		Drying shrinkage (%)		Fired length (cm)	Firing shrinkage (%)	Bending strength (N/mm²)	Water absorption (%)	Mohs Hardness value
		24 hrs	48 hrs	24 hrs	48 hrs					
1	8.025	7.961	7.966	0.798	0.735	7.630	4.922	56.560	7.380	6
2	8.025	7.966	7.966	0.735	0.735	7.590	5.420	58.250	7.520	6
3	8.025	7.956	7.956	0.860	0.860	7.610	5.171	51.280	7.890	6
average	8.025	7.961	7.960	0.798	0.809	7.610	5.171	55.360	7.596	6
Kaolinite-bearing sediment 100 vol.%										

The following equations were used to determine:

2.1.1. Drying and Firing Shrinkages

The drying shrinkage is expressed by the formula:

$$S_d = \frac{L_p - L_d}{L_p} \times 100$$

where: S_d is the linear drying shrinkage (%), L_p is the plastic length of the test specimen (cm) and L_d is the dry length (cm) of the test specimen.

The firing shrinkage is expressed by the formula:

$$S_t = \frac{L_p - L_f}{L_p} \times 100$$

where: S_t is the total linear shrinkage (%), L_p is the plastic length of the test specimen (cm) and L_f is the fired length (cm) of the test specimen.

2.1.2. Water Absorption

The water absorption is the ratio of the mass of water absorbed to the mass of the dry specimen. The water absorption can be expressed by the formula:

$$A = \frac{M - D}{D} \times 100$$

where: A is the water absorption (%), M is the weight of the saturated tile and D is the weight of the dry tile.

2.1.3. Bending Strength

Bending strength can be determined by the formula:

$$MOR = \frac{3}{2} \times \frac{\sigma L}{h}$$

where: σ is the applied bending strength, L is the distance between the supporting rollers (constant 6.24 cm) and h is the thickness of the test specimen (cm).

2.1.4. Mohs Hardness

Hardness is the resistance of a material to being scratched. The test is conducted by placing a sharp point of one specimen on an unmarked surface of another specimen and attempting to produce a scratch. This measurement was performed comparing the hardness of the ceramic specimen with Mohs hardness value (hardness of selected minerals).

2.1.5. Fired Colour

To test the colour of the raw material and the colour of the ceramic specimen slabs, the Munsell colour chart classification (2010) was used.

2.2. Dehydroxylation of the kaolinite: Low-grade mullite formation

A kaolinite-bearing sediment sample composed of quartz (56 vol.%), kaolinite (18 vol.%), muscovite (21 vol.%) and feldspar (<5 vol.%) (Fig. 2) was collected from the deposit in Micaya (Fig. 1).

The mixed powder was first homogenized and concentrated (clay fraction grain sizes <2 μm) by gravity concentration in an aqueous medium for 2 hours. Fifteen tests were performed for the low-grade mullite formation study (table 4). Bulk specimens were heated in air by using a ramp/hold firing method

Table 4: Ramp/hold firing programmes used during the low-grade mullite formation studies.

Sample name	Number of samples	Number of ramps	Temperature (°C)	Rising time (h)	Rising temperature (°C/h)	Holding time (H)
C	3	3	0–570	0,5	1140	0,25
			570–1100	1,5	733	1,5
			1100–1250	1	1250	1,25
D	3	5	0–570	0,5	1075	0,25
			570–800	0,5	1600	0,75
			800–1000	0,5	2200	0,75
			1000–1150	0,25	4600	0,75
			1150–1250	0,5	2500	0,5
E	3	3	0–570	0,75	760	1,5
			570–1100	1,75	639	1,5
			1100–1250	1	1150	1,5
F	3	2	0–570	0,75	760	1,5
			570–1250	1,75	680	1
G	3	4	0–570	0,5	1075	0,25
			570–800	0,5	1600	0,75
			800–1100	0,5	2200	0,75
			1100–250	6	200	0,75

that creates a programmed differential burning by raising the temperature from 0°C to 1250°C following a segmented curve with clearly defined burning times. Therefore, each temperature segment consists of a "ramp of burning" and a "hold time of temperature", which are defined by the starting temperature, the rate of temperature increase, the final temperature to be reached, and the holding time under the final condition. The number of segments in each procedure was set according to the mineralogical phase shifts that occur in a ceramic material during burning, and the kaolinite-mullite transformation changes. After the tests, a burning programme consisting of three segments was established (table 4).

2.3. Analytical and Technical Tests

2.3.1. Thermo-gravimetric Analysis

Thermo-gravimetric analyses (Figs. 3 and 4) were carried out using a Netzsch STA 409C (simultaneous thermal analysis) equipment coupled with a mass spectrometer gas analysis system connected to the heated furnace outlet with a rotary pump. The sample carrier is located at the top of a highly sensitive analytical balance, located in a vacuum tight casing. The high-temperature furnace is heated by tubular SiC heating elements and operates at temperatures from 25°C to 1550°C with possible heating rates between 0.1 and 50°C/min. The differential thermal analysis (DTA) and thermo–gravimetric analyses (TG) were performed to understand the changes due to the composition of the ceramic body (clay and feldspars) and the firing behaviour of the mixture at high temperatures.

2.3.2. Chemical Composition

The chemical composition of the raw materials and of the separated raw material from the kaolinite-bearing sediment (table 2) was determined by ICP-AES using 0.1 g of dehydrated sample, which was dissolved with 15 ml HF, 2 ml HCl, 2 ml HNO_3 and 2 ml H_2O homogenized to temperatures above 1000° C, at ALS Scandinavia AB in Luleå, Sweden.

2.3.3. Mineralogical Assemblage

X-ray diffraction analysis (Figs. 2, 5, 6 and 7) was carried out for mineralogical phase identification of the ceramic slabs and for the identification of the low-grade mullite samples; the analyses were performed using a X'Pert3 PanAlytical instrument using Cu Kα radiation and time step increments of 0.010°/s. For the mineralogical phase identification, the X'Pert PanAlytical High Score software was applied at IGEMA in La Paz.

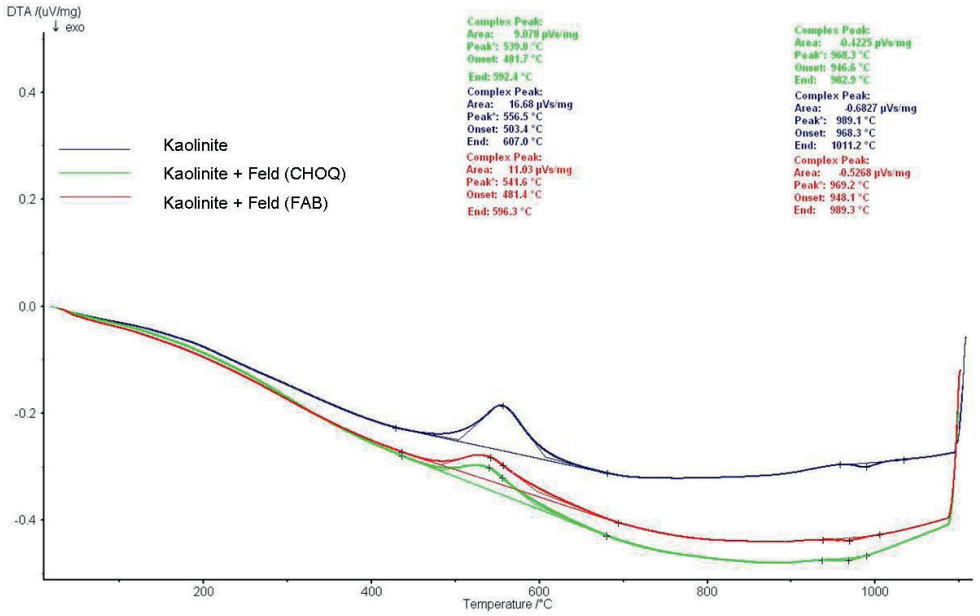

Figure 3: Differential thermal analysis (DTA) of the raw materials: kaolinite-bearing sediment from the Micaya deposit and mixtures with the kaolinite and feldspars from the Choquetanga and La Fabulosa deposits.

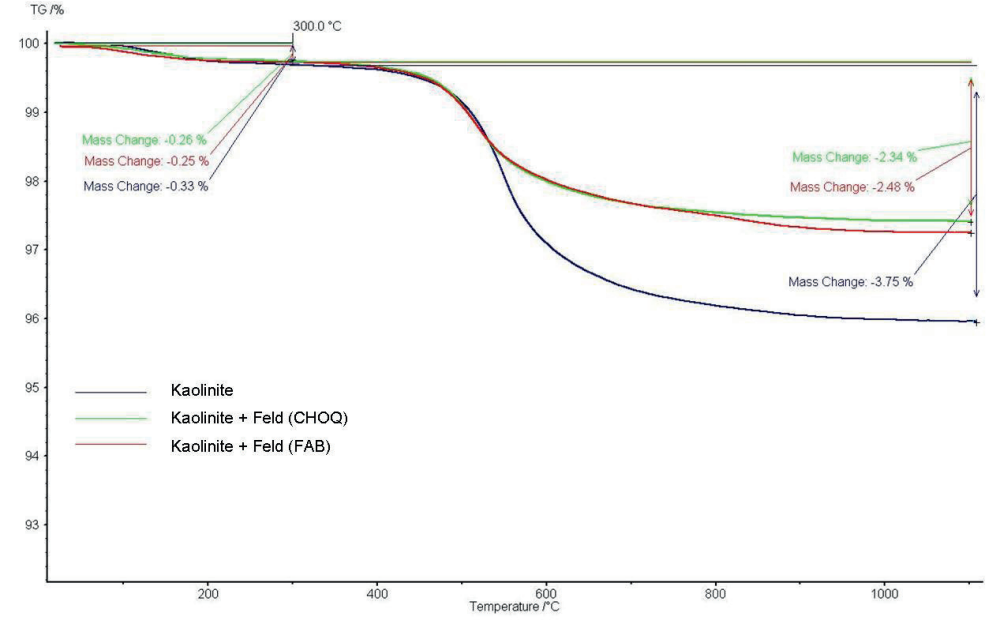

Figure 4: Thermo-gravimetric analysis (TG) of the raw materials: kaolinite-bearing sediment from the Micaya deposit and mixtures with the kaolinite and feldspars from the Choquetanga and La Fabulosa deposits.

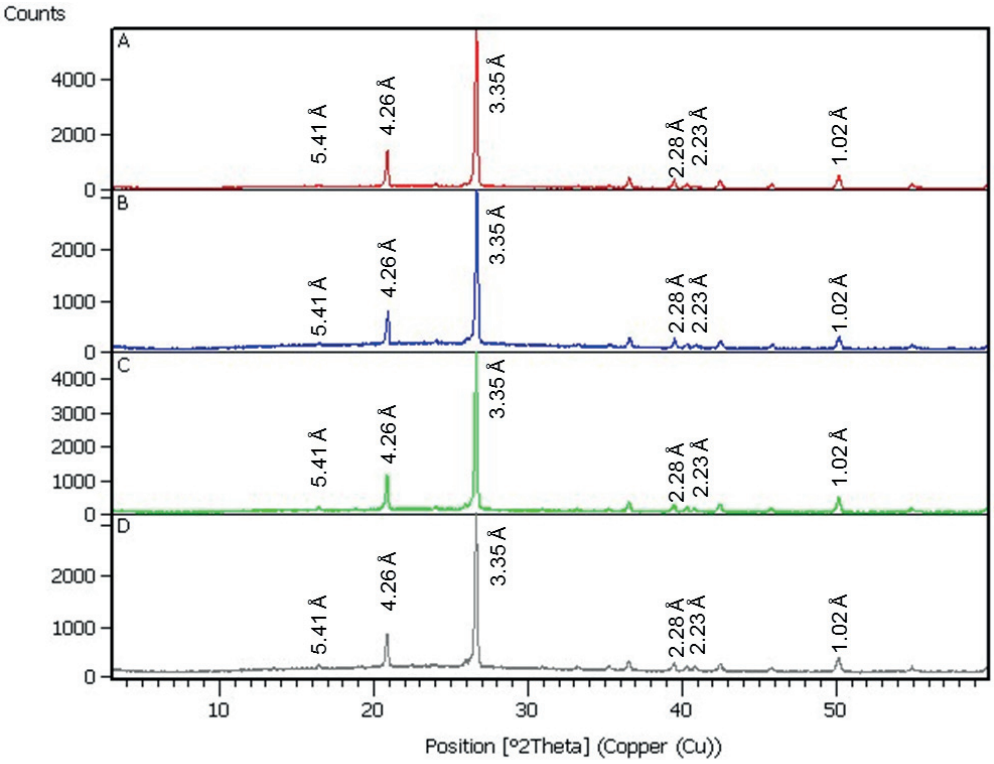

Figure 5: XRD pattern of the ceramic slabs. **A)** 70 vol.% kaolinite-bearing sediments and 30 vol.% feldspar (Choq). Quartz (3.35 Å, 4.26 Å, 2.28 Å, 1.02 Å) and mullite (5.41 Å, 2.23 Å) peaks were identified; **B)** 70 vol.% kaolinite-bearing sediments and 30 vol.% feldspar (Fab). Quartz (3.35 Å, 4.26 Å, 2.28 Å, 1.02 Å) and mullite (5.41 Å, 2.23 Å) peaks were identified; **C)** 80 vol.% kaolinite-bearing sediments and 20 vol.% feldspar (Choq). Quartz (3.35 Å, 4.26 Å, 2.28 Å, 1.02 Å) and mullite (5.41 Å, 2.23 Å) peaks were identified; **D)** 80 vol.% kaolinite-bearing sediments and 20 vol.% feldspar (Fab). Quartz (3.35 Å, 4.26 Å, 2.28 Å, 1.02 Å) and mullite (5.41 Å, 2.23 Å) peaks were identified.

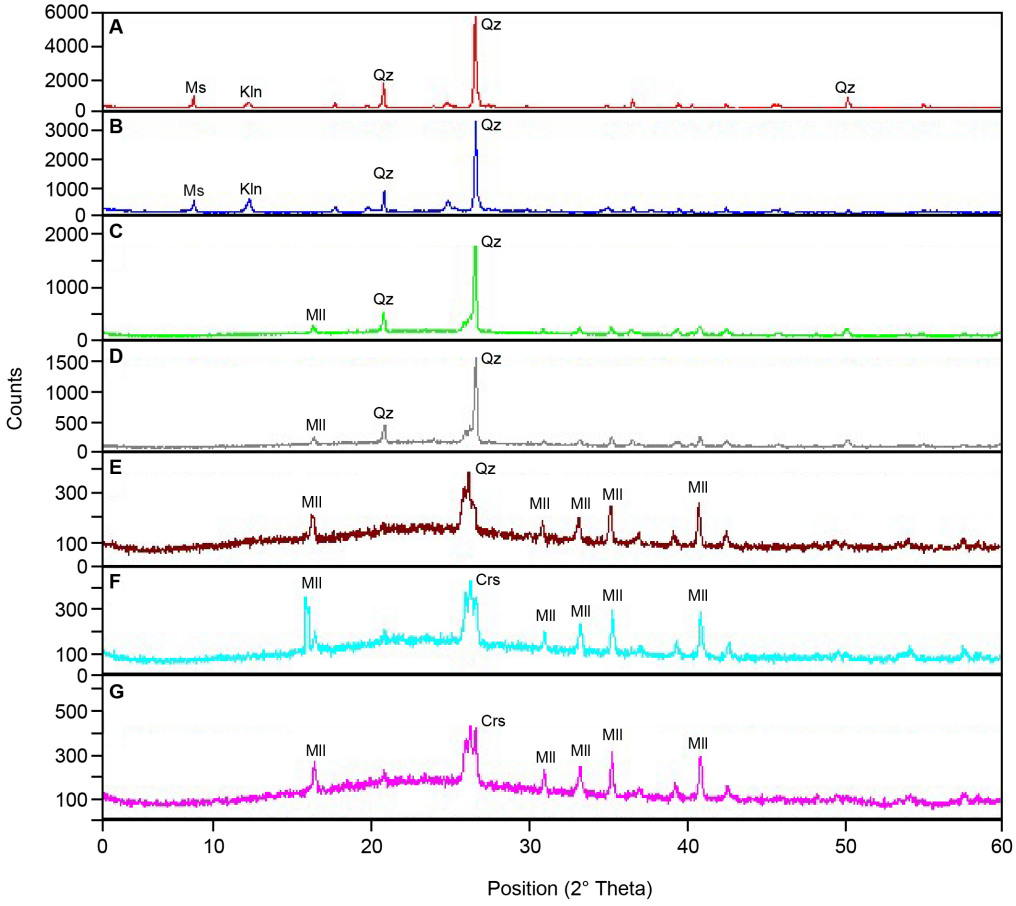

Figure 6: A) XRD patterns of the kaolinite-bearing sediment from the Micaya deposit; **B)** XRD patterns of the low quartz kaolinite-bearing sediment from the Micaya deposit; **C-G)** XRD patterns of the fired raw materials with different ramp/hold burning programmes.

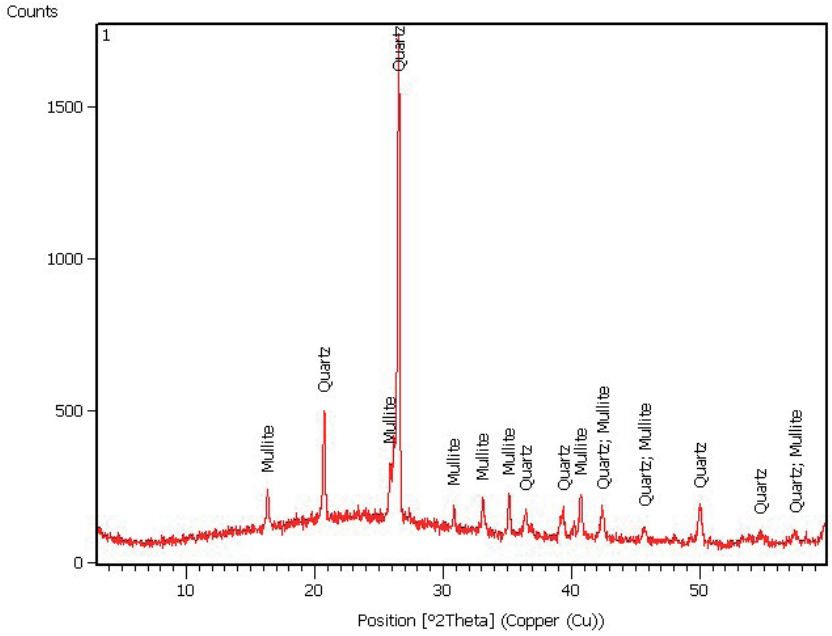

Figure 7: XRD pattern of the low-grade mullite material.

2.3.4. Scanning Electron Microscopy

The microstructure of the fired kaolinite-bearing sediment for low-grade mullite formation was evaluated by scanning electron microscopy (SEM, Magellan UHR) and energy dispersive X-ray spectroscopy (EDX, X-MAX 80 mm2, Oxford Instruments, Oxford, United Kingdom), at the microanalytical laboratory at Luleå University of Technology, Sweden.

3. RESULTS

The results from the physical tests are shown in table 3. According to the Munsell colour chart classification (2010), the ceramic slabs generally exhibit a white colour (8/1) for the mixture with La Fabulosa feldspar and a light grey colour (7/1) for the mixture with the Choquetanga feldspar.

The differential thermal (DTA) diagram of the kaolinite-bearing sample (Fig. 3) shows an endothermic peak at 490°C which is related to dehydroxylation of the kaolinite, forming metakaolinite, overlapped by a broad exothermic peak at 556.5°C, related to the $\alpha \rightarrow \beta$ quartz transition. The endothermic peak at 989.1°C is related to the formation of a silicon spinel phase, followed by the formation of the mullite phase up to 1100°C. The presence of the exothermic peak is supported by the mass loss observed at 573°C in the thermo-gravimetric curve (Fig. 4). The

thermo-gravimetric curve exhibits a two-step weight loss. The first step, in which the kaolinite loses its adsorbed water, occurs when it is heated to approximately 300°C. The wider interval between 400°C - 600°C, reflects 1) the loss of structurally bonded water and 2) the volume changes during quartz transition. The total loss of the kaolinite sample was determined to be 4.08 wt.%.

In the prepared mixtures of kaolinite with feldspar from Choquetanga and La Fabulosa, the endothermic peaks related to the dehydroxylation of the kaolinite are overlapped by the exothermic $\alpha \rightarrow \beta$ quartz transition peak at 539.8°C and 541.6°C, respectively. Similarly as the kaolinite-bearing sample, the occurrence of the endothermic peaks at 968.3°C and 969.2°C, respectively, was due to a phase transformation to a silicon spinel phase. The TG curve of the prepared specimens (Fig. 4) exhibits a two-step weight loss, similar to the kaolinite-bearing sample. The total mass loss was determined to be 2.60 wt.% for the kaolinite mixed with Choquetanga-feldspar and 2.73 wt.% for the kaolinite mixed with La Fabulosa-feldspar (Figs. 3 and 4).

The mineralogical analysis of the initial raw material shows four mineral phases: quartz (3.35Å and 4.26 Å), muscovite (9.99 Å), kaolinite (7.18 Å) and feldspar (3.23 Å). Among them, quartz is the most abundant mineral (Fig. 2a). After the mixture and calcination, two mineral phases were identified in the kaolinite-bearing sample, as well as in the ceramic mixtures (Fig. 2b). These were quartz (3.35 Å and 4.26 Å and 1.02 Å) and mullite (5.41 Å and 2.23 Å) (Fig. 5).

The chemical composition of the raw material indicates a silica-rich kaolinite-bearing sediment (71.30–70.10 wt.%) and alkali-rich samples from the Choquetanga and La Fabulosa deposits (6.55–10.80 wt.%). This chemistry is due to the presence of quartz and feldspars. In table 2, it is shown that the iron content of the kaolinite-bearing material is low, as well as for the La Fabulosa feldspar sample. The iron content of the Choquetanga samples (3.33 wt.%) is directly related to the biotite content of the rock (table 2).

3.1. Mineralogical Results for the low grade-Mullite procedure

During the kaolinite–mullite transformation, XRD analyses were carried out (Figs. 6 and 7) as follows: i) The XRD pattern of the raw material (Fig. 6A) indicates quartz, muscovite, and kaolinite to be the main mineral components. ii) The XRD pattern of the raw material with less quartz (Fig 6B) indicates the presence of quartz, muscovite, and kaolinite, although an increase in the clay fraction is perceived, effectively corroborating with the chemical composition of the separated material (table 2). iii) The XRD patterns of the fired raw material samples (Figs. 6C–6G) show mullite peaks at different

intensities (5.41 Å, 2.23 Å, 2.55 Å, 2.70 Å and 2.89 Å). Among them, the 5.41 Å peak is the most intense, as well as quartz peaks at 3.35 Å and 4.26 Å (Fig. 7). The D, E, F and G XRD patterns are consistent with an enrichment of amorphous phase.

4. DISCUSSION

The chemical composition of a raw material is an important factor in the ceramic processing of tiles and is related to the mineralogy of the material, especially the amount of quartz, kaolinite and feldspars present. Those minerals that exhibit a similar crystalline structure, such as quartz and feldspar, form a generalized silicon-aluminium-oxygen network during firing (Ismailova et al., 1972), which is responsible for the mechanical strength of the ware and is directly proportional to the total alkali content of the material (Moharem and Alla Eldin, 2007). The feldspar is used as a source of alumina and alkali, and the presence of alkali will lower the melting point and increase the bending strength, which are important factors that influence the manufacturing quality and marketing of the final product, saving energy during the firing process (Rodas, 2003; Potter, 2006).

Clays are used because of their plasticity, inertness and stability, providing specific properties, such as a unique rheology, for specific industrial use. Kaolinite is the clay mostly used in manufacturing of sanitary ware, wall tiles and floor tiles, providing the white fired colour and the necessary plasticity to form the ceramic body. The raw material from the Micaya deposit exhibit a white colour (Zeballos et al., 2016), and a suitable mineralogical and chemical composition for ceramic purposes (Fig. 8a), and preliminary physical tests show desirable characteristics for the ceramic industry (Zeballos et al., 2016). There are two primary factors controlling the suitable end use of a ceramic product: 1) the porosity of the ceramic and 2) the bending strength of the ceramic. Porous ceramic materials always have lower bending strengths and elasticities than non-porous materials. The pores and other microscopic imperfections act as stress concentrators, reducing the resistance to mechanical stress (Gonzales, 2003). The pure kaolinite ceramic slabs exhibit high water absorption values (table 3), a property which is directly related to the porosity. The porosity itself can be related to both the grain size of the material (Figs. 8a and 8b) and to the temperature at which the specimen was fired. Muscovite is an important component of the studied raw material (Figs. 2a and 8a) as well as it is in any ceramic mixture. At high temperatures muscovite tends to expand, thus developing coarse pores in the mixture (Cole and Crook, 1968) which increases the porosity in the ceramic product.

The amount of quartz in the ceramic raw material is important since the volume of the ceramic increases during the transition of low quartz to high quartz (Frondel,

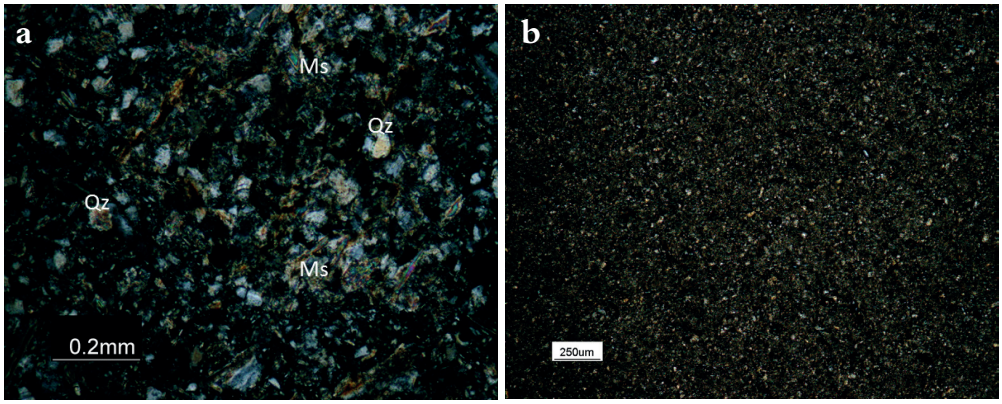

Figure 8: Photograph of the starting raw material for the ceramic mixtures. **a)** Fine-grained quartz and muscovite are visible; **b)** Ceramic slabs raw material after grinding, showing the homogeneity of the mixture.

1962; Schüller, 1979). This volume change occur because of the rapid transition during the firing process, and it affects the final product since fractures may develop (Schüller, 1979). The kaolinite-bearing sediment exhibits a considerable amount of quartz (Figs. 2a and 8a), which could affect the thermal behaviour of the raw material at high temperature (Figs. 3 and 4). Therefore, a slow firing process through the temperature where the structural shift occur is recommended in order to avoid fractures in the ceramic slabs.

Shrinkage by drying and firing is related directly to the amount of clay minerals and physical water present in the plastic clay (Lassinantti et al., 2011). Kaolinite-rich samples exhibit higher values (table 3) than those where feldspar has been added to the mixture (table 3). The role of feldspars in ceramic mixtures, especially those used to fabricate floor tiles, is not only to lower the melting point of the mixture but also to increase the translucency and the bending strength. The bending strength of the ceramic slab is directly related to the water absorption and the amount of feldspars in the ceramic paste (table 3). According to Lassinantti et al. (2011), the feldspar decreases the porosity due to the viscous sintering; the addition of feldspar increases the alkali content rendering the liquid melt, thus promoting the sintering process. The studied samples show a decrease in water absorption when the feldspar content increases (table 3). This is due to the densification of the melting, which is promoted by the sintering process and therefore reduces the porosity and increases the bending strength of the ceramic slabs (table 3).

The term stoneware is applied to tiles with low porosity and high technical performance (Dondi et al., 1999, Martín et al., 2009) with a maximum water absorption of 0.5 vol.% (ISO 13006). The results presented in table 3 show bending strength values higher than those of the current tiles commercialized

in the Bolivian market (55 N/mm^2, Fábrica Boliviana de Cerámica, 2018 and 35 N/mm^2, Gladymar, 2015), as well as a higher hardness (Uriarte, 2007, IBNORCA, 2014). It is suggested in this study that the high bending strength of the ceramic slabs (table 3) is related to the mullite formation during firing (Reyes et al., 2013). When feldspar is added to the mixture, this promotes the lowering of the melting point of the mixture and initiates the mullite formation.

4.1. Low-grade mullite formation

The reaction of kaolinite with alumina relates to the production of mullite by reaction sintering (Liu et al., 1994). Although many researches have studied the implementation of new techniques for mullite synthesis, most studies have been related to the addition of new molecules, such as an extra aluminium phase, pure kaolin or gibbsite ($Al(OH)_3$), into the structure as sintering aid. This addition enhances the mullite phase content at low temperature, ensuring the formation of secondary mullite (Zhou et al., 2011). TiO_2 and Fe_2O_3 are mineralizers that promote or anticipate the nucleation and crystallization of mullite (Souza et al., 2013, Hou et al., 2016). The implementation of Cr_2O_3 allows materials to be obtained with no vitreous phase and homogeneous microstructure (Villar et al., 2004). Depending on the synthesis conditions, mullite may incorporate Ti^{3+}, Ti^{4+}, V^{3+}, V^{4+}, Cr^{3+}, Mn^{2+}, Mn^{3+}, Fe^{2+}, Fe^{3+} and Co^{2+}, although in considerably different amounts (Schneider, 1990). The ions Na^+, K^+ and Ca^+ are called modifiers because they enter the interstices of the lattice of the glass, weaken the connections and cause a decrease in melting temperature, facilitating the formation of glass (Souza et al., 2013). The presence of glass thus involves the degradation of its mechanical properties (Villar et al., 2004).

According to Hou et al. (2016) the rate of the controlled step of crystallization growth is the dissolution velocity of Al_2O_3 into the SiO_2-rich liquid phase; when adding sintering aids, the silica-rich ternary phase is formed at lower temperature.

On this basis and based on the observation of mullite formation in the ceramic slabs (Figs. 2b and 5) from a low alumina mixture (table 2), a set of ramp/hold burning programmes were carefully designed to promote the above mentioned mullite formation (Table 4). The idea of their design is to show the importance of the crystallization timing during its transformation as much as it is the chemical composition of the raw material itself.

Brindley et al. (1959a, 1959b, 1959c) have stated an ideal formula of a raw material suitable for mullite transformation from kaolinite $3Al_2O_32SiO_2$. Therefore,

a procedure to decrease the SiO_2 content of the kaolinite-bearing sediment was carried out (table 2). However, the procedure does not imply the total elimination of quartz since this component is also found in abundance in finer fractions (Figs. 2, 6 and 8a). The resultant material is a mixture composed of SiO_2 and Al_2O_3 in a 2:1 ratio (table 2).

At 1250°C is observed a mullite formation from the kaolinite-bearing sediment (Fig. 9B). The mullite peaks are relatively small (Figs. 6C-G) due to the Si and Al content of the mixture. However, needle-shaped crystals are observed immersed in a vitreous phase (Fig. 9B). The amorphous phase is also visible in the images and the xrd patterns (Figs. 6D-G).

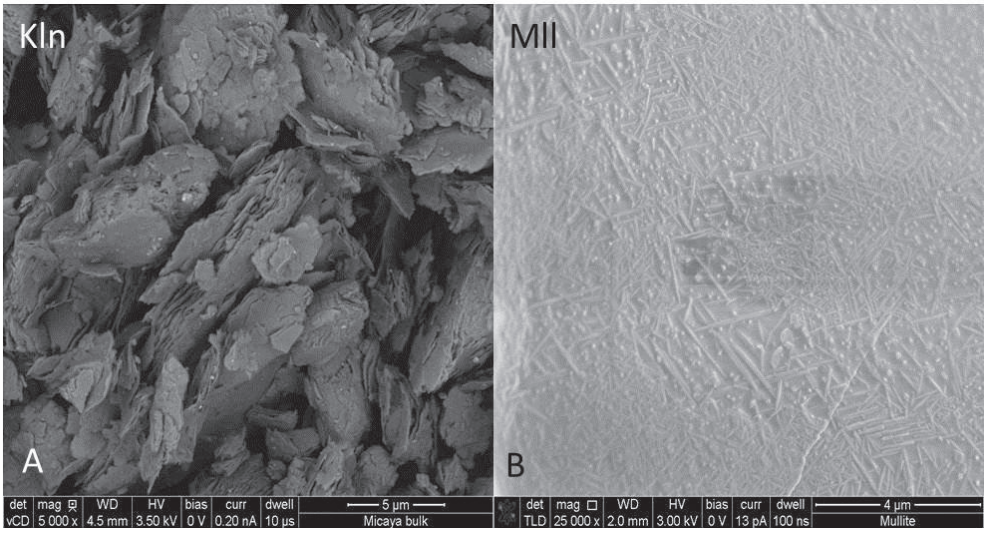

Figure 9: SEM images: (a) kaolinite plate like crystals of the raw material from the Micaya deposit; and (b) needle-shaped crystals, as a result of the low-grade mullite formation after ramp/hold burning programme at 1250°C.

The mullite mineral has been extensively studied (Lu et al., 2004; Cheng et al., 2004; Zhou et al., 2011; Reyes et al., 2013; Sahraoui et al., 2016) for its refractory properties, but also for enhancing the technical properties of floor tile ceramics (Xu et al., 2015; Hou et al., 2016), especially those used as porcelain stoneware (Martín et al., 2009).

5. CONCLUSIONS

A porcelain stoneware slab with a high bending strength and low porosity was produced from a kaolinite-bearing sediment.

The technical characteristics of the porcelain stoneware were enhanced by the addition of feldspar and by mullite formation, sintered from the same kaolinite-bearing sediment.

The distance to market plays an important role in the development of the industry because transportation influences the price. In this context the Bolivian deposits are ideal due to their location, with easy access and proximity to the potential local market.

6. ACKNOWLEDGEMENTS

This study was supported by the Swedish International Development Cooperation Agency (SIDA). We are grateful to the Institute of Geological and Environmental Research (IGEMA) at the San Andrés University, La Paz, Bolivia

REFERENCES

Brindley GW and Nakahira M (1959a) The kaolinite-mullite reaction series: I. A survey of outstanding problems. Journal of the American Ceramic Society, 42: 311-314.

Brindley GW and Nakahira M (1959b) The kaolinite-mullite reaction series: II. Metakaolin. Journal of the American Ceramic Society, 42:315-318.

Brindley GW and Nakahira M (1959c) The kaolinite-mullite reaction series: III. The high temperature phases. Journal of the American Ceramic Society, 42:319-324.

Chen YF, Wang MC, Hon MH (2004) Phase transformation and growth of mullite in kaolin ceramics. Journal of the European Ceramic Society, 24: 2389 – 2397.

Cole WF and Crook DN (1968) High-temperature reaction of clay mineral mixtures and their ceramic properties: IV, dimensional and weight changes on refiring and the pore-size distribution of fired kaolinite-muscovite-quartz mixtures with 25 wt.% quartz. Journal of the American Ceramic Society, 51(2): 79–84.

Dondi M, Ercolani G, Melandri C, Mingazzini C and Marsigli M (1999) The chemical composition of porcelain stoneware tiles and its influence on microstructural and mechanical properties. Interceram 48(2): 75–83.

Enrique NJE and Amorós JL (1985) Tecnología Cerámica: Introducción a la Tecnología cerámica, materia primas cerámicas. Instituto de Química Técnica. Universidad de Valencia Vol.1, 155 p.

Fábrica Boliviana de Cerámica (2018) Normas y especificaciones. Recuperado de http://www.faboce.com.bo.

Frondel C (1962) The system of mineralogy, vol.3: Silica minerals (7th edition), Wiley, New York, 334 p.

Gladymar (2015) Aspectos técnicos del porcelanato. Recuperado de http:// www.gladymar.com.bo.

Gonzales GF, Romero AV, García RG and Gonzáles RM (1990) Firing transformation of mixtures of clays containing illite, kaolinite and calcium carbonate used by ornamental tile industries. Applied Clay Science, 5 (4): 361-375.

Gonzales DI (2003) Arcillas cerámicas de construcción y cerámica fina: Impacto ambiental provocado por su extracción. Mineralogía Aplicada de Emilio Galán Huertos, Editorial Sintesis S.A.: 83-104.

Hou Z, Cui B, Liu L and Liu Q (2016) Effect of the different additives on the fabrication of porous kaolin-based mullite ceramics. Ceramics International 42: 7254 – 17258.

Instituto Boliviano de Normalización y Calidad (IBNORCA) (2014) Catálogo de Normas Bolivianas. NB/ISO 10545-4:2005 Baldosas cerámicas— Determinación de la resistencia a la flexión y de la carga de rotura (correspondiente a la norma ISO 10545-4:1995 - NB-259-78) Dirección General de Normas y Tecnología – Bolivia, Ministerio de Industria y Comercio, 14 p.

Ismailova MA and Borisova KhB (1972) Low temperature bodies for ceramic tile. Journal of Glass and Ceramics. Vol. 29(8): 535-536.

ISO 10545-4 (2004) Determination of modulus of rupture and breaking strength. ISO, Geneva 20. www.iso.org

ISO 10545-3 (1995) Determination of water absorption, apparent porosity, apparent relative density and bulk density. ISO, Geneva 20. www.iso.org

ISO/FDIS 13006 (1998) Ceramic tile – definitions, classification, characteristics and marking. ISO/TC 189.

King RJ (2009) Minerals explained 49: kaolinite. Geology Today, 25 (2): 75-78.

Lassinantti MG, Romagnoli M and Gualtieri A (2011) Influence of body composition on the technological properties and mineralogy of stoneware: A DOE and mineralogical–microstructural study. Journal of European Ceramic Society, 31(5): 673–685.

Liu KC, Thomas G, Caballero A, Moya J and de Aza S (1994) Time-Temperature-Transformation curves for kaolinite-α – Alumina. J. Am. Ceram. Soc. V. 77(6): 1545 – 1552.

Lu HY, Wang WL, Tuan WH and Lin MH (2004) Acicular Mullite Crystals in Vitrified Kaolin. Journal of the American Ceramic Society, 87: 1843-1847.

Martín MJ, De la Torre AG, Aranda MA, Rincón J and Romero M (2009) Journal of the American Ceramic Society 92(1): 229–234.

Moharem AF and Alla Eldin MS (2007) Properties and suitability of Wadi Zarieb Feldspars for ceramic industries in Egypt. Journal of Applied Science, 7 (19): 2794 – 2799.

Munsell Color (Firm). (2010) Munsell soil color charts: with genuine Munsell color chips. Grand Rapids, MI: Munsell Color.

Murray HH (1988) Kaolin Minerals: Their genesis and Occurrences. Hydrous Phyllosilicates, 19 p.

Murray HH and Keller DW (1993) Kaolins, kaolins and kaolins: In kaolin genesis and utilization. Special publication no.1. The Clays Minerals Society; pp.1-24.

Murray HH (2007) Applied Clay Mineralogy: Occurrences, Processing and Application of kaolins, bentonites, palygorskite –sepiolite and common clays. Elsevier First Edition, 189 p.

Potter JM (2006) Feldspars. In Kogel J., Trivedi N., Barker J. and Krukowski S. (Eds.) Industrial Minerals & Rocks, 7th Edition, Society for Mining, and Exploration Inc., pp 451-460.

Reyes SY, Serrato J and Sueyoshi S (2013) Microstructural characterization of sanitaryware, the relationship spinel and mullite. Journal of Ceramic Processing Research, 14(4): 492–497.

Rodas M (2003) Minerales Industriales: Feldespato, magnesita y talco. Mineralogía Aplicada de Emilio Galán Huertos. Editorial Síntesis S. A., pp 51-70.

Sahraoui T, Belhouchet H, Heraiz M, Brihi N and Guermat A (2016) The effects of mechanical activation on the sintering of mullite produced from kaolin and aluminium powder. Ceramics International, 42: 12185–12193.

Sanfeliu T and Jordan MM (2009) Geological and Environmental management of ceramic clay quarries: A review. Environmental Geology, 57: 1613 – 1618.

Schneider H (1990) Transition metal distribution in mullite. Ceramic Trans. 6: 135–158.

Schneider H and Komarneni S (2005) Mullite. WILEY-VCH Verlag GmbH & Co. KGaA, Weinheim, 506 p.

Schüller KH (1979) Porcelain. Ceramic Monographs: A Handbook of Ceramic. Verlag Schmidt GMBH. Freiburg.

Souza AE, Teixeira SR, Santos GTA and Longo E (2013) Addition of sedimentary rocks to kaolinitic clays: influence on sintering process. Ceramica 59: 147 – 155.

Uriarte (2007) Estudio de las características físico – mecánicas de las baldosas cerámicas que se fabrican y ofertan en el mercado nacional. Revista del Instituto de Ensayo de Materiales. Carrera de Ingeniería Civil – UMSA. Año 2 (2): 29 – 40.

Villar MP, Gago-Duport L and García R (2004) Comportamiento de mullitas a alta temperatura: Estudio mediante Difracción de Rayos X. Boletin de la Sociedad Española de Ceramica y Vidrio. 43(2): 135-137.

Xu X, Lao X, Wu J, Zhang Y, Xu X and Li K (2015) Microstructural evolution, phase transformation, and variations in physical properties of coal series kaolin powder compact during firing. Applied Clay Science, 115: 76–86.

Zeballos A, Weihed P, Blanco M and Machaca V (2012) Granitic rocks as a source of K_2O + Na_2O for ceramic applications in Bolivia. Acta Mineralogica-Petrographica, Abstract Series, Szeged, Vol. 7, pp 162.

Zeballos A, Weihed P, Blanco M and Machaca V (2016) Geological, mineralogical and chemical characterization of Devonian kaolinite-bearing sediments for further applications in the ceramic (tiles) industry in La Paz, Bolivia. Environ Earth Sci 75: 1-15.

Zhou H-M, Qiao X-C and Yu J-G (2011) Preparation of Mullite from Low-grade kaolin. Journal of Wuhan University of Technology, 33(2): 121 – 125.

PAPER IV

Characterization of some nonmetallic resources in Bolivia: an overview of their potentiality and their application in specialized formulations

Ariana Zeballos, Pär Weihed, Mario Blanco and Vladimir Machaca

Published in:

Environmental Earth Sciences

(2017) 76:754

Environ Earth Sci (2017)76:754
DOI 10.1007/s12665-017-7094-7

ORIGINAL ARTICLE

Characterization of some nonmetallic resources in Bolivia: an overview of their potentiality and their application in specialized formulations

Ariana Zeballos[1,2] · Pär Weihed[1] · Mario Blanco[2] · Vladimir Machaca[2]

Received: 21 May 2016 / Accepted: 23 October 2017

Abstract Bolivia has several nonmetallic occurrences widespread in the country. Unfortunately, they are poorly studied and slightly characterized. In the present work, several nonmetallic occurrences located in La Paz, Oruro, Potosí and Santa Cruz were studied. The results of the chemical and mineralogical characterization of the materials will be presented, in order to approach their applicability in specialized industrial formulations. A preliminary test of the final products besides an overview of their potentiality will be exposed and a current view of the commercialization as well.

Keywords Bolivian raw materials · Zeolites · Diatomite · Mullite · Clays · Kaolins

Introduction

It is becoming increasingly difficult to ignore the importance of the industrial minerals in the present life. The industrial minerals and rocks cover a wide range of uses, from everyday products such as ceramics, soaps and medicine to high technology such as molecular sieves to rocket components.

However, the literature shows nothing or little work about the potential of Bolivia as a nonmetallic raw material miner as well as a producer. Most studies on the nonmetallic potentiality have been only carried out in a small number of occurrences, and the literature commonly refers those nonmetallic minerals as gangue minerals or alteration products from hydrothermal processes that are commonly associated with metallic mineralizations. The construction industry is one of the largest industries in Bolivia. The red brick producers at Llojeta in La Paz (Fig. 1) send the majority of the production to the border towns near Chile and Perú. The kaolin materials from La Bella in Santa Cruz are well known for the white tile manufacturing which captures the internal consumption. For several years, the bentonites from Coro Coro and Río Mulatos were mined to produce cat litters and drilling muds, respectively. Despite of, a little literature exists about these prosper resources, the quality of the raw materials are unknown.

This paper will examine the potentiality of Bolivia in nonmetallic minerals as well as its capability to transform nonmetallic raw materials in specialized products such as building materials and zeolites. This paper first gives results about the chemical and mineralogical characterization of four important raw materials such as diatomites, clays, zeolites and refractory minerals and finally will give and overview of their potential application in the daily life.

In the last 10 years, the nonmetallic resources and their consumption have been growing up (Fig. 2). In countries such as Bolivia that is known as a potential mineral producer, the mineral resource exploration is focused in metallic ores such as tin, silver, lead, zinc or gold, leaving aside the nonmetallic minerals such as clays, feldspars (Fig. 3) and the industrial minerals, remain unstudied and poorly understood.

✉ Ariana Zeballos
Ariana.Zeballos@ltu.se

[1] Division of Geoscience and Environmental Engineering, Luleå University of Technology, 971 87 Luleå, Sweden

[2] Instituto de Geología y del Medio Ambiente, Universidad Mayor de San Andrés, La Paz, Bolivia

Published online: 10 November 2017

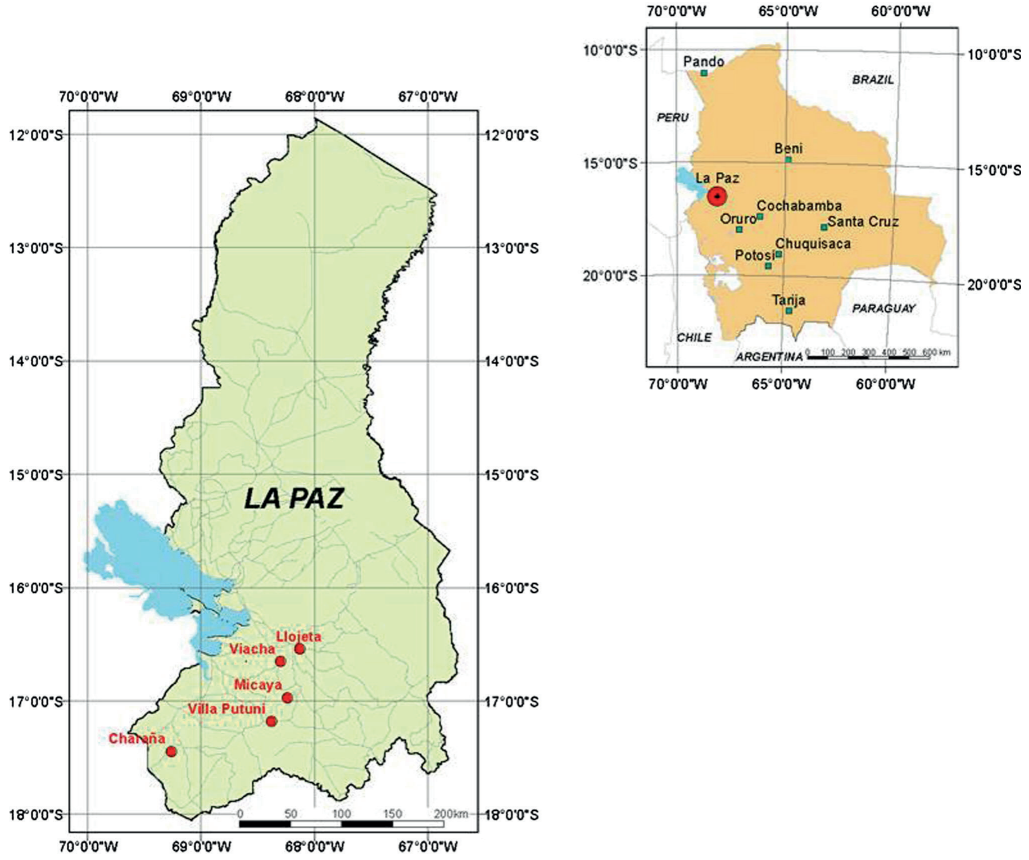

Fig. 1 Location map of the studied deposits in La Paz, Bolivia

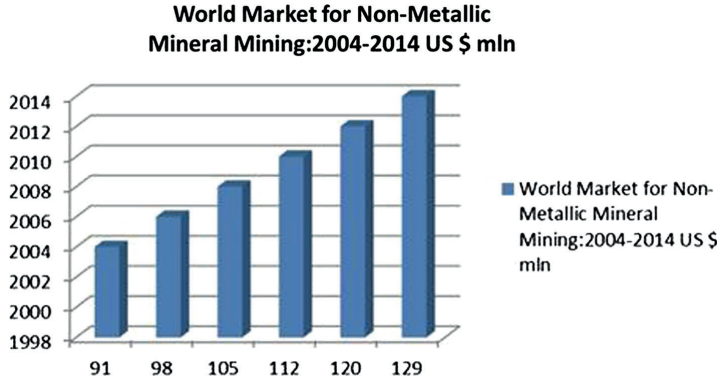

Fig. 2 World Market from nonmetallic mineral mining (2004–2014), data source from Parker (2008)

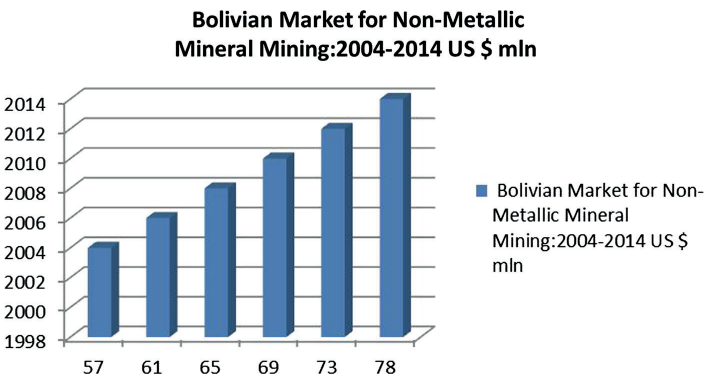

Fig. 3 Bolivian market for nonmetallic mineral mining

Materials and methods

The availability of raw materials was obtained through geological mapping and sampling. In the Micaya (Fig. 1), Charaña (Fig. 1) and Murmutani deposits, geological mapping was performed in a 1:20,000 scales (Zeballos et al. 2016; Acarapi 2013). In Rio Mulatos, Corque and Santa Cruz, chemical and mineralogical analyses were performed. The chemical analyses were carried out in the ALS laboratory in Sweden, according to the EPA method (modified) 200.8 (ICP-SFMS), where 0.1 g sample was fused with 0.4 g $LiBO_2$ and dissolved in HNO_3. LOI (loss on ignition) is done at 1000 °C. The mineralogical characterization was done using a PANalytical Empyrean X-ray Diffractometer equipped with Cu LFF HR X-ray tube, a graphite monochromator and a PIXcel3D detector. The diffractometer was operated at 30 mA and 40 kV. The scanning region of the diffraction angle 2θ was from 5° to 50° with a 0.026 step size and time per step of 250 s in the LTU laboratories in Luleå, Sweden, and a X'Pert3 PANalytical instrument using Cu Ka radiation and time step increments of 0.010_/s, at the IGEMA laboratory, in La Paz. Mineral identification and quantification were determined with the help of the X'Pert High Score Plus software according to the X-ray spectral peak (Brown and Brindley 1980; Moore and Reynolds 1997).

Results and discussion

Synthetic and natural zeolites

Zeolites were first identified in 1756 as a group of minerals by a Swedish mineralogist, Baron A.F. Cronstedt (Eyde and Holmes 2006). Zeolites are hydrated aluminosilicates with a three-dimensional SiO_4 tetrahedral framework-type structures with molecular cavities and molecular channels (Chang 2002). Zeolites minerals can contain loosely bounded alkali and alkaline earths metals that could be easily exchanged for other cations or molecular water (Eyde and Holmes 2006). More than 48 natural zeolites have been well characterized and more than 100 were produced synthetically (Chang 2002; Eyde and Holmes 2006).

Recent studies with local raw materials (Garcia et al. 2015) such as those located in Charaña (Fig. 1) are pointed out, as well as diatomites and montmorillonites from Río Mulatos located in Potosí to be used as raw materials besides kaolin to produce synthetic zeolites to be used in catalytic cracking and detergent industry. Garcia et al. (2015) performed a synthetization of a submicron FAU-type zeolite using an acid-treated diatomite from a diatomaceous earth deposit, as well as zeolite "A" using a natural clay, and montmorillonite from the smectite family (García et al. unpublished results); both are raw materials from two deposits located in Potosí, Bolivia. On the other hand, chemical analysis (Table 1) and mineralogical analysis (Table 2) performed on the samples reveal similar applications of those materials (diatomaceous earth) at Charaña and those minerals (montmorillonitic clay) from Villa Putuni (Fig. 4) located in La Paz. The studied similar geological conditions of origin and preliminary tests (García personal communication.) are also similar. The geological features, chemical analyses and preliminary applications of these nonmetallic minerals will be discussed below.

Diatomaceous earth resources in La Paz

- At the western side of the Bolivian Altiplano in the Pacajes Province is located the Charaña town, at 250 km from La Paz city (Fig. 1) above 4069 m.a.s.l. In the area, diatomaceous earth's resources are present. Diatomites or diatomaceous earths are siliceous

Table 1 Chemical analyses of the studied materials

Kaolinite Micaya	Kaolinite La Bella	Kaolinite Benton	Illite Llojeta	Illite Viacha
70.5–74.2	49.3	49.8–49.9	48.8–55.8	51.6–53.7
17–17.9	34.5	29.3–29.1	22.4–18.1	18.8–22.7
0.13–0.14	< 0.08	< 0.08	0.16–0.17	0.45–1.01
1.27–1.32	< 0.1	0.13–0.12	5.0–5.34	7.06–8.04
3.82–4.01	1.86	3.89–5–16	3.18–3.72	2.92–3.98
0.67–0.70	< 0.02	0.019	1.32–1.60	1.60–1.62
0.02–0.03	0.0137	0.01	0.01–0.02	0.12–0.19
0.09–0.11	0.521	0.10–0.19	0.81–0.84	0.75–1.10
0.07	< 0.009	0.0099	0.06–0.08	0.12–0.13
0.94–0.98	0.0027	0.0059	0.72–0.74	0.81–0.93

Table 2 Mineralogical analyses of the studied materials, using XRD method

Samples	Mineralogical phases
Diatomite "Charaña"	Halite; phlogopite; montmorillonite
Zeolite "Corque"	Mordenite; montmorillonite
Diatomite "Murmutani"	Halite; tridymite; muscovite
Montmorillonite "Villa Putuni"	Montmorillonite; mordenite
Montmorillonite " Río Mulatos"	Montmorillonite; anorthite
Kaolinite "Micaya"	Quartz; kaolinite; muscovite; orthoclase
Kaolinite "La Bella"	Kaolinite; sanidine
Kaolinite "Benton"	Kaolinite; sanidine; phlogopite
Illite "Llojeta"	Quartz; muscovite; montmorillonite; sanidine; clinochlore
Illite "Viacha"	Quartz; clinochlore; muscovite

Fig. 4 Montmorillonite layers from Putuni, La Paz

sedimentary rocks consisting mainly of fossilized remains of microscopic aquatic plants (diatoms); they are highly porous, and their major industrial uses are as a filter aid and as a functional filler in paint, paper, rubber and plastics (Chang 2002; Eyde and Holmes 2006).

The diatomites from the Bolivian Altiplano were first studied by Frenguelli (1939), and later on Servant-Vildary (1978) pointed out 34 species of diatom algae in some lacustrine sediments of the Altiplano. In the Charaña area were recognized three of these species for the lacustrine sediments: Nitzschia amphibia Grun, Navicula salinarum Grun and Navicula plicata Donkin (Servant-Vildary 1978). Mastoglia atacamae Hustedt was determined later on as a new species, a species from the *M. elliptica* group identified in the sediments of the Charaña Fm. at Charaña

(Servant-Vildary and Blanco 1984). Servant-Vildary and Blanco (1984) have also identified Rhopalodia gibberula and Nitzschia punctate Grun, which have been also identified in the new collected samples (Fig. 5a, b).

In 1975, a research board conformed by the US Geological Survey and the Bolivian Geological Survey (1992) reported several deposits of diatomaceous earth. All the material located in lacustrine sediments associated with evaporitic deposits southward the Altiplano, which consist of 10^6 tons of diatomaceous earth in 65–91% of purity; the above-mentioned material is located also in the Tauca Fm as well as in the Charaña Fm. at Charaña (U.S. Geological Survey and the Bolivian Geological Survey 1992). The Charaña Formation lies discontinuously above the Perez ignimbrite dated at 2.2–3 Ma. The Charaña Formation was dated in feldspars and biotites by the K–Ar method (Everden et al. 1966). The volcano-sedimentary sequence of the Charaña Fm is composed of diatomaceous layers of about 40–60-m-thick of plio-pleistocene age (Servant-Vildary and Blanco 1984). Chemical analysis of diatomaceous earth samples from Charaña (Table 1) shows a high content of silica, that corroborates the mineralogical analysis along with halite, phlogopite and montmorillonite as impurities in the mixture (Table 2).

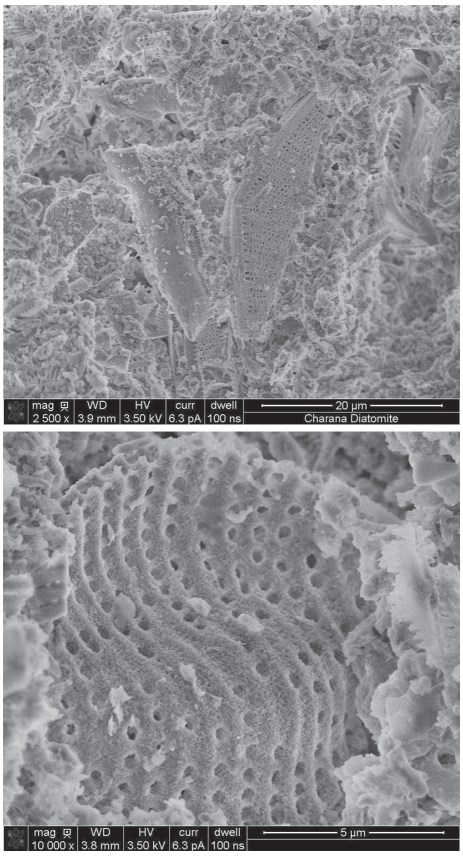

Fig. 5 SEM backscattered images from the diatomaceous earth of Charaña: **a** Rhopalodia gibberula and **b** Nitzschia punctate Grun (Servant-Vildary and Blanco 1984)

Blanco et al. (2003) pointed out a new application of the diatomaceous earth located in Charaña. The use of the diatomaceous material along with $CaCO_3$ (p.a.) in a synthetization process of wollastonite ($CaSiO_3$) a calcium silicate with acicular crystal habit. The wollastonite is used in ceramic formulations to promote dimensional uniformity, low shrinkage and fast firing, as well as in paints and plastics as filler (Chang 2002). The synthetization has been achieved by calcination of the diatomaceous earth and $CaCO_3$ mixture in relation 2:1, in a muffled oxidizing environment by natural air flow at 1100 °C for 48 h (Blanco et al. 2003).

Acarapi (2013) has studied the Charaña material for use in water purification in which work, a study on its potential as a mineral resource has been carried out concluding an approximate reserve of 16,414,200 m^3, which is present as a whitish layer 10 m thick over 1.64 km^2 of lacustrine sediments from the Charaña Fm.

Associated with the lacustrine sedimentary units and tuffs in the Charaña basin, in amygdales of the basaltic quaternary units, some zeolite minerals have been also identified (Soria-Escalante, unpublished results, 1990). The Charaña basin is an enclosed basin in the Altiplano and has been occupied by alkaline lakes and salars during the Holocene, which were formed in the presence of volcanic activity; therefore, according to Ludington et al. (1992) in the Charaña basin the zeolites were formed under the same conditions as those formed southward the Altiplano.

Literature about natural zeolite occurrences in Bolivia is poor, and chemical or mineralogical description of these occurrences is scarce. Arduz and Mobarec (1994) and Mobarec et al. (1996) in their study about the geology of the Corque area located 68 km from Oruro, in the Toledo-Huachacalla rout, have described a whitish layer from the upper level of the Huayllamarca Formation which conformed with gray sandstones; the whitish layer has been recognized as a zeolite occurrence derived from hydrothermal alteration of a dacitic sill 200 m long and 50 cm wide; 1000 tons of material was estimated (Rivas 2002). In this work, chemical (Table 1) and mineralogical analyses (Table 2) were performed on the collected samples and a zeolite type named as mordenite was identified (Fig. 6).

The layer is a zeolitic sill intruding sedimentary units associated with hydrothermal alteration of igneous rocks.

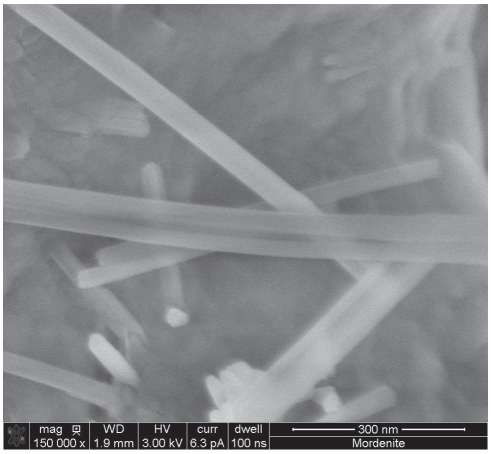

Fig. 6 Acicular crystals of mordenite from Corque

The mineralogical analysis (Table 2) confirms a mordenite-type zeolite in the rock with montmorillonite as a minor component; the chemical analysis shows 59.2 wt.% SiO_2, 15.2 wt.% Al_2O_3 as major components and 2.83 wt.% CaO and 4.34 wt.% MgO as minor components. The Si/Al relationship is 3:1, characteristic from a mordenite-type zeolite (Fig. 6).

Diatomaceous earth resources in Bolivia

Shenk (1991) has pointed out basinal characteristics for diatoms accumulations: (1) extensive, shallow basins for photosynthesis; (2) an abundant supply of soluble silica and nutrients; (3) an absence of toxic or growth-inhibiting constituents; (4) sustained high rates of diatom reproduction; (5) minimal clastic, chemical and organic contamination and (6) a low-energy environment for the preservation of the delicate diatom structure. Into the Altiplano, all these parameters were present during the past time. From the beginning of the quaternary age, lacustrine extensions have been developed due to the high volume of water as result of melting glaciers (Servant and Fontes 1978) that originated several lakes in the central basin such as Mataro lake, Cabana lake, Ballivian lake, Minchin lake, Tauca lake and nowadays the Titicaca lake (Lavenu 1991); therefore, occurrences of diatomites are common. For many years, several authors have identified diatoms occurrences in the Altiplano (Servant-Vildary 1978; Ballivian and Risacher 1981; Servant-Vildary and Blanco 1984; Ludington et al. 1992), and in the "Laguna Colorada" in South Lipez Province of Potosí, these deposits have been described by Orris et al. (1992) along with borates and sulfates in the basin.

Located in Potosí near Llica town a diatomaceous earth deposit has been mentioned by Rivas (2002) and first studied by Blanco and Zeballos (unpublished results, 2010) and Acarapi (2013); in his studies about diatomaceous resources for water purifying application, the material was described and the area was geologically characterized. The material is described as light in color and highly porous, geologically characterized by strato-volcanic series, Miocene in age, folded and faulted overlaid by tuff sequences (Cortez and Lima 2002). Rivas (2002) calculated 150,000 tonnes of the material with 80% of purity distributed in layers of 1.30 m of thickness. The mineralogical analyses (Table 2) performed in this work show amorphous material as a major component followed by tridymite, halite and muscovite. Scanning electron microscopy analyses (Fig. 7a, b) show diatoms as the major component of the

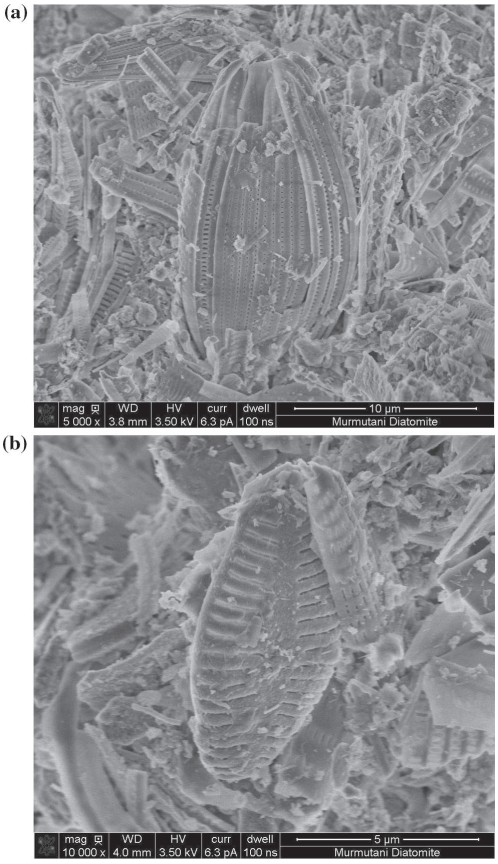

Fig. 7 SEM backscattered images from the diatomaceous earth of Murmutani, Llica

rock, corroborating this way the higher silica oxide content in the chemical analyses (Table 1).

A lacustrine sedimentary basin is located 50–60 km south of Tarija and constitutes the Padcaya basin in which diatomite horizons are present within three sectors: Padcaya, Huacanqui–Potrero and Phayo (Troëng et al. 1993). The horizons vary between 0.1 and 1.1 m in the Padcaya sector with a relatively low silica content compared with the fairly high alumina and iron, the 0.5-m and 3-m-thick outcrop in the Huacanqui–Potrero area (Troëng et al. 1993) and one horizon of 2.0–3.6 m thickness at the Phayo sector (Arduz et al. 1991).

Montmorillonitic clay resources in La Paz

- Villa Putuni (Fig. 1) is located in the Pacajes Province 102 km away from La Paz city. Located close to the Coro Coro mine, which hosts the most important copper mineralizations of Bolivia. The area hosts important resources of bentonites which are already in exploitation for the pet litter industry; although the resources belong to the community, a few families are benefited by them.

The montmorillonites are members of the silicate family with dioctahedral structure and could be highly expanded minerals if wet (Chang 2002).

The clay mineralization in the area is distributed in three thick layers from the Kollu Kollu Formation and has been identified as montmorillonite (Table 2; Fig. 4), green, red and gray in color due to some elemental characteristic of each layer. Chemical and mineralogical analyses show purity in the studied materials, allowing it to be used in zeolite synthetization (Panoso 2015). Tables 1 and 2 show mineralogical and chemical results of the collected samples. Panoso (2015) has calculated an exploitable material of 10,949,450 m^3, especially to be used in zeolitic synthetization, due to its purity.

Montmorillonitic clay resources in Bolivia

In the geological descriptions of Bolivia, two montmorillonitic deposits were referred as important in the literature, "La Encontrada" and "Rio Mulatos." La Encontrada deposit at the Coro Coro district area in La Paz has been identified as bentonitic occurrences associated with copper. The Rio Mulatos deposit is located in Potosi and is represented by bentonitic materials associated with polymetallic vein ores.

Located in the northern part of the Altiplano is the Coro Coro mine. Coro Coro is the main copper mine of Bolivia, where several studies and mining works have been carried out in the area. The studies were focused on the geological knowledge and the chemical analyses in the copper content in the sedimentary units. Near the Coro Coro town is located the Coro Coro mining district, which is composed of sediments from the Ballivian (formerly Vetas Fm.) and Caquiaviri (formerly Ramos Fm) formations. The literature refers to copper replacement clays as a geological model of the copper assemblage (Entwistle and Gouin 1955; Cox et al. 1992) although the clay was not identified and properly characterized, being the metallic mineralogy more important than the nonmetallic minerals; in this work, several samples were collected in the Coro Coro area and chemical analyses (Table 1) and mineralogical test (Table 2) were performed on the clay minerals. In the Chacarilla district as well as in the Coro Coro district, bentonized sediments were studied (Guerra and Ascarrunz 1964a, b). In "La Encontrada mine," tertiary bentonized tuff bed on the west flank of a northwest trending anticline has been identified and analyzed; the altered bed is composed of 85–99% montmorillonite as the main phase along with quartz, biotite and iron oxides (Guerra and Ascarrunz 1964a, b).

In both areas, the montmorillonitic clay appears to be the result of the hydrothermal alteration which originated the copper mineralization. The montmorillonite clay is probably that material described by Cox et al. (1992) in some other copper mines such as in the Pisaqueri mine.

Río Mulatos is another polymetallic mining district located in Potosí; veins of Au–Ag–Sb represent the disseminated mineralization; also uranium occurrences and alluvial gold are present along with important nonmetallic mineralization determined as montmorillonites from altered massive ignimbrites (Almendras et al. 2002). Close to the Río Mulatos mining district, in the Phasa Kollu Hill and the Maria Eugenia Hill, bentonite-bearing rocks with 70–90% of purity have been discovered and estimated reserves of 200,000 tons and 900,000 tons, respectively, calculated (Rivas 2002). Encinas et al. (2007) in their study about cadmium absorption properties of clays pointed out the use of clays and natural zeolites as metal absorbents of surficial waters around mining districts. They performed the studies using a montmorillonitic raw material from Río Mulatos and a natural zeolite from Corque, aforementioned; however, neither the mineralogical nor the chemical analyses of both raw materials were presented in the results. In this work, several analyses were carried out in both areas. In the Río Mulatos area, the mineralogical analyses (Table 2) show montmorillonite as the main component of the mixture and anorthite as impurity, and the chemical analyses (Table 1) show 53.0–57.1 wt.% SiO_2 and 19.7–21.5 wt.% Al_2O_3 as major components and 2.49–2.95 wt.% CaO and 3.71–3.85 MgO as minor components. The mineralogical and chemical analyses of the zeolite have been presented above.

Clays for building materials

The term applied to building materials covers any material to be used with construction purposes such as red bricks, cement, aggregates, tiles, etc. In this section, three sedimentary deposits in La Paz will be discussed (Fig. 1), a kaolinitic material from a residual deposit (Zeballos et al. 2016) and two well-known illitic-rich clay deposits currently in exploitation as raw materials for the red brick industry.

The economic evaluation of a clay deposit is related not only to the nature of the materials, but also to the exploitation, the cost of transportation and the processes to achieve the finished product from the raw material as well. All these parameters will play an important role in the final price of the product. The manufacturing processes are almost the same in all ceramic formulations; the process as many authors pointed out (Carty and Senapati 1998; Moharem and Saleh 2007; Sanfeliu and Jordán 2009) starts with shaping the raw material using specialized equipment according to the finished product obtained. Drying is the second step necessary to avoid fractures during the firing stage: firing it to a certain temperature according to the desired finished product and the mineralogical composition of the raw materials used in the product. In the specific case of tile manufacture, the final step is the glazing. Sanfeliu and Jordán (2009) pointed out the importance of the geological work in the deposits; besides, the analytical methods to determine the quality of the clay to obtain the best quality finished product have also been indicated.

According to the National Statistical Institute from Bolivia (2013), the exportation of ceramic product for the construction area has grown over 300-fold in the past 10 years, while the ceramic importation has grown over 500-fold in the past 10 years.

In this review, geological features, chemical analyses and an overview of final applications of the three deposits and end uses in ceramic will be discussed below.

Kaolinitic clay resources from Micaya

- Micaya town is located 75 km away from La Paz city (Fig. 1) and has a population of 300 inhabitants who live mainly from the agricultural work. In Micaya, a kaolinitic deposit has been found (Blanco et al. 2003) and it has been described firstly by Zeballos et al. (2009), described as whitish material, residual in origin, hosted between the layers of the Vila Vila Formation (Zeballos et al. 2016, Fig. 8).

At the bottom of the Devonian sedimentary sequence is located the Vila Vila Formation, composed of quartzitic sandstones and siltstones, overlaid by the Belen Fm.

Fig. 8 Kaolinitic deposit from Micaya, La Paz

(siltstones), Sica Sica Fm. (sandstones) and Collpacucho Fm. (sandstones), discordant to the Devonian sequence is the Neogene Umala Fm. and Remedios Formation, which is composed of tuffs (Zeballos et al. 2009). According to Soria (1980), the Remedios Formation is a result from the Cenozoic magmatism in the Altiplano. Preliminary studies in the material (Fig. 8) (Blanco et al. 2003; Zeballos et al. 2009) show quartz and kaolinite as the main components in the mixture. Plasticity test (Zeballos et al. 2014, 2016) demonstrated their suitability in the ceramic industry; the material has been worked out for the local population to handmade kitchenware (pots and dishes). Geological mapping and several analyses, such as chemical (Table 1), mineralogical (Table 2), structural (Fig. 9) and physical tests on the kaolinitic material, pointed out a presumable

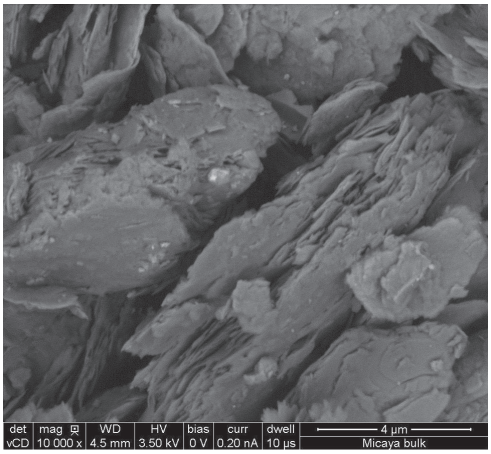

Fig. 9 SEM backscattered images from the kaolinitic sediments of Micaya

use of these materials in the construction field as suitable raw materials for floor tile manufacture (Zeballos et al. 2016).

The raw material from Micaya is a whitish mixture that exhibits very fine grain size and is composed of quartz, kaolinite, muscovite and feldspar (Zeballos et al. 2016). Chemical analyses (Table 1) show 70.5 wt.% SiO_2, 17 wt.% Al_2O_3 and 1.27 wt.% Fe_2O_3, suitable composition for white ceramic formulations, due to the minimal iron content.

Kaolinitic clay resources in Bolivia

Kaolinitic occurrences in Bolivia are registered in several places, but they are poorly characterized and scarce data are available; in the current paper, some chemical and mineralogical analyses will be provided as general knowledge. In some deposits, the kaolinitic materials are associated with metallic ores like the deposit in the Santa Rosa mine located in La Paz, where mineralogical studies show the kaolin occurrence as a by-product of the hydrothermal alteration in the rocks which at the same time originated Pb, Au and Ag anomalies. In Santa Cruz, several occurrences of kaolin were reported; those occurrences are mainly associated with pegmatitic rocks and tantalum/beryllium mineralization such as in the Ñuflo de Chavez Province, which are widely mined due to the tantalum content in the rock. In Oruro, the Itos deposit is a well-known kaolin occurrence, and it is related to the Sn-Ag mineralization in the Itos mine.

In the Santa Rosa mine, the argillization occurs associated with polymetallic veins where sandstones from the Tiwanaku Fm. were intruded by the Quimsachata dacitic porphyditic body (Orris et al. 1992; Rivas 2002). Several kaolinized areas were exploited by open-pit methods in the Quimsachata district following the metallic mineralization. Chemical analyses of the kaolinized alterations performed by Escobar et al. (1999) show 70.24 wt.% SiO_2, 14.81 wt.% Al_2O_3, 3.55 wt.% K_2O and 3.15 wt.% Fe_2O_3, mapped as kaolinitic alteration; the silica–alumina relation shows poor kaolinization of the host rock. Available data of the raw materials point out the main application in the refractory ceramic industry, besides paints and absorbents. Escobar et al. (1999) have compared the Quimsachata kaolin deposit with the Itos deposit located in Oruro first studied by Chase (1948a). The Itos deposit was an important ore of metallic minerals such as Ag–Pb–Sn (Arduz et al. 1994). Chase (1948a) has described intense alteration in the Itos stock which is composed of 60% of feldspar, 20% of quartz and 20% of biotite. Although in his studies he mentions an intense alteration such as in the San Jose Breccia where the matrix is altered to sericite and kaolin and also a 20-cm-thick alunite and kaolinite veins at the Grande vein, mineralogical analyses are not available. Moricz et al. (2009) in their work about the mineralogy in the tails of the Itos mine report illite as the main clay phase in the mixture probably the sericitic material that Chase (1948b) mentioned before, which is present in an average of 20 wt.% in contrast to 2 wt.% of kaolinite of the total volume. The Itos deposit covers an extension of 300 m length, 30 m width and 6 m of thickness with a potential of 140,000 tonnes of material (Arduz et al. 1994).

The Altiplano and Cordillera Occidental several mines have been described with kaolinized sediments as a result of hydrothermal alteration along with metallic mineralization. Despite the geological data, chemical and mineralogical analyses are not available (See Geology and Mineral Resources of the Altiplano and Cordillera Occidental, Bolivia, 1992).

In Santa Cruz, economic occurrences of kaolinite are known and have been mined as ceramic raw materials for the local industry. Centellas (1990) has pointed out kaolinite occurrences associated with tantalum–columbite minerals in Santa Cruz as well as gold mineralization (Fernández 2012). Fernández (2012) in an important review about the mining industry in Bolivia has pointed out the mineralogy of the Concepcion district, which is composed of Cu-, Pb-, Zn-, Ag- and Au-rich schist belts associated with quartz veins enriched in Au-, Sn-, W-, Nb-, Be-rich pegmatitic complexes besides kaolin as an alteration product; although the mineralogy was studied, no mineralogical or chemical results have been reported. The kaolin resources in Santa Cruz are the only kaolin resources proved to be of a good quality and are important resources (Fernández 2012), although the quality of the material and chemical and mineralogical results are not available.

For research purposes, in the present work several samples were analyzed from three deposits located in Santa Cruz; this will provide reliable data about kaolinite occurrences in the area: La Bella deposit is a kaolinite-rich pegmatitic complex intruded during the Sunsas orogeny (Litherland 1984; Arduz and Mobarec 1994) near to San Ramon town; the kaolinite in the deposit is a result of feldspar alteration, which is the main component in the pegmatites, and kaolin is the only mineral mined in the deposit; La Bella mine covers an extension 250 m long and 150 m wide, and the thickness varies from 1.50 to 33 m with a 112,000 tones reserve (Feraudy and Ruiz 1974); La Bella mine was formerly worked as an beryllium and muscovite ore (Rivas 2002). Located between San Ramon and Concepcion is the Misabo deposit in the Concepcion district, a well-known gold district in Santa Cruz, and it is associated with Au-rich kaolinized pegmatites where kaolinite and tantalum are by-products from the gold mining; 80 km from San Javier is located the Benton mine

where tantalum/niobium-rich kaolinized pegmatitic rocks (Fig. 10) are mined for the tantalite mineral which is highly radioactive (10 mR/h).

Mineralogical analyses show kaolinite as the main component for the collected samples from the deposits; Misabo deposit exhibits < 20% quartz and feldspar content in the composition, in contrast to La Bella and Benton deposits which exhibit higher alumina content (Table 1). Morphological analyses (Fig. 11) on the feldspar-free samples exhibit a particular kaolinite habit, especially in La Bella, where needle-shape kaolinite crystals are highly widespread in the sample, as well as in the Benton 1 and Benton 2 samples where the acicular crystals (Fig. 12) are also present besides a clay matrix, in which kaolinite's platelets are easily identified.

Common clay resources in La Paz

Common clay resources in Llojeta

- Llojeta is located in La Paz city (Fig. 1), a well-known area in La Paz because vast clay resources from the La Paz Formation (Fig. 13) are exposed; several companies in the red brick commercialization are settled down in the area to minimize the transportation cost. The La Paz Formation consists in discontinuous beds of poorly consolidated sand, silt, gravel, clays (Dobrovolny 1955) and tuffaceous beds (Lavenu 1978; Thouveny and Servant 1989), tertiary in age (Posnansky 1920; Branisa 1954; Escobar et al. 1999) and fluvial in origin (Dobrovolny 1955).

These materials are in almost 70% of the La Paz red brick consumption and along with other factories in Cochabamba and Santa Cruz are in 90% of the national red brick consumption (Bustillos et al. 2004). The chemical analysis (Table 1) and the XRD results (Table 2) reveal quartz as a major component along with muscovite and Illite as the principal clay constituent, a typical composition of a red brick raw material. A previous work (Escobar et al. 1999) in other areas, such as in Mallasa, Aranjuez, Cota Cota, pointed out La Paz Formation outcrops used, as well as in Llojeta, as raw materials for local red bricks producers.

Fig. 10 Kaolin occurrences from Benton deposit, Santa Cruz

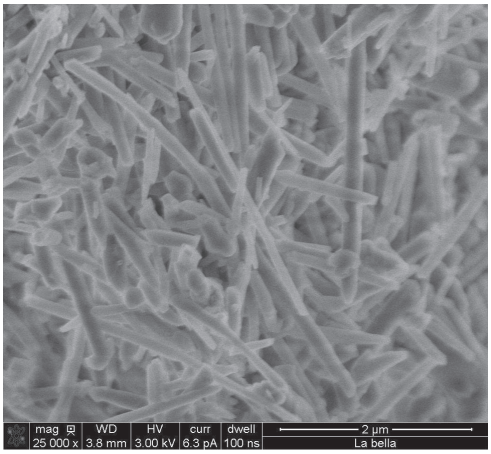

Fig. 11 Needle-shape kaolinite from La Bella deposit, Santa Cruz

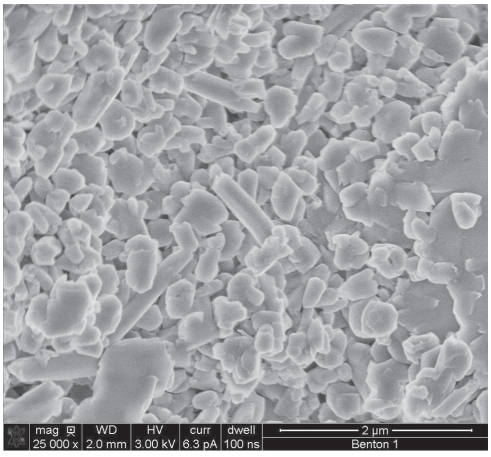

Fig. 12 Mixture of needle-shape kaolinite and platelets of kaolinite form Benton deposit, Santa Cruz

Common clay (ball clay) resources in Viacha

- The Viacha municipality is located 18 km from "El Alto" city (Fig. 1), where ceramic factories are located

Fig. 13 Illitic clays deposit from Llojeta, La Paz

around the town. The clay deposit owned by INCERPAZ, one of the major ceramic producers in Bolivia, is located 4 km from Viacha, The INCERPAZ's deposit consists of brownish clays intercalated with siltstones and fine-grained sand from the Ulloma Formation which is lacustrine in origin. Tables 1 and 2 show the chemical and mineralogical analyses performed in the collected samples.

Ball clays resources in Bolivia

Ball clay resources are widespread in Bolivia, although most of the deposits are not well described or studied; the red brick industry has worked on most of them, and some of those deposits will be described below.

Paleozoic sediments

The Belén Formation, Devonic in age, is composed of siltstones, mudstones and fine-grained sandstones, marine in origin; the finest lithology has been exploited for ceramic purposes in three areas close to Batallas town: Chillu, Karhuisa and Warmimarka (Escobar et al. 1999). The Chillu deposit located at 1.5 km from Batallas belongs to the lower sediments of the Belen Fm. which consist mainly of mudstones, and it is approximately 200 m long and 20 m thick. The raw material is composed of 60.25 wt.% SiO_2, 21.69 wt.% Al_2O_3 and 6.30 wt.% Fe_2O_3 (Escobar et al. 1999), used in pottery.

The Karhuisa deposit is located 7 km from Batallas; it consists of altered mudstones, yellowish in color between the siltstones and sandstones in the Belen Fm. The Karhuisa deposit is composed of 55.52 wt.% SiO_2, 19.93 wt.% Al_2O_3 and 6.83 wt.% Fe_2O_3 (Escobar et al. 1999); the raw material has been used since 1992 in the red brick manufacturing. The Warmimarka deposit exhibits the same lithological characteristics as the Karhuisa deposit; the chemical composition 63.94 wt.% SiO_2, 18.48 wt.% Al_2O_3 and 3.99 wt.% Fe_2O_3 (Escobar et al. 1999) reveals the possible application of the material in the ceramic industry.

In the central Altiplano, tertiary clay sediments have been described in several locations: at the Kollu Kollu Fm in Laja and Chua municipalities, at the La Paz Fm in La Paz city and the Ulloma Fm in Jesús the Machaca municipality; additionally, some deposits have been registered and studied in Potosí and Cochabamba.

Paleogene sediments

The Catavi deposit located 52 km from La Paz over the Kollu Kollu Fm is composed of red shales and sandstones besides those evaporitic layers such as gypsum and limestone that have been identified. The Catavi deposit is chemically composed of 52.50 wt.% SiO_2, 23.43 wt.% Al_2O_3, 1.23 wt.% CaO and 6.73 wt.% Fe_2O_3, although not commercially developed; some local workers have used the raw material for brick manufacture (Escobar et al. 1999). Another deposit from the Kollu Kollu Formation is the Chua Grande deposit located 22 km from Huarina; in this section, the sedimentary unit is composed of sands, tuffs and clays, yellowish in color and has an extension of 10,000 m^2 mined by hand methods with an alumina content of 20.4 wt.% Al_2O_3 (Escobar et al. 1999).

Neogene sediments

In Potosí, the Sacaca deposit is located 7 km away of Sacaca town in the Jachuma Hill; the deposit is located in a sedimentary basin within small hills, consisting of small clay occurrences; the origin of the sediments is unknown; nevertheless, a lacustrine evaporation process is suggested due the gypsum content in the sediments; the sedimentary units are undetermined, although Claure et al. (1996) assign the Bolivar Fm as the sedimentary unit. The Sacaca deposit consists of a basal conglomerate overlain by a white silty–sandy bed, a horizon of a coarse-grained sand, a light color clay bed with 20% of gypsum, 28 m thick and 600 long and of 1.6 m^3, and composed of illite and kaolinite (Claure et al.1996).

In La Paz city, the well-developed La Paz Formation is composed mainly of clays and gravel fluvio-glacial in origin. The clay has been used for many years as a raw material for the red brick industry as the main source of ceramic-building materials besides Cochabamba to import in Bolivia.

The La Paz Fm. crop out in several places; in the La Paz basin, the most exploited deposits are those located in Llojeta described before in this study; other deposits are located in Mallasilla where the production is over 7000 units/d, from a deposit 100 m long and 15 m high (Escobar et al. 1999); In the Achumani zone, the BRIKO factory reports that the used raw material belongs to siltstones layers from la Paz Fm, is gray in color and used mainly in roofing ceramics. Those deposits located in the Kantutani

zone are small in size and are used in the local commercialization with 1700 units/d (Escobar et al. 1999); along with these deposits, several others were sketched from the sediments of the La Paz Fm. located in Ovejuyo, Cota Cota, Aranjuez and Achachicala; no production data are available.

Quaternary sediments

The Ulloma Formation hosts vast clay resources used in the manufacture of red bricks as well as those raw materials from the La Paz Fm. The Tocari and Jilakhata deposits are located near Jesús de Machaca and are constituted by clays, siltstones and gravel of fluvio-lacustrine origin; the clays of the Tocari deposit are composed of 57.33 wt.% SiO_2, 14.16 wt.% Al_2O_3, 9.95 wt.% CaO and 5.29 wt.% Fe_2O_3; the sediments are distributed in 3–4-m-thick layers in the Ulloma Fm (Escobar et al. 1999). The khellani deposit materials are currently used in the manufacture of bricks with a production rate of 6000 units/day constituted of clays and siltstones with calcareous crusts; the mineralogical analysis shows quartz and illite as major components.

The Altiplano is an infill basin of lacustrine sediments, sediments that came from the oldest Minchín lake and the old Ballivian lake; as lacustrine sediments, the predominant mineralogy are illitic-rich clays, widely used in the manufacture of bricks and roofing tiles. The local ceramic manufacture represents an important economical movement in some municipalities such as San Andrés de Machaca, Viacha, Tiahuanacu, Batallas and Achacachi in the La Paz department (Escobar et al. 1999) and between Challacollo and Toledo in Oruro where the deposit consist of 2-m-thick reddish horizon; Claure et al. (1996) pointed out illite as the major component in the clay sediment, along with kaolinite and montmorillonite as the minor components.

Asher-Bolider et al. (1992) describe the CORDEOR clay pit, located in Oruro, in lacustrine deposits to be quaternary in origin and illitic in composition; 2,000,000 tons have been approximately calculated by Montes de Oca (1982) as raw material to be used in local red brick factories.

Mullite

The mullite is a rare mineral discovered in Mull (Scotland), seldom found in nature, but produced artificially by heating silica and alumina. C-E Minerals dominate a synthetic mullite production by mixing and heating various grades of bauxitic clays (Sweet et al. 2006). Synthetic mullite are generally produced by four processes: (1) melting alumina and silica or bauxite and kaolin at 1914 °C; (2) sintering alumina-rich minerals such as kaolin, bauxita or kyanite at 1763 °C; (3) calcining kyanite at 1300 °C or (4) sintering siliceous bauxite or mixtures of bauxite and kaolin at 1561 °C.

The mullite mineral imparts to the products in which it is used high refractoriness and low coefficient of thermal expansion; it confers them great resistance to thermal shock and resistance to the chemical corrosion. In Bolivia, no occurrences of this mineral have been detected.

Comeforo et al. (1948) working in mullitization from kaolinites studied the thermal behavior of kaolinites from Georgia in this experiment; it is shown mullite crystallized from kaolinites, the firing process develops two stages of crystallization, between 500 and 600 °C the hydroxyl groups are expelled from the structure and at 1000 °C, a crystallization of a new phase starts called “metakaolin” or “pro-mullite.”

From the kaolinitic residual deposit located in Micaya, La Paz (Fig. 1), Zeballos et al. (2013) have proposed a second application, a synthetization of mullite. The raw material used in the mullite synthetization was discussed above; a geological background and chemical analyses were presented in the building materials section.

Based on chemical analyses (Table 1) and XRD mineral peak position (Table 2), Zeballos et al. (2013) performed a mullite synthetization using kaolinite-bearing sediments as raw material from Micaya. The performed process is a ramp/hold firing program, where the heating rate process is timely controlled as well as the cooling process leaving a slow crystallization process. Three heating and holding stages were defined: (1) 0 °C–570 °C/30 min, (2) 570 °C–1100 °C/30 min and (3) 1100 °C–1250 °C/30 min, and the resulting material was a mixture where acicular mullite crystals are visible (Fig. 14).

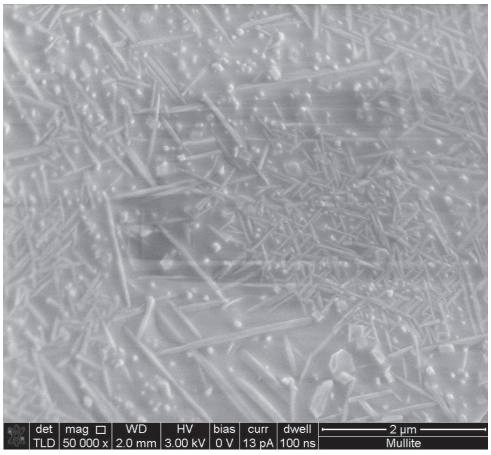

Fig. 14 Acicular mullite crystals, synthetized from kaolinitic sediments

Refractory minerals in Bolivia

Sanz et al. (2003) reported refractory minerals widely widespread in Oruro, in areas such as San Pedro, Corque, Pampa Aullagas, Andamarca, Isla de Panza and Salinas de Garcí Mendoza; no specifications in the mineral composition in these studied areas were reported.

Close to La Paz city in the Zongo Valley, 15-cm-long crystals of andalucite were discovered in the metamorfized Coroico Fm. with a 10 wt.% concentration (Rivas 2002). Ávila-Salinas (1989) determined quiastolite from the andalucite family as the main mineral, whitish in color due to the 2% concentration of Fe_2O_3 and of 5.8 million tons.

Nonmetallic market in Bolivia (import–export)

Bolivia is an important player in mineral exportations and has been one of the export leaders in tin, lead, zinc among others. In (1970), Arthur D. Little Inc. made a first survey about the opportunities of the nonmetallic minerals industry in Bolivia, and the conclusions indicate construction materials, glass, ceramic tile, magnesite, asbestos and vitreous plumbing as good opportunities of resources, market and technology.

The mining industry was for several years the main income of Bolivia, and now it became important again thanks to the Mutún at the eastern part of Bolivia and the Uyuni salt lake at the western side of the country. Bolivia has been characterized as a mining country since the days of the colony; beginning of 1545 is the year that is given to the cycle of mining, in which mineral exploitation begins, mainly silver. Around 1900, the ore mineral deposits were worked by private owners as the likes of Patiño, Aramayo and Hochschild. In 1952 comes the nationalization of mines and COMIBOL (Bolivian Mining Corporation) is founded. COMIBOL is the company responsible for the old mine workings as well as the current ones.

The Uyuni Salar flat is the main nonmetallic mining prospect in Bolivia and has a surface of 10,582 km^2, home for 70% of the lithium reserve with a 100 million tons of reserve (Office of Evaporitic Resources 2010). The nonmetallic mineral deposits in general are slightly known and less exploited due the low trade value; nevertheless, some nonmetallic minerals acquire relative importance as raw materials, such as limestones, dolomite and clays.

In 2010, the median mining contributed with 36.73%, the small mining and cooperative mining with 55.80% and the state-owned mining with 7.45% (Ministry of Mining and Metallurgy 2010). The nonmetallic minerals are represented in the small mining, in minerals such as ulexite (97,302.03 m^3), barite (7844.67 m^3), amethyst (485,390 m^3), bentonite (440,000 m^3) casing stones (728,604 m^3), tantalite (3416 m^3) and limestone (111,450 m^3). During 2010, the export value reached a value of USD 3,410,254 with an export volume of 3,156,069 fine metric tons (Ministry of Mining and Metallurgy 2010). During 2010, Bolivia has exported 42% to Asia, 28% to Europe, 28% to America and 2% to Oceania and Africa (Ministry of Mining and Metallurgy 2010).

The cement Industry in Bolivia

Cement is one of the main industrial products made of nonmetallic minerals, which uses limestone, clay and gypsum which is added to control the setting. Bolivia produces portland cement and pozzolanic cement that mix clinker with 30% of pozzolana increasing the resistance of the salt water attack and fracturing. The clinker occurs as lumps or nodules, usually 3 to 25 millimeters in diameter, produced by sintering limestone and aluminosilicate materials such as clay during the cement kiln stage.

The pozzolans are materials bound to volcanism or materials that exhibit pozzolaneity. The pozzolaneity is a reaction developed between the silica of the raw material itself and the calcium hydroxide of the cement in the presence of water; among the materials used are tuffs and ignimbrites. Deposits of tuffs are located near the city of Sucre, in the Huayllas and Calera occurrences, whose materials are whitish to greenish gray with varying contents of biotite and silty clay sediments (Arduz et al. 1992). In La Paz area, 25 km southwest to La Paz, the Ventilla deposit is composed by rhyodacitic tuff horizons intercalated with sand and clays from the Umala Fm. The important horizon is 2.0–3.0 m thick and 100 m long; close to Villa Remedios, the same horizon from the Umala Fm is 4.8 m thick (Arduz and Buitrago 1992).

The cement industry in Bolivia is represented by six companies, SOBOCE (La Paz), FANCESA (Sucre), COBOCE (Cochabamba), ITACAMBA (Santa Cruz), YURA (Perú), ITAÚ (Brasil). In 2015, the cement industry has grown in over 8.4%, leading the sales SOBOCE accounting for a 1,537,012 tons in 2015 (SOBOCE 2015), FANCESA with a 989,563 tons, COBOCE with a 677,821 tons, ITACAMBA with a 168,270 tons and Yura with a 296,972 (Press report, 2016). Four plants will be installed in the future: the state company ECEBOL (Oruro) will initiate operation in 2019 with 3000 tpd, Itacamba (Santa Cruz) will operate 2000 tpd in 2017, FANCESA (Sucre) will operate 2000 in 2019 (Press report, 2016) and SOBOCE will initiate operation in a new plan in Santa Cruz de la Sierra accounting for 1000 tpd in 2020 (SOBOCE 2015).

Acknowledgements This study was funded by the Swedish Development Agency (SIDA). We express our enormous gratitude to the Institute of Geology and Environment (IGEMA).

References

Acarapi W (2013) Estudio y aplicación de los recursos diatomaceos de las localidades de Charaña y Bella Vista, departamentos de La Paz y Potosí. Dissertation, Universidad Mayor de San Andrés, La Paz, Bolivia

Almendras AO, Menacho LM, Miranda AV (2002) Depósitos metálicos y áreas prospectivas de la región de Río Mulatos. Final Proc. Bolivian Conf. of Geology. Santa Cruz, Bolivia, pp 12–17

Arduz M, Buitrago O (1992) Minerales y rocas industriales en Bolivia: Una alternativa de diversificación. Bol Soc Geol Boliv La Paz 27:12–13

Arduz TM, Mobarec CR (1994) Final Proc. Bolivian Conf. of Geology. Santa Cruz, Bolivia, pp 340–342

Arduz M, Burgos G, Quiroga J (1991) Programa de Investigación de minerales industriales en el Departamento de Tarija – Bolivia. Informe inédito, GEOBOL

Arduz M, Troncoso D, Asebey J, Camacho A (1992) Proyecto de exploración y evaluación de minerales industriales en el Departamento de Chuquisaca - Bolivia. Informe inédito, GEOBOL

Arduz TM, Almeida L, Claure H (1994) Final Proc. 7° Chilean Conf. of Geology: Volume II. Concepción, Chile, pp 720–724

Asher-Bolinder S, Soria EE, Orris JG (1992) CORDEOR clay pit. In: Cox PD, Carrasco R, Andre RO, Hinojosa VA, Long RL (eds), Cooper deposits in sedimentary rocks United States Government Press Office, pp 206–207

Arthur D Little Inc., Prudencio Claros y Asociados (1970) Estudio de Oportunidades para la industria Boliviana. Industria de Metales No-Ferrosos, Ministerio de Gobierno, vol 2, p 29

Ávila-Salinas W (1989) Perspectivas sobre la explotación y aplicación industrial de la andalucita de Yani – Zongo. CEDOMIN No 11

Ballivian O, Risacher F (1981) Los salares del Altiplano boliviano; métodos de estudio y estimación económica: Paris and La Paz. L 'Office de Ia Recherche Scientifique et Technique Outre - Mer and Universidad Mayor de San Andres

Blanco M, Conde J, Cabrera S (2003) Síntesis de wollastonita a partir de precursores naturales (toba y diatomite). Final Proc. Bolivian Conf. of Geology, Oruro, Bolivia, pp 357–361

Branisa L (1954) Geología del Valle de La Paz. El Diario and La Nación newspaper reporting, La Paz, Bolivia

Brown G, Brindley GW (1980) X-ray diffraction procedures for clay mineral identification. In: Brindley GW, Brown G (eds) Crystal structures of clay minerals and their X-ray identification. Miner Soc Monogr 5:305–359

Bustillos R, Carrasco C, Duran L (2004) Determinación de los Impactos Ambientales de la viruta de cromo empleada para la fabricación de ladrillos. Final report, National Chamber of Industry –IIDEPROQ

Carty MW, Senapati U (1998) Porcelain-raw materials, processing, phase evolution, and mechanical behaviour. J Am Ceram Soc 81(1):3–20

Centellas CR (1990). Algunas manifestaciones de minerals de rendimiento económico. In: Yacimientos Petrolíferos Fiscales Bolivianos Technical journal, Final Proc. IX Bolivian Geological Conference, vol. 11(2–3), pp 317–321

Chang LY (2002) Industrial mineralogy: materials, processes and uses, 1st edn. Prentice Hall, Upper Saddle River

Chase MF (1948a) Tin-Silver veins of Oruro, Bolivia (I Part). Bull Econ Geol 43(5):333–383

Chase MF (1948b) Tin-Silver veins of Oruro, Bolivia (II Part). Bull Econ Geol 43(6):435–470

Claure VH, de Oliveira AL, Arduz TM (1996) Deposits of industrial minerals and rocks. In: Troëng B, Riera KC (eds) Thematic maps of mineral resources of Bolivia, Uncía geological sheet. Bulletin Geological Survey of Bolivia, vol 7, pp 43–62

Comeforo E, Fischer R, Bradley W (1948) Mullitization of Kaolinite. J Am Ceram Soc 31(9):254–259

Cortez R, Lima CE (2002) Resultados de prospección geoquímica en el area Llica – Bella Vista. Final Proc. Bolivian Conf. of Geology. Santa Cruz, Bolivia, pp 275–278

Cox PD, Carrasco R, Andre RO, Hinojosa VA, Long RL (1992) Cooper deposits in sedimentary rocks. In: U. S. Geological Survey editors, United States Government Press office, pp. 95–209

Dobrovolny E (1955) Preliminary report of the geology of the Upper Las Paz valley, Bolivia. U.S. Geological Survey, Report

Encinas E, Zubieta E, Rojas J (2007) Remoción de Cadmio proveniente de la actividad minera mediante materiales arcillosos. In: J. Feyen, L. Aguirre, M. Moraes (Editors), International Congress on Development, Environment and Natural Resources: Multi-level and Multi-scale Sustainability, Cochabamba – Bolivia, pp 873–880

Entwistle PL, Gouin OL (1955) The chalcocite-ore deposits at Coro coro, Bolivia. Bull Econ Geol 50(6):555–570

Escobar DA, Bellot J, Jurado AE (1999) Minerales y rocas industriales. In: Riera KC, Troëng B, Diaz ME, Jurado AE (eds) Integrated studies of the mineral resources of Bolivia. La Paz and Copacabana Geological sheet. Geological Survey of Bolivia, Bulletin, vol 22, pp 75–117

Everden F, Kriz S, Cherroni C (1966) Correlaciones de las formaciones terciarias de la cuenca altiplánica a base de edades absolutas determinadas por método potasio - argon. Report (1). Geological Survey of Bolivia

Eyde HT, Holmes AD (2006) Zeolites. In: Kogel J, Trivedi N, Barker J, Krukowski S (eds) Industrial minerals & rocks, 7th edn, Society for Mining, and Exploration Inc., pp 1039–1064

Feraudy C, Ruiz G (1974) Kaolin project: Evaluation and reserves calculation of kaolin deposits. Geological Survey of Bolivia, Bulletin GE-61

Fernández TJ (2012) La minería y la problemática medioambiental en Bolivia. In: Fernandes A, Furtado L (eds) Minería y actuación del ministerio público en Latinoamérica. Latin American network of Environmental Public Prosecutor, Brazil, pp 67–93

Frenguelli J (1939) Diatomeas del Lago Titicaca. Notes Mus, La Plata, vol 4, pp 175–196

Garcia G, Aguilar-Mamani W, Cabrera S, Hedlund J, Mouzon J (2015) Preparation of zeolite A with excellent optical properties from clay. J Alloys Compd 619:771–777

Guerra M, Ascarrunz KR (1964a) Informe sobre el estudio de yacimiento bentonítico mina La Encontrada: Bolivia. Report (DNG-M-342), Geological Survey of Bolivia

Guerra M, Ascarrunz KR (1964b) Informe sobre orientación técnica mina cuprífera La Encontrada: Bolivia. Report (DNG-M-343), Geological Survey of Bolivia

I. N. E. (2013) Estadísticas de la actividad de la Construcción. Statistical National Institute from Bolivia. Statistical report. La Paz, pp 33–36

Lavenu A (1978) Néotectonique des sédiments Plio-Quaternaire du nord de L'Altiplano Bolivien (région de La Paz-Ayo Ayo-Umala). Cah ORSTOM Sér Géol X(1):115–126

Lavenu A (1991) Formación Geológica y Evolución. In: Dejoux C, Iltis A (eds) El Lago Titicaca – Síntesis del Conocimiento limnológico actual. ORSTOM, Hisbol Press, La Paz, pp 19–27

Litherland M (1984) Precambrian Geological Sheet. GEOBOL-BGS, esc. 1:1000000. Cook, Hammond & Kell, Inglaterra

Ludington S, Orris GJ, Cox DP, Long KR, Asher-Bolinder S (1992) Mineral deposit models. In: U. S. Geological Survey editors, United States Government Press office, pp 63–89

Ministry of Mining and Metallurgy of Bolivia (2010) Data Base of the Ministry

Mobarec CR, Murillo SF, Arduz TM (1996) Deposits of industrial minerals and rocks. In: Troëng B, Riera KC (eds) Thematic maps of mineral resources of Bolivia, Corque and Payachata snow Hills geological

Moharem AF, Saleh AE (2007) Properties and suitability of Wadi Zarieb Feldspars for ceramic industries in Egypt. J Appl Sci 7(19):2794–2799

Montes de Oca I (1982) Geografía y recursos naturales de Bolivia. Superel Ltd Press, La Paz

Moore D, Reynolds R (1997) X-ray diffraction and the identification and analysis of clay minerals. Oxford University Press, Oxford, p 371

Moricz F, Walder FI, Madai F (2009) Geochemical and mineralogical characterization of waste material from the Itos Sn-Ag deposit, Bolivia. Final Proc. Int. Conf. Securing the Future and 8th ICARD, Skellefteå, Sweden

Office of Evaporitic Resources of Bolivia (2010) Informative report and memories 2010. La Paz – Bolivia

Orris JG, Asher-Bolider S, Soria EE, Enriquez RR, Bailey AE (1992) Laguna Colorada. In: Cox PD, Carrasco R, Andre RO, Hinojosa VA, Long RL (eds) Cooper deposits in sedimentary rocks. United States Government Press Office, pp 201–202

Panoso Y (2015). Estudio Geológico y Caracterización del Depósito Bentonítico y sus aplicaciones Potenciales, en la Localidad Putuni – Condoroca, Provincia Pacajes, Departamento de La Paz. Dissertation, Universidad Mayor de San Andrés, La Paz, Bolivia

Parker MP (2008) The 2009–2014 World outlook for Non-metallic mineral mining and quarrying. ICON Group International, Inc Press, San Diego, p 191

Posnansky A (1920) Bolivia. Soc. Geogr (28:51–52), La Paz

Rivas S (2002) Minerales No-Metálicos, Rocas Industriales y Gemas de Bolivia. Landivar Press, Bolivia, p 355

Sanfeliu T, Jordán MM (2009) Geological and environmental management of ceramic clay quarries: a review. Environ Geol 57:1613–1618

Sanz MF, Gutierres ZF, Echeverria MP (2003) Potencial económico-social del Departamento de Oruro, Bolivia. Cartagena agreement team –Andean Cooperation Program to Bolivia, Oruro

Servant M, Fontes JC (1978) Les lacs quaternaires des hauts plateaux des Andes boliviennes. Premieres interprétations paléoclimatiques. Cah ORSTOM Sér Géol 10(1):9–23

Servant-Vildary S (1978a) Les diatomées des dépôts lacustres quaternaires de I' Altiplano bolivien. Cah ORSTOM Sér Géol X(I):25–35

Servant-Vildary S (1978b) Les diatomées des dépôts lacustres quaternaires de I' Altiplano bolivien. Cah ORSTOM sér Géol X(I):55–102

Shenk JD (1991) Lacustrine diatomite. In: Orris GJ, Bliss JD (eds) Some industrial mineral deposit models-descriptive deposit models: U.S. Geological Survey Open-File, Report 91-11A, pp 23–25

Sociedad Boliviana de Cemento (2015) Escenario Competitivo de la industria. Informe Interno

Soria FA (1980) Estudio hidrogeológico del área Viacha, Surusaya y Villa Remedios. Thesis, Universidad Mayor de San Andrés, La Paz, Bolivia

Sweet P, Dixon G, Snoddy J (2006) Industrial Minerals & Rocks. In: Kogel J, Trivedi N, Barker J, Krukowski S (eds) Kyanite, Andalusite, Sillimanite and Mullite: Society for Mining, and Exploration Inc., pp 553–560

Thouveny N, Servant M (1989) Palaeomagnetic stratigraphy of Pliocene continental deposits of the Bolivian Altiplano. Palaeogeogr Palaeoclimatol Palaeoecol 70:331–344

Troëng B, Claure H et al (1993) Thematic maps of the Mineral Resources of Bolivia, Tarija and Villazon Sheets

U.S. Geological Survey and Bolivian Geological Survey (1992) Geology and Mineral Resources of the Altiplano and Cordillera Occidental, Bolivia. In: U.S. Trade and development program. United States Government Press office

Zeballos A, Blanco M, Machaca V (2009) Caracterización Mineralógica y Fisicoquímica de una Lutita Blanca de la Localidad de Micaya, La Paz. Memorias Congr. Nal. Geología XIV, Potosí-Bolivia, 2009. Ed. Comisión Científica Nacional, pp 230–233

Zeballos A, Weihed P, Blanco M, Machaca V (2013) Mullite synthetization at low temperature. Final Proceedings of the International Conference Mineral deposit research for a high-tech world, Uppsala, Sweden, pp 1784–1786

Zeballos A, Weihed P, Blanco M, Machaca V (2016) Geological, mineralogical and chemical characterization of Devonian kaolinite-bearing sediments for further applications in the ceramic (tile) industry in La Paz, Bolivia. Environ Earth Sci 75(5):1–15